

The hMSSM with a Light Gaugino/Higgsino Sector: Implications for Collider and Astroparticle Physics

GIORGIO ARCADI¹, ABDELHAK DJOUADI^{2,3}, HONG-JIAN HE^{4,5},
JEAN-LOIC KNEUR⁶ and RUI-QING XIAO^{4,7}

¹ Dipartimento di Scienze Matematiche e Informatiche, Scienze Fisiche e Scienze della Terra,
Universita degli Studi di Messina, Via Ferdinando Stagno d'Alcontres 31, I-98166 Messina,
Italy

² Centro Andaluz de Física de Partículas Elementales & Departamento de Física Teórica y del
Cosmos, Universidad de Granada, E-18071 Granada, Spain

³ NICPB, Rävala pst. 10, 10143 Tallinn, Estonia

⁴ T. D. Lee Institute & School of Physics and Astronomy, Key Laboratory for Particle
Astrophysics and Cosmology (MOE), Shanghai Jiao Tong University, Shanghai, China

⁵ Institute of Modern Physics and Physics Department, Tsinghua University, Beijing, China;
Center for High Energy Physics, Peking University, Beijing, China

⁶ Laboratoire Charles Coulomb (L2C), UMR 5221 CNRS-Université de Montpellier II,
F-34095 Montpellier, France

⁷ Department of Physics, King's College London, Strand, London WC2R 2LS, UK

Abstract

The hMSSM is a special parameterization of the minimal supersymmetric extension of the Standard Model (MSSM) in which the mass of the lightest Higgs boson is automatically set to the LHC measured value, $M_h = 125 \text{ GeV}$, by adjusting the supersymmetric particle spectrum such that it provides the required amount of radiative corrections to the Higgs boson masses. The latter spectrum was in general assumed to be very heavy, as indicated by the present exclusion limits of the LHC, not to affect the phenomenology of the Higgs sector. In this work, we investigate the impact on the hMSSM by a light gaugino and higgsino sector, that is allowed by the present LHC data. In particular, we discuss the radiative corrections due to charginos and neutralinos to the Higgs boson masses and couplings and show that an hMSSM can still be realized in this context. We first describe how this scenario is implemented in the package SuSpect that generates the MSSM Higgs and supersymmetric spectra. We then analyze the possible impact of Higgs boson decays into these new states, as well as the reverse cascade channels with Higgs bosons in the final states, for the constraints on the MSSM Higgs sector at the LHC. We further explore the cosmological constraints on the hMSSM with a light gaugino–higgsino spectrum. We analyze the relic abundance of the lightest neutralino as a candidate of the dark matter in the Universe and the constraints on its mass and couplings by the present and future astroparticle physics experiments.

Contents

1	Introduction	2
2	Theoretical Setup	5
2.1	Formulation of the hMSSM	5
2.2	Light Neutralinos and Charginos in the hMSSM	7
2.3	Implementation in the Program SuSpect	9
2.4	Direct Corrections to the Higgs-Fermion Couplings	14
3	Constraints on the Gaugino-Higgsino Sector	17
3.1	LHC Searches for Charginos and Neutralinos	17
3.2	LHC Constraints on the Gaugino-Higgsino Parameters	20
4	Collider Constraints on the Higgs sector	24
4.1	Higgs Production and Decay	24
4.1.1	Higgs Cross Sections and Decay Branching Fractions	24
4.1.2	Diphoton Decay Rates of Higgs Bosons	25
4.1.3	SUSY Corrections to Higgs Production and Decays	26
4.2	Constraints on the Parameter Space of the Higgs Sector	29
4.3	Higgs Decays into Charginos and Neutralinos	32
5	Astrophysical Constraints of the hMSSM	37
5.1	$M_1 \simeq \frac{1}{2}M_2$	39
5.2	$M_1 \simeq M_2$	41
5.3	$M_1 \ll M_2$ and $M_2 \ll M_1$	44
5.4	Summary of the DM constraints	46
6	Conclusions	49

1 Introduction

The search for Higgs bosons, in addition to the one discovered by the ATLAS and CMS collaborations in 2012 [1] which completed the particle spectrum of the Standard Model (SM), is one of the main missions of the LHC experiments. Such particles are predicted in a plethora of extensions of the SM. This is particularly the case of supersymmetric theories [3, 4] which address one of the main theoretical issues of the SM Higgs sector, namely the hierarchy problem and the instability of the Higgs boson mass against very high energy scales. In its most economical version, the minimal supersymmetric SM (MSSM) [4, 5], the theory requires the existence of two Higgs doublet fields that lead to five Higgs states in the particle spectrum: two CP-even h and H , a CP-odd or pseudoscalar A and two charged H^\pm states [6, 7]. While the h boson is identified with the one which has been observed at the LHC and measured to have a mass of $M_h = 125.09 \text{ GeV}$ and SM-like couplings to the known fermions and weak gauge bosons [2], the other Higgs particles are expected to be heavy enough as to escape detection at the current stage of the experiments [8].

One of the attractive features of the MSSM is that, despite of its complexity, the Higgs sector can be described by two free parameters at the tree level, compared, for instance, to the 7 parameters needed in the case of a general two-Higgs doublet model [9]. This allows the model to have some predictability despite of its rich Higgs sector and to allow for rather straightforward phenomenological analyses. Unfortunately, such a simple picture is spoiled when radiative corrections, which turn out to be quite important in the Higgs sector [10], are taken into account. In this case, the numerous SUSY parameters enter the characterization of the Higgs sector and make any analysis a daunting task. One solution to ease the problem is to resort to benchmark scenarios that are representative of the phenomenology of the model, in which one keeps free the two basic input parameters and fixes all the additional ones entering the loop corrections. These benchmarks have been proposed quite early [11][12] and have been used for a long time by theorists and experimentalists in MSSM Higgs studies, in particular before the discovery of the h boson.

One drawback of these benchmark scenarios is that, when varying the relevant input parameters, the mass of the h Higgs state which is extremely sensitive to radiative corrections has to also vary and might exceed significantly the experimental value of $M_h \simeq 125$ GeV. One way out of this problem, would be to enforce the h mass to be equal to its true value and, hence, to use it as an input from the very beginning; this is the essence of the hMSSM scenario proposed a decade ago [13][14]. This is made feasible by the fact that by far the dominant correction that enters in the MSSM Higgs sector and, hence, in the CP-even Higgs masses, appears in one single block [16][17] that can be traded against the mass parameter M_h^2 . Hence, to an approximation which has been shown to be very good [12][13][14] (see also Ref. [15]), one can still describe the radiatively corrected MSSM Higgs sector with only two parameters as at the tree level, while keeping the h mass at its measured value. This is particularly true for very large masses of the superpartners of the SM fermions, in particular those of the top squark which have the largest Higgs couplings and hence contribute mostly to the loop corrections¹.

The hMSSM is currently used by the ATLAS and CMS collaborations in their study of the MSSM Higgs sector and in setting the constraints on its parameter space from their searches of the heavier Higgs states H , A and H^\pm , in the various discovery channels. One implicit assumption of the hMSSM, though, is that all SUSY particles should be heavy enough (or should couple very weakly) to these Higgs states. While this can be certainly true in the case of the strongly interacting superparticles, the squarks and the gluinos, which should be (have been) constrained to have masses above a few TeV (at least 2 TeV) from the negative LHC searches [19], this is not the case of the weakly interacting superparticles. Nevertheless, for the $\mathcal{O}(1 \text{ TeV})$ masses that are being currently probed at the LHC, sleptons generate small contributions to the radiative corrections and have a limited impact on the MSSM Higgs sector in general. In turn, the charginos and neutralinos, the mixtures of the gauginos and higgsinos, the superpartners of the gauge and Higgs bosons, are expected to be lighter and might couple substantially to the Higgs particles.

One should therefore allow, in the context of the hMSSM, for the description of the phenomenology of these particles and their interplay with the Higgs sector. This is par-

¹For a recent different M_h input setup in the MSSM, that does reduce the number of input parameters but rather determines semi-analytically the trilinear coupling $A_t(M_h)$, see Ref. [18].

ticularly important as in the next Run II and the higher luminosity LHC runs [20], a large data sample could be collected which would allow to have sensitivity to the channels in which the MSSM Higgs bosons could decay into charginos and neutralinos. In fact, this is also important for the reverse processes in which it is these weakly interacting superparticles that could decay into the various Higgs bosons, including the heavier Higgs states, which will be closely studied by the up coming experiments.

From a rather different perspective, another very interesting and attractive feature of supersymmetry in general, and the MSSM in particular, is that the lightest SUSY particle (LSP) identified with the lightest of the four neutralinos, can be made absolutely stable by virtue of a discrete symmetry called R-parity [21]. This particle might thus form the dark matter (DM) in the Universe and in fact, for a long time it was thought as the best DM candidate [22]. If the sfermions are very heavy as indicated by current LHC data, the neutral MSSM Higgs states can serve as the privileged portals to the DM neutralino in a large area of the parameter space [23]. The hMSSM should therefore describe these astroparticle aspects too.

Hence, it is necessary to extend the original hMSSM scenario in order to cope with these interesting possibilities for collider searches in the context of an intertwined MSSM Higgs and gaugino-higgsino sectors, and to address the astrophysical issues in which the dark matter formed by the lightest neutralino interacts through the MSSM Higgs portal. This is the main scope of this paper. We will extend the hMSSM in which the Higgs sector is described as usual by two parameters, taken to be the CP-odd Higgs mass and the ratio of vacuum expectation values (vevs) of the two Higgs doublets fields $\tan\beta$, and we link it to the chargino and neutralinos sectors which are described by three additional parameters, namely the two soft-SUSY breaking gaugino mass parameters M_1 and M_2 and the (supersymmetric) higgsino mass parameter μ [24]. The interplay of the two sectors of the theory will be explored in detail.

After discussing how such a scenario is implemented in one of the major numerical packages that generate the supersymmetric spectrum, the program `SuSpect` [25], we will analyze the impact of the radiative corrections of the supersymmetric sector to the Higgs boson masses and couplings, including the so-called direct corrections to the Higgs-fermion couplings. We will then analyze the contributions of these superparticles to loop induced Higgs decays, the impact of the chargino and neutralinos in MSSM Higgs decays and the decays of these SUSY states into Higgs bosons. The impact of these new channels on the LHC constraints on the Higgs sector will be highlighted. Finally, we perform an updated analysis of the phenomenology of the lightest neutralino DM in the hMSSM, study its relic abundance and the constraints and prospects for direct and indirect detection experiments and the complementarity of these searches in connection to those performed at colliders.

The paper is organized as follows. In the section 2, we present the hMSSM including the chargino and neutralino sector and its impact on the radiative corrections to the Higgs masses and couplings, and discuss how the model is implemented in the program `SuSpect`. In section 3, we analyze the LHC constraints on the gaugino-higgsino sector and, in section 4, the collider constraints on the Higgs sector when these new particles are included in the analyses. Section 5 studies systematically the dark matter implications in the hMSSM and how it is tested by the present astroparticle physics experiments. Finally, we present our conclusions in section 6.

2 Theoretical Setup

2.1 Formulation of the hMSSM

In the MSSM, two doublets of complex scalar fields are necessary to spontaneously break the electroweak symmetry, leading to a spectrum of five Higgs states: two CP-even h and H bosons, a pseudoscalar A boson and two charged H^\pm bosons [6, 7]. At tree-level, the Higgs sector can be simply described by two basic parameters, taken usually to be the ratio of vevs $\tan\beta$ and the mass M_A of the pseudoscalar state. For a large value of the latter, $M_A \gg M_Z$, one is in the so called decoupling regime where the three heavy Higgs states are almost degenerate in mass while the lighter one reaches its maximal mass value,

$$M_H \approx M_{H^\pm} \approx M_A \quad \text{and} \quad M_h \simeq M_Z |\cos 2\beta| < M_Z. \quad (2.1)$$

The Higgs couplings to fermions and gauge bosons are given in terms of $\tan\beta$ and the angle α that diagonalises the 2×2 mass matrix of the two CP-even h and H states

$$\mathcal{M}^2 = \begin{bmatrix} M_Z^2 \cos^2 \beta + M_A^2 \sin^2 \beta & -(M_Z^2 + M_A^2) \sin \beta \cos \beta \\ -(M_Z^2 + M_A^2) \sin \beta \cos \beta & M_Z^2 \sin^2 \beta + M_A^2 \cos^2 \beta \end{bmatrix}. \quad (2.2)$$

Compared to their SM values, the Yukawa couplings g_f^ϕ for isospin up- and down-type fermions and the reduced Higgs couplings to the $V = W, Z$ bosons are given by [6, 7]

$$\begin{aligned} g_u^h &= \frac{\cos \alpha}{\sin \beta}, & g_d^h &= -\frac{\sin \alpha}{\cos \beta}, & g_V^h &= \sin(\beta - \alpha), \\ g_u^H &= \frac{\sin \alpha}{\sin \beta}, & g_d^H &= \frac{\cos \alpha}{\cos \beta}, & g_V^H &= \cos(\beta - \alpha), \\ g_u^A &= \cot \beta, & g_d^A &= \tan \beta, & g_V^A &= 0. \end{aligned} \quad (2.3)$$

In the decoupling limit $M_A \gg M_Z$ in which one has $\alpha \rightarrow \beta - \frac{\pi}{2}$, the h couplings reduce to those of the SM Higgs boson, $g_X^h \rightarrow 1$, while those of the H state (as well as the ones of the two H^\pm states) follow asymptotically the A boson couplings, $g_X^H \rightarrow g_X^A$.

This simple description of the MSSM Higgs sector with only two basic parameters is unfortunately spoiled by radiative corrections in which all MSSM parameters in principle enter [10]. Nevertheless, the by far largest correction is contained into one single term: the correction to one of the elements of the CP-even Higgs mass matrix eq. (2.2), $\Delta\mathcal{M}_{22}^2$. This term, coming from the top-stop sector, is quadratic in the top quark mass or Yukawa coupling $\lambda_t = \sqrt{2}m_t/v \sin\beta$ and involves the logarithm of the SUSY scale, defined to be the geometric average of the two stop squark masses $M_S = \sqrt{\bar{m}_{\tilde{t}_1} \bar{m}_{\tilde{t}_2}}$.

One thus has [16]

$$\Delta\mathcal{M}_{22}^2 \sim \frac{3\bar{m}_t^4}{2\pi^2 v^2 \sin^2 \beta} \left[\log \frac{M_S^2}{\bar{m}_t^2} + \frac{X_t^2}{M_S^2} \left(1 - \frac{X_t^2}{12M_S^2} \right) \right], \quad \Delta\mathcal{M}_{11}^2 \sim \Delta\mathcal{M}_{12}^2 \sim 0, \quad (2.4)$$

where X_t is the stop mixing parameter given, in terms of the trilinear coupling A_t in the stop sector and the higgsino mass parameter μ , by $X_t = A_t - \mu/\tan\beta$ and which maximizes the radiative corrections for the special value $X_t = \sqrt{6}M_S$; \bar{m}_t is the running

$\overline{\text{MS}}$ top quark mass introduced to account for the leading two-loop radiative corrections in a renormalisation-group (RG) improved approach. Sub-leading contributions, such as those controlled by the b -quark Yukawa coupling $\lambda_b = m_b/v \cos \beta$ which, at large values of $\tan \beta$, becomes relevant can be included in the component $\Delta \mathcal{M}_{22}^2$. Other non-leading corrections [10] enter in all $\Delta \mathcal{M}_{ij}^2$ terms of the correction matrix, like the ones that are proportional to λ_t^2 or λ_b^2 or those originating from the gaugino sector, which introduce a dependence on the gaugino mass parameters M_1, M_2, M_3 in addition. However, these contributions are much smaller than the leading one and can be ignored in general [10].

In the approximation above, the maximal value of the h mass, $M_h^2 \rightarrow M_Z^2 \cos^2 2\beta + \Delta \mathcal{M}_{22}^2$, is obtained if the following conditions are met (see Ref. [26] for instance): one should be close to the decoupling regime with $M_A \sim \mathcal{O}(\text{TeV})$, have relatively high $\tan \beta$ values, $\tan \beta \gtrsim 5$, such that $\cos^2 2\beta \approx 1$, have very heavy stop squarks, $M_S \gtrsim 1\text{--}3 \text{ TeV}$ to generate the large logarithmic corrections and, eventually, have a stop mixing parameter $X_t \approx \sqrt{6}M_S$ to be in the so-called maximal mixing scenario as to maximize the stop loop contributions [11].

If the parameters are optimized as above, the value of M_h could reach the one measured at the LHC, i.e. $M_h \simeq 125 \text{ GeV}$. However, when this mass value is properly taken into account and only the dominant part of the radiative correction is considered, $\Delta \mathcal{M}_{22}^2$ can be traded against M_h and the MSSM Higgs sector can be, as at tree-level, again described with only two free parameters such as $\tan \beta$ and M_A [13, 14, 27]. Indeed, one can write

$$\Delta \mathcal{M}_{22}^2 = \frac{M_h^2(M_A^2 + M_Z^2 - M_h^2) - M_A^2 M_Z^2 \cos^2(2\beta)}{M_Z^2 \cos^2 \beta + M_A^2 \sin^2 \beta - M_h^2}, \quad (2.5)$$

and obtain the H boson mass and the mixing angle α , which will be simply given by

$$M_H^2 = \frac{(M_A^2 + M_Z^2 - M_h^2)(M_Z^2 \cos^2 \beta + M_A^2 \sin^2 \beta) - M_A^2 M_Z^2 \cos^2 2\beta}{M_Z^2 \cos^2 \beta + M_A^2 \sin^2 \beta - M_h^2}, \quad (2.6)$$

$$\alpha = -\arctan \left(\frac{(M_Z^2 + M_A^2) \cos \beta \sin \beta}{M_Z^2 \cos^2 \beta + M_A^2 \sin^2 \beta - M_h^2} \right), \quad (2.7)$$

while the mass of the charged Higgs state, which is not significantly affected by radiative corrections, can be still expressed by the tree-level relation, namely [28]

$$M_{H^\pm} \simeq \sqrt{M_A^2 + M_W^2}. \quad (2.8)$$

This approach, which was dubbed hMSSM in Ref. [13, 14], has been shown to provide a very good approximation of the MSSM Higgs sector when sfermions and in particular stop squarks, are rather heavy; see also the related analyses of Refs. [12, 15].

In fact, the system defined in eqs. (2.4,2.5) is more constrained in the decoupling regime. Indeed, one would have in this limit

$$\Delta \mathcal{M}_{22}^2 \simeq (M_h^2 - M_Z^2 \cos^2 2\beta) / \sin^2 \beta, \quad (2.9)$$

which means that, for a given $\tan \beta$ value and in a given scenario for stop mixing, such as the no stop mixing $X_t = 0$ or maximal mixing $X_t/M_S = \sqrt{6}$ scenarios, the lightest

Higgs mass is related to $\log(M_S/\bar{m}_t)$. In particular, to achieve the h mass measured value $M_h \simeq 125$ GeV, a very high SUSY scale, $M_S \approx 500$ TeV, is required in the optimistic case of maximal mixing to comply with low $\tan\beta$ values, $\tan\beta \approx 1$ [14]. This SUSY scale reduces to $M_S \approx 1$ TeV for $\tan\beta \gtrsim 10$. In the no-mixing case, the resulting scale M_S in this approximation should be raised by several orders of magnitude to allow for values $\tan\beta \approx 1$ and raised by a factor of three, $M_S \approx 3$ TeV, to allow for $\tan\beta \gtrsim 10$.

In our study here, we consider the usual hMSSM for the Higgs sector with only two inputs $\tan\beta$ and M_A and assume the sfermions to be too heavy to have a phenomenological impact on it, i.e. they will be integrated out and decoupled from the low energy spectrum. To cope with the severe LHC bounds [19], the gluino mass parameter is also assumed to be large, $m_{\tilde{g}} \approx M_3 \gtrsim 3$ TeV. In turn, the gaugino parameters M_1, M_2 and the higgsino one μ that enter the electroweak sector will be assumed to be in the few 100 GeV range, leading to charginos and neutralinos that could be accessible at the LHC and, hence, impact the Higgs sector. We would thus need five basic input parameters in our set-up. We will nevertheless assume some relation between the wino and bino mass parameters to reduce the number of inputs. Besides the GUT relation $M_1 \simeq \frac{1}{2}M_2$, we will mainly study the possibilities of wino and bino masses such that $M_2 = M_1$, $M_2 = 10M_1$ and $M_2 = \frac{1}{10}M_1$ that lead to interesting phenomenological implications.

2.2 Light Neutralinos and Charginos in the hMSSM

Let us now briefly introduce and discuss the gaugino and higgsino sectors of the theory and summarize their interplay, when they involve a relatively light spectrum, with the MSSM Higgs sector. The bino, the three winos and the four higgsinos mix to generate the physical states, namely the four chargino $\chi_{1,2}^\pm$ and the four neutralino χ_{1-4}^0 Majorana particles. The lightest of the neutralino χ_1^0 is in general (and definitely in our case) the lightest SUSY particle or LSP which is assumed to be stable and constitutes the dark matter candidate. The inputs in this sector are taken to be μ, M_1, M_2 together with $\tan\beta$. While the real parameter μ takes both signs, M_2 and M_1 will be assumed to be real and positive.

The chargino mass matrix, in terms of the input parameters above, simply reads [4]

$$\mathcal{M}_C = \begin{bmatrix} M_2 & \sqrt{2}M_W \sin\beta \\ \sqrt{2}M_W \cos\beta & \mu \end{bmatrix}. \quad (2.10)$$

The two chargino (and their CP-conjugate) eigenstates χ_1^\pm and χ_2^\pm as well as their masses are determined via a unitary transformation $U^* \mathcal{M}_C V^{-1} = \text{diag}(m_{\chi_1^\pm}, m_{\chi_2^\pm})$ with U, V being unitary matrices. In the interesting limit $|\mu| \gg M_2$, the lightest (heaviest) charginos correspond to pure winos (higgsinos) with masses $m_{\chi_1^\pm} \simeq M_2$ ($m_{\chi_2^\pm} = |\mu|$). In the opposite $M_2 \gg |\mu|$ limit, the roles of the states χ_1^\pm and χ_2^\pm are simply reversed.

In the case of the neutralinos, the four-dimensional mass matrix depends on the same three parameters above, namely μ, M_2 and $\tan\beta$, and in addition, on the bino mass M_1 .

In the basis $(-i\tilde{B}, -i\tilde{W}_3, \tilde{H}_1^0, \tilde{H}_2^0)$, with the mixing angles β and θ_W , it has the form [4]

$$\mathcal{M}_N = \begin{bmatrix} M_1 & 0 & -M_Z \sin \theta_W \cos \beta & M_Z \sin \theta_W \sin \beta \\ 0 & M_2 & M_Z \cos \theta_W \cos \beta & -M_Z \cos \theta_W \sin \beta \\ -M_Z \sin \theta_W \cos \beta & M_Z \cos \theta_W \cos \beta & 0 & -\mu \\ M_Z \sin \theta_W \sin \beta & -M_Z \sin \theta_W \sin \beta & -\mu & 0 \end{bmatrix}. \quad (2.11)$$

The neutralino eigenstates $\chi_{1,2,3,4}^0$ and their masses are determined with the help of a transformation $Z^T \mathcal{M}_N Z^{-1} = \text{diag}(m_{\chi_1^0}, m_{\chi_2^0}, m_{\chi_3^0}, m_{\chi_4^0})$ where, again Z is a unitary matrix. In this case also, for $|\mu| \gg M_2 > M_1$, two neutralinos will be pure gauginos with masses $m_{\chi_1^0} \simeq M_1$ and $m_{\chi_2^0} \simeq M_2$, while the two others will be pure higgsinos with masses $m_{\chi_3^0} \simeq m_{\chi_4^0} \simeq |\mu|$. In the opposite limit, the roles are again reversed and $m_{\chi_1^0} \simeq m_{\chi_2^0} \simeq |\mu|$, $m_{\chi_3^0} \simeq M_1$ and $m_{\chi_4^0} \simeq M_2$. When $M_2 < M_1$ the role of the two gauginos is reversed.

The couplings of the neutralinos and charginos to the MSSM Higgs bosons, as well as the couplings to the massive gauge bosons, are given in terms of the matrices U, V and Z and we briefly summarize them below. Denoting the Higgs bosons by H_k with $k = 1, 2, 3$, corresponding respectively to H, h, A , and $H_4 = H^\pm$ and normalizing to the electric charge e , the Higgs couplings to chargino and neutralino pairs can conveniently be written as [24]:

$$\begin{aligned} g_{\chi_i^- \chi_j^+ H_k}^{L,R} &= g_{ijk}^{L,R} \quad \text{with} \quad \begin{cases} g_{ijk}^L = \frac{1}{\sqrt{2} \sin \theta_W} [e_k V_{j1} U_{i2} - d_k V_{j2} U_{i1}] \\ g_{ijk}^R = \frac{1}{\sqrt{2} \sin \theta_W} [e_k V_{i1} U_{j2} - d_k V_{i2} U_{j1}] \epsilon_k \end{cases}, \quad (2.12) \\ g_{\chi_i^0 \chi_j^0 H_k}^{L,R} &= g_{ijk}^{L,R} \quad \text{with} \quad \begin{cases} g_{ijk}^L = \frac{1}{2 \sin \theta_W} (Z_{j2} - \tan \theta_W Z_{j1}) (e_k Z_{i3} + d_k Z_{i4}) + i \leftrightarrow j \\ g_{ijk}^R = \frac{1}{2 \sin \theta_W} (Z_{j2} - \tan \theta_W Z_{j1}) (e_k Z_{i3} + d_k Z_{i4}) \epsilon_k + i \leftrightarrow j \end{cases}, \\ g_{\chi_i^0 \chi_j^+ H_4}^{L,R} &= g_{ij4}^{L,R} \quad \text{with} \quad \begin{cases} g_{ij4}^L = \frac{\cos \beta}{\sin \theta_W} [Z_{j4} V_{i1} + \frac{1}{\sqrt{2}} (Z_{j2} + \tan \theta_W Z_{j1}) V_{i2}] \\ g_{ij4}^R = \frac{\sin \beta}{\sin \theta_W} [Z_{j3} U_{i1} - \frac{1}{\sqrt{2}} (Z_{j2} + \tan \theta_W Z_{j1}) U_{i2}] \end{cases}, \end{aligned}$$

with the convention $\epsilon_{1,2} = -\epsilon_3 = 1$. The coefficients e_k and d_k for a given H_k state, together with their limiting values in the decoupling regime $M_A \gg M_Z$, are

$$e_1 = +\cos \alpha \rightarrow \sin \beta, \quad e_2 = -\sin \alpha \rightarrow \cos \beta, \quad e_3 = -\sin \beta, \quad (2.13a)$$

$$d_1 = -\sin \alpha \rightarrow \cos \beta, \quad d_2 = -\cos \alpha \rightarrow \sin \beta, \quad d_3 = +\cos \beta. \quad (2.13b)$$

Note that the Higgs couplings to pairs of the dark matter states χ_1^0 , recalling that $Z_{11}, Z_{12} (Z_{13}, Z_{14})$ are the gaugino (higgsino) components of the Z matrix, vanish if the LSP neutralino is a pure gaugino or higgsino. This feature can be in fact generalized to all the couplings of MSSM Higgs bosons to the various neutralinos and charginos: the Higgs bosons couple only to higgsino-gaugino mixtures or states and do not couple to pure gauginos or pure higgsinos. This makes that Higgs couplings to mixed heavy and light chargino/neutralino states are maximal in the pure gaugino or higgsino regions, while the couplings involving only heavy or light gaugino or higgsino states are suppressed by powers of $M_i/|\mu|$ ($|\mu|/M_i$) for $|\mu| \gg M_i$ ($|\mu| \ll M_i$). Note that some of the Higgs couplings

to neutralinos can also accidentally vanish outside the decoupling limit for certain values of $\tan\beta$ and M_A which enter in the coefficients d_k and e_k given previously.

Finally, we will need the couplings of the charginos and neutralinos to the massive gauge bosons. Using the same ingredients as above, they are given by [24]

$$\begin{aligned} g_{\chi_i^0 \chi_j^+ W}^L &= \frac{c_W}{\sqrt{2}s_W} [-Z_{i4}V_{j2} + \sqrt{2}Z_{i2}V_{j1}], & g_{\chi_i^0 \chi_j^+ W}^R &= \frac{c_W}{\sqrt{2}s_W} [Z_{i3}U_{j2} + \sqrt{2}Z_{i2}U_{j1}], \\ g_{\chi_i^0 \chi_j^0 Z}^L &= -\frac{1}{2s_W} [Z_{i3}Z_{j3} - Z_{i4}Z_{j4}], & g_{\chi_i^0 \chi_j^0 Z}^R &= +\frac{1}{2s_W} [Z_{i3}Z_{j3} - Z_{i4}Z_{j4}], \\ g_{\chi_i^- \chi_j^+ Z}^L &= \frac{1}{c_W} \left[\delta_{ij}s_W^2 - \frac{1}{2}V_{i2}V_{j2} - V_{i1}V_{j1} \right], & g_{\chi_i^- \chi_j^+ Z}^R &= \frac{1}{c_W} \left[\delta_{ij}s_W^2 - \frac{1}{2}U_{i2}U_{j2} - U_{i1}U_{j1} \right]. \end{aligned} \quad (2.14)$$

In contrast to the couplings of the Higgs bosons, the gauge boson couplings to charginos and neutralinos are important only for higgsino- or gaugino-like states.

The gaugino and higgsino states enter the radiative corrections to the MSSM Higgs sector and, in particular, contribute to the CP-even Higgs mass matrix elements \mathcal{M}_{ij} . However, contrary to squarks which mainly contribute to the entry $\Delta\mathcal{M}_{22}$ as discussed above, these will equally contribute to all entries so that one cannot use the approximation $\Delta\mathcal{M}_{22} \gg \Delta\mathcal{M}_{11}, \Delta\mathcal{M}_{12}$ which defines the hMSSM, eqs. (2.4,2.5). This is in fact also the case of the subleading contributions of the electroweak W and Z bosons to the Higgs boson self-energies and which are too small and will not be considered here.

A basic ingredient of our analysis is that, in contrast to the fermion-sfermion contributions (especially the dominant top-stop one), the full one-loop contributions of the gauginos, higgsinos to the Higgs boson self-energies, given e.g. in Refs. [29, 31] for instance, will be kept exactly. While the contribution to the entry $\Delta\mathcal{M}_{22}$ can be added to that of eq. (2.5) to define the hMSSM, the contributions to $\Delta\mathcal{M}_{11}, \Delta\mathcal{M}_{12}$ will act as small perturbations which will modify the hMSSM relations. In particular, these will give extra contributions to the mass M_h and, hence, modify its input value in the hMSSM, $M_h = 125$ GeV. Nevertheless, if these additional corrections are at the level of a few percent at most, they could be acceptable since, as is well known, there is an intrinsic uncertainty in the determination of M_h in the MSSM which is a result of experimental errors (mainly from the values of the top quark mass m_t and the strong coupling constant α_s measurements) and theoretical uncertainties (e.g. from missing higher order effects). This uncertainty has been estimated to be of the order of $\Delta M_h \simeq \pm 3$ GeV [10].

The additional corrections will also modify the values of the parameters α and M_H obtained through eq. (2.7), a modification which is expected to be rather modest too.

2.3 Implementation in the Program SuSpect

In this section, we provide some details on how we implement the chargino and neutralino radiative corrections to the MSSM Higgs boson masses and couplings, as a slight modification of the basic/original hMSSM scenario defined in eq. (2.5). One should note that this relation, being expressed in terms of physical masses, represents in that sense an “all-order” determination for this specific matrix element (at least for those largely dominant contributions from the top-stop sector at large M_S values). Hence, to avoid

double-counting, the known one-loop or higher-loop contributions of this specific sector should be carefully subtracted out, once using eq. (2.5). In particular, one should remove any genuine two-loop corrections in this approximation, which is not included in the renormalisation group improvement of the correction in eq. (2.4), that is expected to provide the dominant contributions in the related approximation where all sfermions are very heavy, $M_S \gg 1$ TeV. Thus, the latter are explicitly decoupled from the contributions to the three matrix elements ΔM_{ij} .

Nevertheless, although eq. (2.5) does not depend on M_S explicitly, in such an hMSSM prescription and as was already mentioned, one should take M_S values such that eq. (2.5) and eq. (2.4) are at least approximately consistent. This implicitly sets the sfermion scale M_S to depend on $\tan \beta$ choices. Typically, in the illustrations that we will give below, we will take $M_S \sim 10$ TeV for $\tan \beta = 10$, while $M_S \sim 100$ TeV e.g. for $\tan \beta \sim 3$.

Next, apart from the corrections that are due to charginos and neutralinos, other radiative contributions from gauge plus heavy Higgs bosons, which are very moderate, will be neglected here. We thus incorporate within the CP-even Higgs mass matrix, on top of eq. (2.5), the contributions of neutralinos and charginos in the matrix elements ΔM_{ij}^2 with exact one-loop expressions, as given e.g. in Ref. [29], and we recalculate consistently from this corrected mass matrix, the CP-even Higgs boson pole masses.

More precisely, we consider the mass eigenvalues as obtained from the corrected CP-even Higgs squared mass matrix:

$$\mathcal{M}^2(p^2) = \begin{bmatrix} M_Z^2 c_\beta^2 + \overline{M}_A^2 s_\beta^2 + \Delta M_{11}^2|_\chi(p^2) & -(M_Z^2 + \overline{M}_A^2) s_\beta c_\beta + \Delta M_{12}^2|_\chi(p^2) \\ -(M_Z^2 + \overline{M}_A^2) s_\beta c_\beta + \Delta M_{21}^2|_\chi(p^2) & M_Z^2 s_\beta^2 + \overline{M}_A^2 c_\beta^2 + \Delta M_{22}^2|_\chi(p^2) + \Delta M_{22}^2 \end{bmatrix} \quad (2.15)$$

where we have used the abbreviations $s_\beta = \sin \beta$ and $c_\beta = \cos \beta$; \overline{M}_A is the running A mass defined at momentum squared transfer p^2 . Here, ΔM_{22}^2 is given by eq. (2.5), while the neutralino and chargino contributions entering the matrix elements $\Delta M_{ij}^2|_\chi$ are

$$\Delta M_{ij}^2|_\chi(p^2) = -\Pi_{s_i s_i}^\chi + t_i/v_i \quad (i = 1, 2), \quad \Delta M_{12}^2|_\chi(p^2) = \Delta M_{21}^2|_\chi(p^2) = -\Pi_{s_1 s_2}^\chi, \quad (2.16)$$

where, explicitly and at momentum squared p^2 , one has

$$\begin{aligned} (4\pi)^2 \Pi_{s_k s_l}^\chi(p^2) &= \frac{1}{2} \sum_{i,j=1}^4 \left[f_{ijs_{kl}}^0 G(p^2, m_{\chi_i^0}, m_{\chi_j^0}) - 2g_{ijs_{kl}}^0 m_{\chi_i^0} m_{\chi_j^0} B_0(p^2, m_{\chi_i^0}, m_{\chi_j^0}) \right] \\ &+ \sum_{i,j=1}^2 \left[f_{ijs_{kl}}^+ G(p^2, m_{\chi_i^+}, m_{\chi_j^+}) - 2g_{ijs_{kl}}^+ m_{\chi_i^+} m_{\chi_j^+} B_0(p^2, m_{\chi_i^+}, m_{\chi_j^+}) \right] \end{aligned} \quad (2.17)$$

for the Higgs two-point functions or self-energies, and for the tadpoles t_i/v_i

$$(4\pi)^2 \frac{t_1}{v_1} = \frac{-g_2^2}{M_W c_\beta} \left[\sum_{i=1}^4 Z_{i3} (Z_{i2} - \tan \theta_W Z_{i1}) m_{\chi_i^0} A_0(m_{\chi_i^0}) + \sqrt{2} \sum_{i=1}^2 V_{i1} U_{i2} m_{\chi_i^+} A_0(m_{\chi_i^+}) \right] \quad (2.18)$$

and a similar expression for t_2/v_2 with the following replacements $Z_{i3} \rightarrow Z_{i4}$ and $V_{i1} \rightarrow V_{i2}$. g_2 is the SU(2) coupling constant and we have used the function

$$G(p^2, m_1, m_2) = (p^2 - m_1^2 - m_2^2) B_0(p^2, m_1, m_2) - A_0(m_1) - A_0(m_2), \quad (2.19)$$

where B_0 and A_0 are the standard Passarino-Veltman [30] two- and one-point loop functions, respectively. In eq. (2.17), the relevant couplings in the s_1, s_2 basis are defined as

$$\begin{aligned} f_{ijs_{kl}} &= g_{\chi_i \chi_j s_k}^L g_{\chi_i \chi_j s_l}^L + g_{\chi_i \chi_j s_k}^R g_{\chi_i \chi_j s_l}^R, \\ g_{ijs_{kl}} &= g_{\chi_i \chi_j s_k}^L g_{\chi_i \chi_j s_l}^R + g_{\chi_i \chi_j s_k}^R g_{\chi_i \chi_j s_l}^L, \end{aligned} \quad (2.20)$$

where in terms of the physical Higgs boson couplings of eq. (2.13), one has

$$\begin{aligned} g_{\chi_i \chi_j s_1}^{L,R} &= \cos \alpha g_{\chi_i \chi_j H_1}^{L,R} - \sin \alpha g_{\chi_i \chi_j H_2}^{L,R}, \\ g_{\chi_i \chi_j s_2}^{L,R} &= \sin \alpha g_{\chi_i \chi_j H_1}^{L,R} + \cos \alpha g_{\chi_i \chi_j H_2}^{L,R}. \end{aligned} \quad (2.21)$$

Similarly, the chargino and neutralino contributions to the Π_{AA} self-energy read

$$\begin{aligned} (4\pi)^2 \Pi_{AA}^X(p^2) &= \frac{1}{2} \sum_{i,j=1}^4 \left[f_{ijA}^0 G(p^2, m_{\chi_i^0}, m_{\chi_j^0}) - 2g_{ijA}^0 m_{\chi_i^0} m_{\chi_j^0} B_0(p^2, m_{\chi_i^0}, m_{\chi_j^0}) \right] \\ &+ \sum_{i,j=1}^2 \left[f_{ijA}^+ G(p^2, m_{\chi_i^+}, m_{\chi_j^+}) - 2g_{ijA}^+ m_{\chi_i^+} m_{\chi_j^+} B_0(p^2, m_{\chi_i^+}, m_{\chi_j^+}) \right] \end{aligned} \quad (2.22)$$

with couplings f_{ijA}^0, g_{ijA}^0 and f_{ijA}^+, g_{ijA}^+ defined similarly as in eq. (2.20). Eq. (2.22) enters the running pseudoscalar A mass defined, in the $\overline{\text{DR}}$ renormalization scheme, in terms of the pole mass M_A (at one-loop order) as

$$\overline{M}_A^2 = M_A^2 + \Pi_{AA}^X(p^2) - \sin^2 \beta t_1/v_1 - \cos^2 \beta t_2/v_2 + \mathcal{O}(\text{higher orders}). \quad (2.23)$$

Note that within the minimal hMSSM setup, namely with only eq. (2.5) included, it is understood that the pole mass M_A is used. In contrast, once accounting for additional chargino and neutralino radiative corrections within eq. (2.15), it is crucial to consistently use the running mass \overline{M}_A in the latter, that involves large cancellations between different one-loop contributions, in particular among the tadpole t_i/v_i and the Π_{AA}^X contributions within eq. (2.23). Indeed, for large $\tan \beta$ and not too large μ values, the chargino and neutralino contributions to eq. (2.23) become rather large, such that \overline{M}_A can be substantially different from M_A . Therefore, while we still take the pole mass M_A as the basic hMSSM input, eq. (2.5) is modified with the replacement $M_A \rightarrow \overline{M}_A$, using eq. (2.23).

This is a rather moderate extension of the basic hMSSM setup in order to guarantee the consistency of eq. (2.15) from which the CP-even Higgs masses are recalculated. Note, however, that interestingly the actual value of M_A used within eq. (2.5) is rather irrelevant: a remarkable feature is that eq. (2.5) depends very little on the value of M_A . Indeed, for large $\tan \beta$ and M_A values, one has

$$\Delta M_{22}^2 \simeq M_h^2 - M_Z^2 + \frac{1}{\tan^2 \beta} \left(M_h^2 + 3M_Z^2 + M_Z^2 \times \mathcal{O}\left(\frac{M_h^2}{M_A^2}, \frac{M_Z^2}{M_A^2}\right) \right) + \mathcal{O}\left(\frac{1}{\tan^3 \beta}\right), \quad (2.24)$$

which remains a very good approximation, only departing by a few percent at most from eq. (2.5), even for moderate $\tan \beta \gtrsim 5$ and $M_A \gtrsim 2M_h$ values.

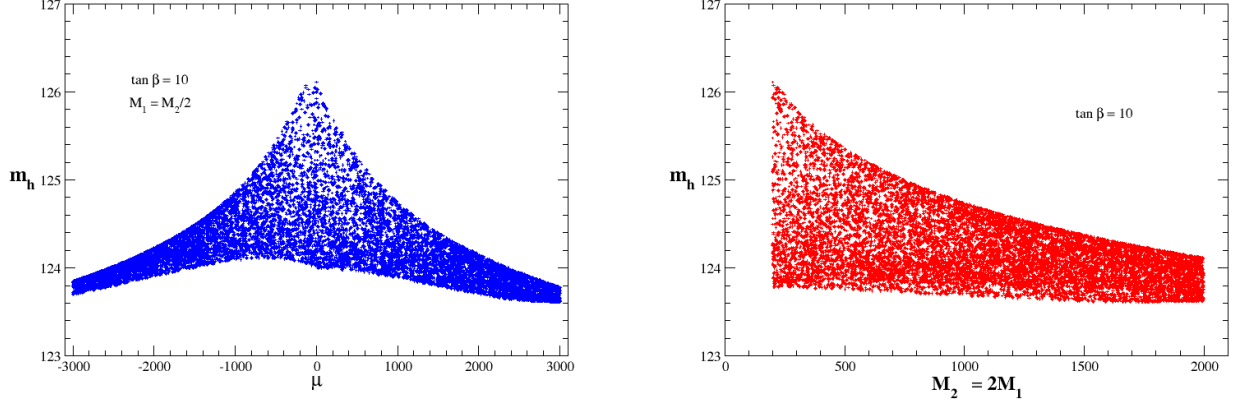


Figure 1: The recalculated lightest CP-even Higgs boson mass M_h in the hMSSM setup, with chargino and neutralino radiative corrections added for $\tan \beta = 10$ and $M_2 = 2M_1$ as a function of μ (left) and $M_2 = 2M_1$ (right).

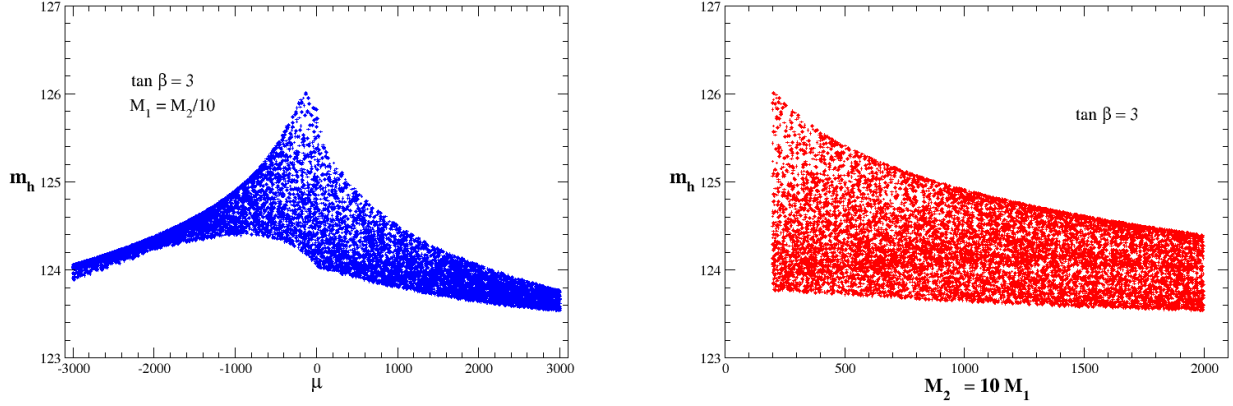


Figure 2: The same as in Fig. 1 for $\tan \beta = 3$ and $M_2 = 10M_1$.

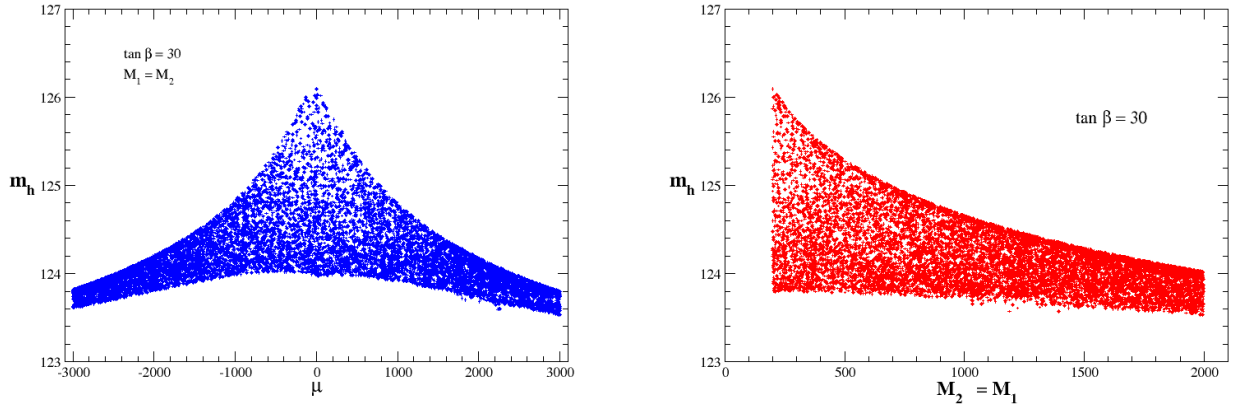


Figure 3: Same captions as in Fig.1 for $\tan \beta = 30$ and $M_2 = M_1$.

For the parameter choice and constraints discussed above, we then perform several scans over the relevant parameters μ, M_2 , for representative choices of $\tan \beta \simeq 3, 10, 30$, to illustrate the impact of the chargino-neutralino corrections. (Note that $M_S = 10$ TeV for $\tan \beta = 10$ and $10^2 - 10^4$ TeV for very low $\tan \beta \leq 3$). The gluino mass is chosen to be $M_{\tilde{g}} \sim 3$ TeV and M_A is fixed to 1 TeV, like the electroweak symmetry breaking scale. The resulting recalculated M_h values are illustrated in the subsequent figures.

As it can be seen, the chargino plus neutralino contributions to the lightest Higgs mass remain rather moderate for most of the parameter space, well below the present theoretical uncertainty on M_h , namely $\Delta M_h \simeq 3$ GeV. The deviations reach a positive maximum of $\approx +1$ GeV for, not too surprisingly, very low $|\mu|$ and M_2 values (close to the 100 GeV limit which is excluded by LEP2 data/searches as will be seen later), and a negative minimum ≈ -1.5 GeV for large $|\mu|$ and M_2 values. The latter is explained by non-decoupling logarithmic dependencies $\propto \log(m_{\chi_i^+}/M_h), \log(m_{\chi_i^0}/M_h)$ that remain moderate as long as the gaugino spectrum is not too heavy. These deviations are not very sensitive to the M_2/M_1 ratio nor to the different values of $\tan \beta$.

We should stress again that the three different $\Delta M_{ij}^2|_{\chi}$ contributions to the CP-even mass matrix can be separately rather large, but large cancellations occur among those within the light Higgs boson mass recalculated from eq. (2.15).

Finally, we also illustrate in Fig. 4 the relative difference, with respect to eq. (2.7), of the recalculated CP-even Higgs mixing angle α , with chargino and neutralino radiative corrections added. Again, the effects remain moderate, reaching a maximum slightly above $\Delta\alpha = 0.03$, and decreasing both for increasing $\tan \beta$ or M_S values.

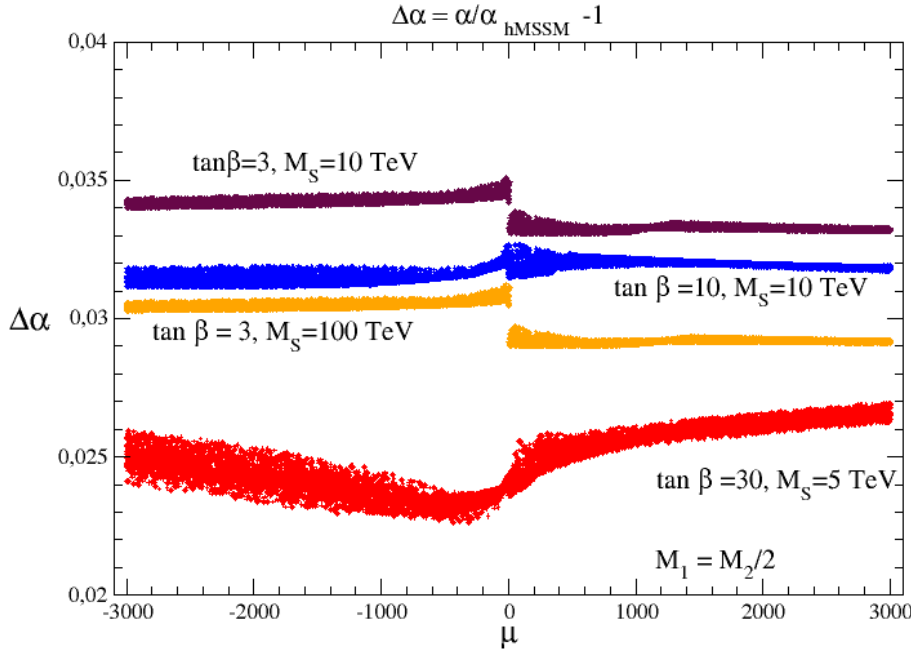


Figure 4: The relative difference of the recalculated CP-even Higgs mixing angle α with chargino and neutralino radiative corrections included with respect to the simple hMSSM value, as a function of the parameter μ for fixed choices $\tan \beta = 3, 30$ and $M_2 = 2M_1$.

The difference between the recalculated heavy CP-even Higgs mass M_H and the one given in eq. (2.7) is even smaller, being at most at the permille level for our considered range of $\tan\beta, \mu, M_2$ values as it is illustrated in Fig. 5. The relatively more pronounced sensitivities seen in Fig. 5 around $|\mu| \sim 500$ GeV correspond to artificial threshold effects, from chargino or neutralino contributions to the H boson self-energies, i.e. when $M_H \sim 1 \text{ TeV} \simeq 2m_{\chi_i^\pm}$ and/or $M_H \simeq 2m_{\chi_i^0}$.

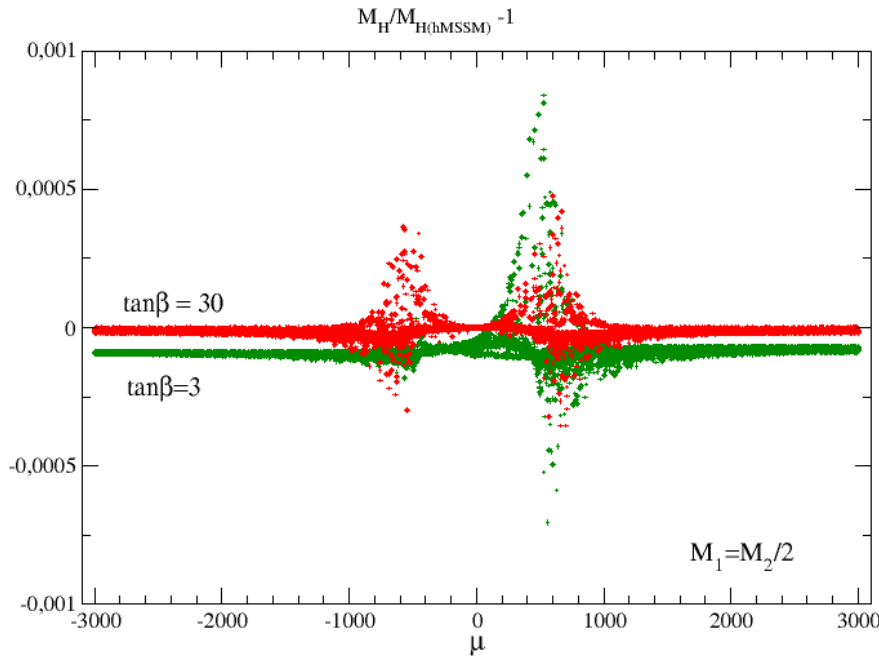


Figure 5: The relative difference of the recalculated CP-even heavy Higgs boson mass M_H with chargino and neutralino radiative corrections included with respect to the simple hMSSM value, as a function of μ for fixed choices of $\tan\beta = 3, 30$ and $M_2 = 2M_1$.

2.4 Direct Corrections to the Higgs-Fermion Couplings

Another type of radiative corrections which is important in the context of the MSSM Higgs sector, is the so-called direct corrections which appear in Higgs decays into third generation fermion pairs. Analogous corrections for Higgs decays into muon and strange quark decays also occur, but they do not play an important role in general and will be ignored here. In the case of Higgs decays into quarks, one encounters large QCD corrections, while the electroweak corrections are in general rather small [32]. The dominant part of these QCD corrections can be absorbed in the running fermion Yukawa couplings when defined in the $\overline{\text{MS}}$ scheme and evaluated at the scale of the corresponding Higgs boson mass [33]. But there also pure SUSY-QCD corrections mediated by gluino-squark exchange [29, 34] and SUSY-electroweak corrections that involve squark and chargino/neutralino exchange that cannot be absorbed in the running quark masses and should be therefore considered separately [32, 34].

These SUSY direct corrections for third generation quarks and leptons, called Δ_f ($f = t, b, \tau$) corrections, modify the effective top, bottom and τ Yukawa couplings \tilde{g}_f^ϕ ($\phi = h, H, A$) of the neutral CP-even h, H and the CP-odd A states, in the following way [34]

$$\tilde{g}_f^h = \frac{g_f^h}{1+\Delta_f} \left[1 - \frac{\Delta_f}{\tan \alpha \tan \beta} \right], \tilde{g}_f^H = \frac{g_f^H}{1+\Delta_f} \left[1 + \Delta_f \frac{\tan \alpha}{\tan \beta} \right], \tilde{g}_f^A = \frac{g_f^A}{1+\Delta_f} \left[1 - \frac{\Delta_f}{\tan^2 \beta} \right] \quad (2.25)$$

with the Yukawa couplings g_f^ϕ for isospin up- and down-type fermions given in eq. (2.3).

Considering first the Higgs couplings to bottom quarks, the Δ_b correction at one-loop order is given by $\Delta_b = \Delta_b^{\text{QCD}} + \Delta_b^{\text{EW}}$ with the individual contributions reading [34]

$$\begin{aligned} \Delta_b^{\text{QCD}} &= \frac{2}{3} \frac{\alpha_s}{\pi} m_{\tilde{g}} \mu \tan \beta I(m_{\tilde{b}_1}^2, m_{\tilde{b}_2}^2, m_{\tilde{g}}^2), \\ \Delta_b^{\text{EW}} &= \frac{\lambda_t^2}{(4\pi)^2} A_t \mu \tan \beta I(m_{\tilde{t}_1}^2, m_{\tilde{t}_2}^2, \mu^2) - \frac{1}{12\pi} \mu \tan \beta \left\{ \right. \\ &\quad \alpha_1 M_1 \left[\frac{1}{3} I(m_{\tilde{b}_1}^2, m_{\tilde{b}_2}^2, M_1^2) + \left(\frac{c_b^2}{2} + s_b^2 \right) I(m_{\tilde{b}_1}^2, M_1^2, \mu^2) + \left(\frac{s_b^2}{2} + c_b^2 \right) I(m_{\tilde{b}_2}^2, M_1^2, \mu^2) \right], \\ &\quad \left. + 3 \alpha_2 M_2 \left[c_t^2 I(m_{\tilde{t}_1}^2, M_2^2, \mu^2) + s_t^2 I(m_{\tilde{t}_2}^2, M_2^2, \mu^2) + \frac{c_b^2}{2} I(m_{\tilde{b}_1}^2, M_2^2, \mu^2) + \frac{s_b^2}{2} I(m_{\tilde{b}_2}^2, M_2^2, \mu^2) \right] \right\}, \end{aligned} \quad (2.26)$$

where α_s denotes the strong coupling constant, $\lambda_t = \sqrt{2}m_t/(v \sin \beta)$ the top quark Yukawa coupling, $\alpha_{1,2} = g_{1,2}^2/4\pi$ the U(1), SU(2) gauge couplings. $s_b/c_b = \sin / \cos \theta_b$ are the sine and cosine of the sbottom mixing angle θ_b , while the function I is given by

$$I(a, b, c) = \frac{ab \log(a/b) + bc \log(b/c) + ca \log(c/a)}{(a-b)(b-c)(a-c)}. \quad (2.27)$$

At high values of the parameters $\tan \beta$ and μ and for not too large gluino and squark masses (the corrections are damped by terms $\max(\tilde{m}_q^2, \tilde{m}_{\tilde{g}}^2)$ from the denominator), the full SUSY-QCD corrections can reach the level of a factor of two in extreme cases, while the SUSY-electroweak corrections are much smaller and can reach at most 10% only.

In the case of the Higgs coupling to tau leptons, there is no contribution from strong interaction and the corresponding Δ_τ term receives only contributions from the electroweak gauge couplings $\alpha_{1,2}$. The SUSY direct corrections are small in this case, again at the 10% level at most and in general much less.

Similarly to what occurs in the case of the Higgs couplings to b -quarks, direct corrections also affect the Higgs couplings to top quarks but, contrary to the case above, they are suppressed by $\tan \beta$ factors and could only be important at low $\tan \beta$ values, $\tan \beta \approx 1$. The corresponding $\Delta_t = \Delta_t^{\text{QCD}} + \Delta_t^{\text{EW}}$ SUSY-corrections is dominantly given by

$$\Delta_t = \mu \cot \beta \left[\frac{2\alpha_s}{3\pi} m_{\tilde{g}} I(m_{\tilde{t}_1}^2, m_{\tilde{t}_2}^2, m_{\tilde{g}}^2) + \frac{\lambda_b^2}{(4\pi)^2} A_b I(m_{\tilde{b}_1}^2, m_{\tilde{b}_2}^2, \mu^2) \right], \quad (2.28)$$

Hence, only the first term, i.e. the SUSY-QCD correction, gives rise to large contributions because $\lambda_b = \sqrt{2}m_b/(v \cos \beta)$ is expected to be tiny for small $\tan \beta$ values.

The supersymmetric-QCD corrections involving the gluino gives large radiative corrections only to the heavy A, H and H^\pm coupling to heavy quarks. The corresponding

corrections in the context of the SM-like h boson decouple and are thus extremely small in general as will be seen later (see also the recent analysis performed in Ref. [35]). The Δ_b corrections are also potentially enhanced for large $\tan\beta$ values due to top-charginos contributions. In Fig. 6, we illustrate the deviations in the coupling $g_{Ab\bar{b}}$ and $g_{Hb\bar{b}}$ which are similar in the decoupling regime, for two representative $\tan\beta$ values and from a scan over the μ , M_2 parameters, and see where deviations are expected to be enhanced. Very low values, $\tan\beta \simeq 3$, give tiny deviations that are not illustrated.

Note that the gluino mass is taken to be $m_{\tilde{g}} = 3$ TeV which is above the present limit from the negative LHC searches, such as to maximize deviations since, as can be seen from eq. (2.26), Δ_b^{QCD} increases with $m_{\tilde{g}}$ as long as $m_{\tilde{g}} \lesssim m_{\tilde{b}_{1,2}}$. Note also that in our numerical analysis, we rather use exact (one-loop) expressions for the particularly sensitive QCD corrections Δ_b^{QCD} , that differ from the large $\tan\beta$, $\mu \gg M_2$ approximations in eq. (2.26), the latter being thus not valid for small $\tan\beta$, μ also considered in our analysis. Indeed, the exact expressions tend to increase those corrections, by up to 30 – 40% for $\tan\beta \simeq 3$ for which Δ_b is however very small, $\sim 10^{-3}$.

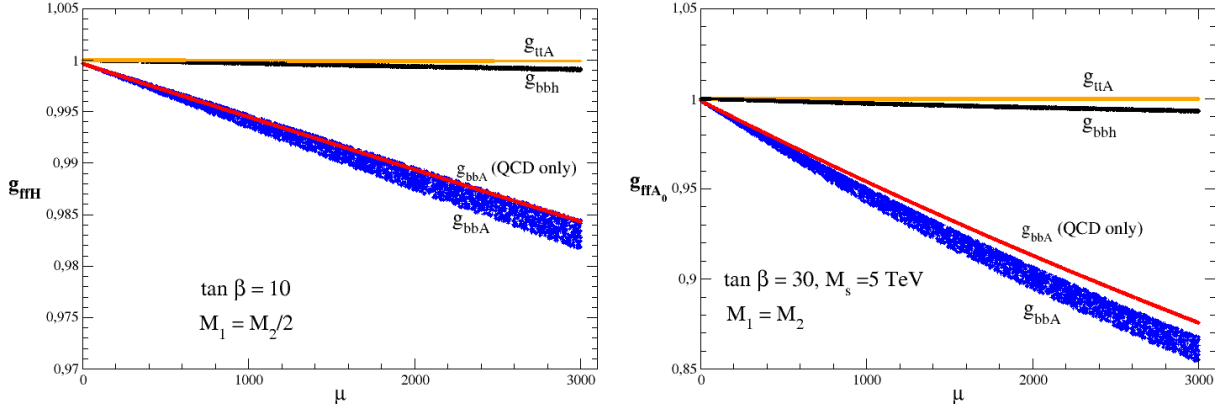


Figure 6: The direct corrections to the coupling $g_{Ab\bar{b}}$ as a function of μ for $\tan\beta = 10$ and $M_2 = 2M_1$ (left) and $\tan\beta = 30$ and $M_2 = M_1$ (right). In red, only the SUSY-QCD correction is displayed for $m_{\tilde{g}} = 3$ TeV, while in blue, the additional contributions of the electroweak corrections are shown. We also display the very small corrections to the g_{ttA} (in orange) and g_{bbh} (in black) couplings.

As can be seen from Fig. 6, deviations in $g_{Ab\bar{b}}$ remain very moderate unless $\tan\beta$ is large enough, so that for instance for $\tan\beta \sim 30$, they can reach the 10% level (respectively 15%) for $|\mu| \sim 2$ TeV (respectively 3 TeV). Note that the dependence is very symmetrical for $\pm\mu$ and, thus, we only illustrate the effects for positive μ values in Fig. 6.

Finally, we also compare in Fig. 6 the other relevant deviations in $g_{hb\bar{b}}$ and $g_{At\bar{t}}$, that both remain extremely moderate, illustrating the decoupling of the corresponding contributions in the first case and the absence of enhancement of the contribution at low $\tan\beta$ values, in the latter case.

3 Constraints on the Gaugino-Higgsino Sector

In this section, we investigate the impact on the hMSSM by a light gaugino and higgsino sector, which is allowed by the present LHC data. In section 3.1, we study the LHC search limits on the charginos and neutralinos. Then, in section 3.2, we analyze the LHC constraints on the Gaugino-Higgsino parameter space. For these analyses, we will use the SuSpect package [25] to generate the supersymmetric particle spectra, and use the packages SDECAY [41] and SUSY-HIT [42] to evaluate the decays of the heavier neutralinos and charginos into the lighter ones plus Higgs and gauge bosons.

3.1 LHC Searches for Charginos and Neutralinos

Several searches for charginos and neutralinos have been performed by the ATLAS and CMS collaborations in various production channels and final state topologies. Following the spirit of our extended hMSSM framework, in which we assume the sfermions and in particular the squarks to be rather heavy and inaccessible at the LHC, we will ignore all channels in which the charginos and neutralinos originate from cascade decays of squarks. In addition, to simplify the discussion, we will assume that gluinos are also heavy and out of the LHC reach so that there are no gluino cascade decays either. Thus, the main channel for the direct production of charginos and neutralinos is the Drell–Yan process:

$$pp \rightarrow q\bar{q} \rightarrow \chi_i^\pm \chi_i^\mp, \chi_i^\pm \chi_j^0, \chi_i^0 \chi_j^0. \quad (3.1)$$

Of particular interest is the final state containing the lightest chargino and the next-to-lightest neutralino,

$$q\bar{q}' \rightarrow W^* \rightarrow \chi_1^\pm \chi_2^0, \quad (3.2)$$

which are produced only through the s -channel W -boson exchange. Another interesting channel should be the pair production of the lightest chargino through photon and Z -boson exchange and the next-to-lightest neutralino via Z -boson exchange only

$$q\bar{q} \rightarrow \gamma^*/Z^* \rightarrow \chi_1^\pm \chi_1^\mp, \quad q\bar{q} \rightarrow Z^* \rightarrow \chi_2^0 \chi_2^0. \quad (3.3)$$

The production cross sections are known up to next-to-leading order (at least) in QCD [36] and can be evaluated using, for instance, the program Prospino [37].

For the first of the processes above, the most interesting decay products in the final state include the trileptons and missing energy from the channels ($\ell = e, \mu$)

$$\chi_2^0 \rightarrow \chi_1^0 Z^{(*)} \rightarrow \chi_2^0 \ell\ell \quad \text{and} \quad \chi_1^\pm \rightarrow \chi_1^0 W^{(*)} \rightarrow \chi_1^0 \ell\nu, \quad (3.4)$$

but we can also look for the possibility of the lightest Higgs boson in the final state,

$$\chi_2^0 \rightarrow \chi_1^0 h. \quad (3.5)$$

In the case of chargino pair production, a powerful search channel is the one leading to two charged leptons and missing energy from the decay mode

$$\chi_2^\pm \rightarrow W^* \chi_1^0 \rightarrow \ell^\pm \nu \chi_1^0. \quad (3.6)$$

If the charginos and neutralinos are very heavy and the phase space is favorable, they could also decay in channels in which the heavier Higgs bosons of the MSSM are present [38, 39, 40]:

$$\chi_i \rightarrow \chi_j H_k, \quad (3.7)$$

where χ_i generically stand for the heavier neutralinos or charginos, χ_j for the lighter ones and H_k to the MSSM Higgs bosons as already defined in section 2.2 with $k = 1, 2, 3$ and 4, corresponding respectively to the H, h, A and H^\pm states.

The partial decay widths of heavier charginos and neutralinos χ_i , decaying into lighter ones χ_j and gauge $V = W, Z$ or Higgs H_k bosons are given by [38, 40]:

$$\Gamma(\chi_i \rightarrow \chi_j V) = \frac{\alpha}{8c_W^2} m_{\chi_i} \lambda^{\frac{1}{2}}(\mu_{\chi_j}, \mu_V) \left\{ -12 \sqrt{\mu_{\chi_j}} g_{\chi_i \chi_j V}^L g_{\chi_i \chi_j V}^R \right. \quad (3.8a)$$

$$\left. + \left[(g_{\chi_i \chi_j V}^L)^2 + (g_{\chi_i \chi_j V}^R)^2 \right] (1 + \mu_{\chi_j} - \mu_V) + (1 - \mu_{\chi_j} + \mu_V)(1 - \mu_{\chi_j} - \mu_V) \mu_V^{-1} \right\},$$

$$\Gamma(\chi_i \rightarrow \chi_j H_k) = \frac{\alpha}{8} m_{\chi_i} \lambda^{\frac{1}{2}}(\mu_{\chi_j}, \mu_{H_k}) \left\{ \left[(g_{\chi_i \chi_j H_k}^L)^2 + (g_{\chi_i \chi_j H_k}^R)^2 \right] (1 + \mu_{\chi_j} - \mu_{H_k}) \right. \quad (3.8b)$$

$$\left. + 4 \sqrt{\mu_{\chi_j}} g_{\chi_i \chi_j H_k}^L g_{\chi_i \chi_j H_k}^R \right\},$$

with the usual two-body phase space function defined as $\lambda(x, y) = 1 + x^2 + y^2 - 2(xy + x + y)$ and given in terms of the reduced masses $\mu_X = m_X^2/m_{\chi_i}^2$. The couplings among charginos, neutralinos and the Higgs or massive gauge bosons have been presented in eq. (2.13) and eq. (2.14), respectively. The magnitude of these decays strongly depends not only on the phase-space, i.e. on the relative masses of the various chargino/neutralino states and the Higgs and gauge bosons, but also on the texture of the charginos and neutralinos and, hence, on the values of the $M_{1,2}$ and μ parameters.

To illustrate how the decay widths of, for instance, the χ_2^0 and χ_1^\pm states behave, let us ignore the masses of the decay products for simplicity and assume the decoupling limit with very heavy H, A, H^\pm bosons that we ignore. One can then express the partial decay widths of these two, supposedly light, particles in units of $G_F M_W^2 |\mu| / (8\sqrt{2}\pi)$, as follows

$$\Gamma(\chi_1^+ \rightarrow \chi_1^0 W^+) \approx \Gamma(\chi_2^0 \rightarrow \chi_1^0 h) \approx \sin^2 2\beta, \quad \Gamma(\chi_2^0 \rightarrow \chi_1^0 Z) \approx \cos^2 2\beta (M_2 - M_1)^2 / 4\mu^2. \quad (3.9)$$

The first two decay widths are large at low $\tan\beta$ values when $\sin 2\beta \approx 1$, while the last channel is important at high $\tan\beta$ when $\cos 2\beta \approx 1$ and when $M_{1,2} \gg |\mu|$ to make the two neutralino states higgsino-like with a non-suppressed coupling to the Z boson.

We present in Fig. 7 the branching fractions for the decays of the heavier neutralinos $\chi_2^0, \chi_3^0, \chi_4^0$ and chargino χ_2^\pm into the lighter ones plus Higgs and gauge bosons. They have been evaluated with the programs SDECAY [41] and SUSY-HIT [42] in which we have generated the supersymmetric particle and Higgs spectra using the modified version of the SuSpect code [25] as discussed in the previous section. We have assumed that the sfermions, and also the gluinos ($m_{\tilde{g}} \gtrsim 3$ TeV), are too heavy to have an impact on the numbers. The branching ratios are given as functions of the μ parameter which takes both signs and we have set the other inputs to $\tan\beta = 3$, $M_A = 600$ GeV and $2M_1 = M_2 = 1$ TeV.

For this parameter set, the next-to-lightest neutralino has two decay modes, $\chi_2^0 \rightarrow \chi_1^0 h$ and $\chi_2^0 \rightarrow \chi_1^0 Z$. The lightest chargino can only decay into one channel, $\chi_1^\pm \rightarrow W^\pm \chi_1^0$.

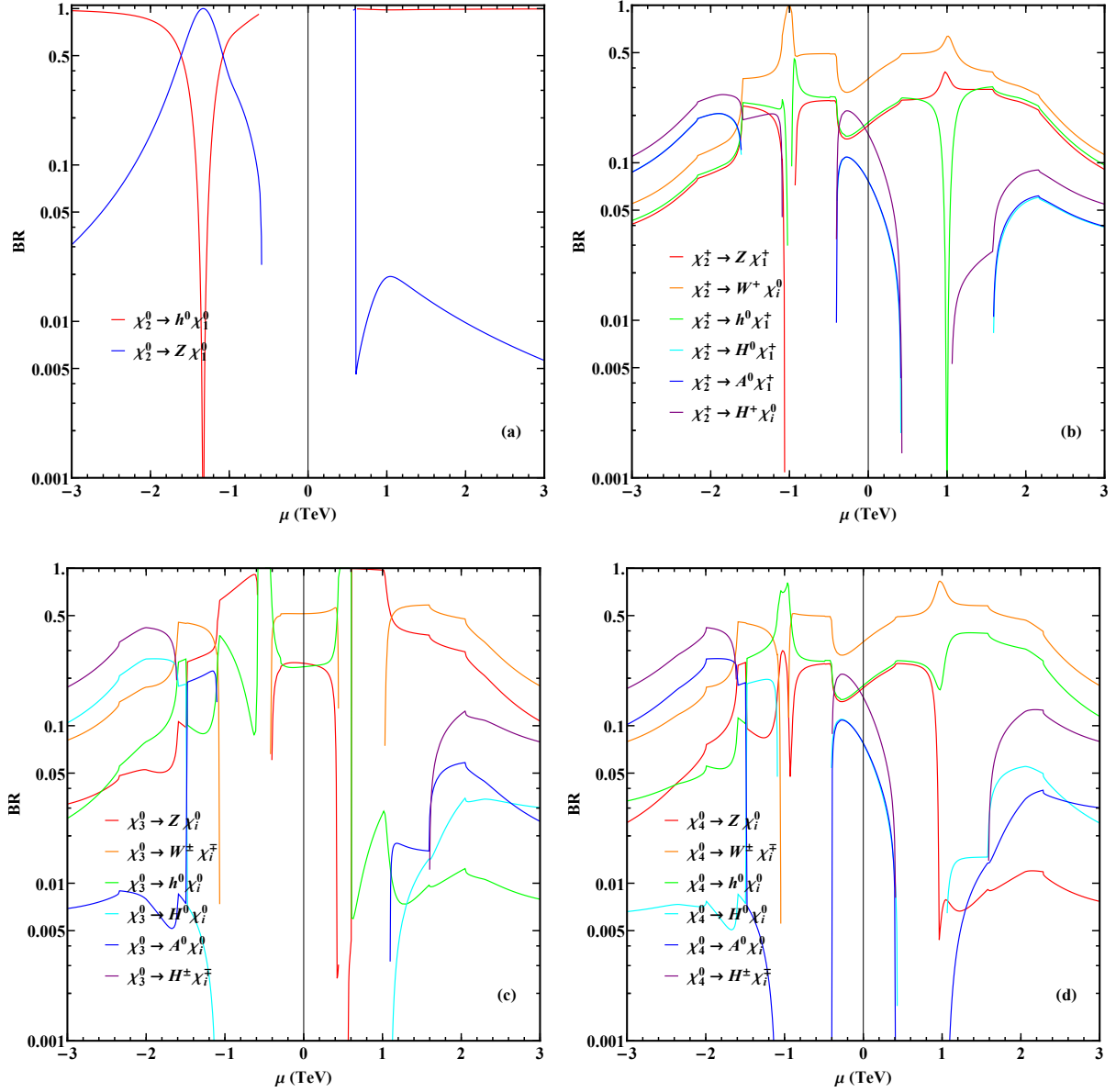


Figure 7: Branching fractions of the various charginos and neutralinos decaying into gauge and Higgs bosons in the hMSSM, as functions of the μ parameter and for the set of input parameters $\tan\beta = 3$, $M_A = 600$ GeV and $2M_1 = M_2 = 1$ TeV.

Heavier charginos and neutralinos can decay not only into the light h and Z, W bosons, but also into the heavier A, H, H^\pm states. The branching fractions can vary significantly around some critical points, such as $|\mu| = M_1$ and $|\mu| = M_2$. This is because these μ, M_1, M_2 values determine how the gauge eigenstates form the physical mass eigenstates.

As can be seen from the figures, the decay pattern in this case is rather involved as many possibilities could be allowed. The mass difference between the parent and daughter particles should be large enough, firstly to avoid phase-space suppression for decays with W, Z, h final states and secondly to open the possibility for cascade decays into the heavier MSSM $H/A/H^\pm$ bosons. The decays into Higgs bosons are particularly relevant if the

lighter χ states are higgsino-like (gaugino-like) and the heavier ones are gaugino-like (higgsino-like), which maximize the couplings as mentioned previously. Those involving the $H/A/H^\pm$ final states can be important, reaching sometimes the level of a few times 10%, but the decays into gauge bosons are in general dominant, in particular for large μ values.

3.2 LHC Constraints on the Gaugino-Higgsino Parameters

Constraints on the gaugino-higgsino mass parameter space come mainly from LHC searches of the lighter chargino and neutralinos in the simple processes (without cascades)

$$pp \rightarrow \chi_2^0 \chi_2^0, \chi_2^0 \chi_1^\pm, \chi_1^\pm \chi_1^\mp \rightarrow \chi_1^0 \chi_1^0 + XX \rightarrow XX + E_T^{\text{mis}}, \quad (3.10)$$

where E_T^{mis} is the transverse missing energy due to the escaping LSP neutralinos and the final states X stand for the lightest Higgs and the massive gauge bosons, $X = W^\pm, Z, h$. If the mass difference between the χ_2^0, χ_1^\pm and the χ_1^0 states is small, the W and Z boson could be off-shell and would decay into (almost) massless quarks and leptons, off-shell h bosons can be ignored as the total width $\Gamma_h^{\text{tot}} = 4.07 \text{ MeV}$ [85] is too small.

In most cases, only final state topologies with leptonic decays, that are subject to a significantly smaller QCD background than events with final state quarks, have been analyzed. The most famous signatures are the trilepton events, mainly from $q\bar{q} \rightarrow \chi_2^0 \chi_1^\pm \rightarrow ZW + \chi_1^0 \chi_1^0 \rightarrow \ell^+ \ell^- \ell'^\pm + E_T^{\text{mis}}$ (with $\ell, \ell' = e, \mu$) which has a large cross section times branching ratio, or the same sign dilepton events from processes such as the one quoted above but with one lepton which has not been detected.

Three or four leptons can also be obtained in the processes $q\bar{q} \rightarrow \chi_2^0 \chi_2^0 \rightarrow ZZ \chi_1^0 \chi_1^0$, which nevertheless have a smaller cross section than the one above. Mono- Z and mono- h events from the process $q\bar{q} \rightarrow \chi_1^0 \chi_2^0$ which is more favored by phase-space and $\chi_2^0 \rightarrow \chi_1^0 Z$ or $\chi_2^0 \rightarrow \chi_1^0 h$ with $Z \rightarrow \ell^+ \ell^-$ and $h \rightarrow b\bar{b}$ (and eventually $h \rightarrow \gamma\gamma$ as the much lower branching ratio could be compensated by the much smaller QCD background) are also considered but the rates are even smaller in general.

Finally, the process $q\bar{q} \rightarrow \chi_1^\mp \chi_1^\pm \rightarrow WW \chi_1^0 \chi_1^0 \rightarrow \ell^\mp \ell'^\pm + E_T^{\text{mis}}$, as it is also mediated by s -channel photon exchange, has a significant cross section independently of the chargino texture, but the topology with opposite-sign leptons is subject to a larger background.

As already mentioned, the corresponding backgrounds, which mainly come from rare SM processes such as pair production of W or Z bosons or associated W, Z bosons with top quarks or from events in which the leptons have been misidentified or missed, or result from decays of hadrons, are in general rather small.

The experimental measurements on these channels have been performed by the ATLAS [51] and CMS [52] collaborations and a very recent summary has been given in Ref. [19]. As already alluded to in the previous discussion, the strongest constraints arise from the searches in the $pp \rightarrow \chi_2^0 \chi_1^\pm \rightarrow \ell\ell\ell\nu + E_T^{\text{mis}}$ topology.

In the case where the lightest chargino and the next-to-lightest neutralino are almost degenerate in mass with the LSP, the above searches are inefficient as the leptons or the other accompanying particles are too soft to be detected. In this case, one would have long-lived χ_1^\pm and χ_2^0 states and the so-called “disappearing track” signature. This is mainly

done in the pair production process of the lightest charginos $q\bar{q} \rightarrow \chi_1^\mp \chi_1^\pm + g$ in which a high transverse momentum gluon is emitted in the initial state. Such signatures have also been searched for by the CMS [53] and ATLAS [54] collaborations, and constraints on the mass difference with the LSP χ_1^0 neutralino or the lifetimes of the χ_1^\pm and χ_2^0 states have been obtained.

In this case of χ_1^0 being bino-like and χ_2^0/χ_1^\pm being wino-like, the production rate of $p \rightarrow W^{\pm*} \rightarrow \chi_2^0 \chi_1^\pm$ is not sensitive to μ and $\tan\beta$ as shown in eq. (2.14) with $(i, j) = (2, 1)$, and χ_2^0/χ_1^\pm can only decay to χ_1^0 regardless of the parameter space. Almost all LHC experimental searches give bounds of $m_{\chi_1^0}$ and $m_{\chi_2^0, \chi_1^\pm}$ on this option.

For other options such as $M_1 < |\mu| < M_2$ or $|\mu| \ll M_{1,2}$, the reactions in eq. (3.10) are sensitive to μ and $\tan\beta$ because higgsino involved in the final states. The LHC experimental studies impose bounds on these options, but they used certain fixed μ and $\tan\beta$ values. Different experimental studies had different choices of fixed parameters, so we do not have universal bounds on these options. These experimental studies mostly gave the model-independent bounds on $\epsilon \times \sigma$, where ϵ is the detection efficiency which can be obtained only by detector-level simulations. This would require detector-level simulations for the whole parameter space. Thus it is valuable to further perform systematic experimental analysis in the near future.

In the following, we will give a concrete example on how the constraints can be imposed on the viable parameter space in the plane of $[m_{\chi_1^\pm, \chi_2^0}, m_{\chi_1^0}]$ by using the current experimental searches and analyses. The latter have been done mostly for the wino-bino (\tilde{W}, \tilde{B}) scenario as described above and the combination of all these experimental limits for this (\tilde{W}, \tilde{B}) model are presented in Fig. 8. We have implemented the hMSSM in the package Suspect [25] as discussed in section 2.3, generated the chargino, neutralino and Higgs spectra, and performed the following scan on the hMSSM parameter space:

$$\tan\beta \in (1, 50), \quad M_A \in (0.5, 2)\text{TeV}, \quad M_2 \in (0, 2)\text{TeV}, \quad \mu \in (-3, 3)\text{TeV}. \quad (3.11)$$

For the remaining bino mass parameter M_1 , we will study four benchmark scenarios in which it is connected to the wino mass parameter M_2 in the following way:

- (a). $M_1 \ll M_2$ which will describe the pure bino-like possibility at large $|\mu|$ values.
- (b). $M_1 = \frac{1}{2}M_2$ which features the GUT-like possibility with $M_2/M_1 = \alpha_2/\alpha_1$.
- (c). $M_1 = M_2$ which leads to the scenario where the bino and wino are mass degenerate.
- (d). $M_1 = 2M_2$ in which the LSP can be wino-like and mass degenerate with χ_1^\pm .

As already stated, we set the other MSSM parameters such as the SUSY scale (which governs the sfermion masses) and the gluino mass parameter M_3 (which governs the gluino mass), to be large enough, so their effects on the current collider searches are negligible. Since the scenarios (c) and (d) have no intersection with the (\tilde{W}, \tilde{B}) model, we analyze their parameter space just for the comparison with the scenarios (a) and (b).

We present the viable parameter space of the lightest gaugino mass in Fig. 8. The shaded blue regions are excluded by LEP2 searches of charginos which require $m_{\chi_1^\pm} > 104$ GeV, and by the current direct searches at the LHC. We see that sizable regions of the masses $m_{\chi_2^0}, m_{\chi_1^\pm} \lesssim 1$ TeV have been excluded by the LHC. For the case of $M_1 \ll M_2$ (we use the range $M_1 < 0.1M_2$) in Fig. 8(a), one can deduce that $m_{\chi_1^0} \lesssim m_{\chi_2^0}, m_{\chi_1^\pm}$. For

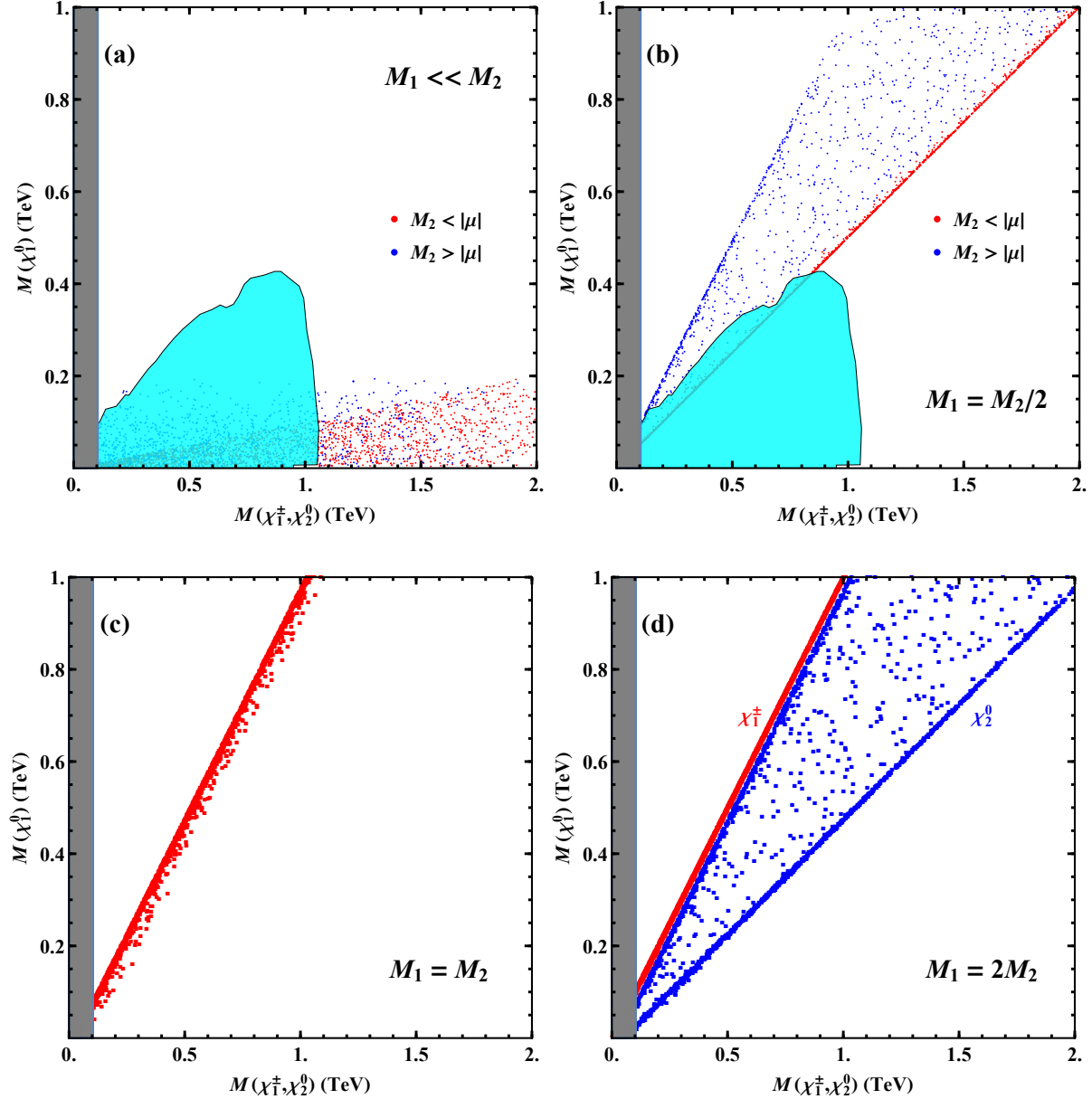


Figure 8: Allowed mass range of the lightest gaugino under the constraints from the gaugino and Higgs searches at the LHC, where the dots represent the hMSSM parameter space and the shaded blue regions are excluded by the existing LHC searches in the (\tilde{W}, \tilde{B}) model ($M_1 < M_2 < |\mu|$) at the 95% C.L. The analysis is presented for the four sample scenarios, $M_1 \ll M_2$ in panel (a), $M_1 = M_2$ in panel (b), $M_1 = \frac{1}{2}M_2$ in panel (c), and $M_1 = 2M_2$ in panel (d). In the panels (a)–(b), the red dots correspond to the possibility $M_2 < |\mu|$ while the blue dots correspond to the possibility $M_2 > |\mu|$.

the case of $M_1 = \frac{1}{2}M_2$ in Fig. 8(b), one infers the condition $\frac{1}{2}m_{\chi_2^0}, \frac{1}{2}m_{\chi_1^\pm} < m_{\chi_1^0} < m_{\chi_2^0}, m_{\chi_1^\pm}$ while for the case of $M_1 = M_2$ in Fig. 8(c), one finds $m_{\chi_1^0} \lesssim m_{\chi_2^0}, m_{\chi_1^\pm}$. Then, for the case of $M_1 = 2M_2$ in Fig. 8(d), one deduces $\frac{1}{2}m_{\chi_2^0} < m_{\chi_1^0} \lesssim m_{\chi_1^\pm} < m_{\chi_2^0}$. Finally, from the panels (a) and (b) of Fig. 8, one sees that for the (\tilde{W}, \tilde{B}) model, one of the two conditions must

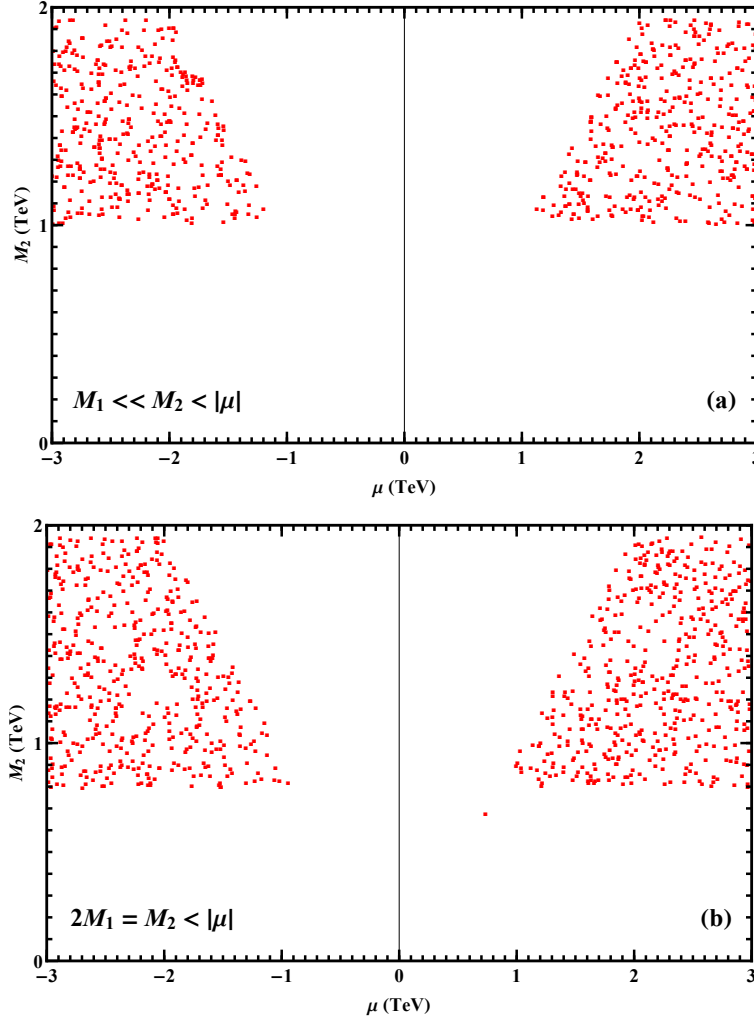


Figure 9: Allowed parameter space in the plane $[\mu, M_2]$ under the constraints (95% C.L.) from gaugino searches at the LHC. The analysis is presented for the two representative scenarios, $M_1 \ll M_2 < |\mu|$ for panel (a) and $2M_1 = M_2 < |\mu|$ for panel (b).

be satisfied: $150 \text{ GeV} < m_{\chi_1^0} < m_{\chi_2^0}, m_{\chi_1^\pm}$, or $m_{\chi_1^0} \ll 1 \text{ TeV} < m_{\chi_2^0}, m_{\chi_1^\pm}$.

Next, we further present in Fig. 9 the corresponding viable parameter space in the plane $[\mu, M_2]$, where the constraints at the 95% confidence level are derived from the negative searches of wino-like χ_2^0/χ_1^\pm , bino-like χ_1^0 and Higgs bosons. The parameters M_A and $\tan \beta$ which appear in the Higgs sector, are mainly constrained by the searches of the heavy Higgs states at the LHC and by the precision measurements of the lighter h couplings to SM fermions and gauge bosons, which will be summarized in the next section. This analysis has been performed for the two representative scenarios $M_1 \ll M_2 < |\mu|$ for panel (a) and $2M_1 = M_2 < |\mu|$ for (b).

Then, using the constraints of Fig. 8, one can further derive bounds on the $[\mu, M_2]$ parameter space as illustrated in Fig. 9 for the two possibilities $M_1 \ll M_2 < |\mu|$ and $2M_1 = M_2 < |\mu|$. The two panels show that the parameter regions with small $|\mu|$ and M_2 values have been excluded by the existing searches at the LHC. To be more specific,

we find that the regions of $|\mu| \lesssim 1.2 \text{ TeV}$ and $M_2 \lesssim 1 \text{ TeV}$ are excluded for the case $M_1 \ll M_2 < |\mu|$ as in plot (a), while the regions of $|\mu| \lesssim 1 \text{ TeV}$ and $M_2 \lesssim 0.8 \text{ TeV}$ are excluded for the case $2M_1 = M_2 < |\mu|$ as in plot (b). These bounds have already covered the the bound of LEP2 searches of charginos ($M_2, |\mu| \gtrsim 100 \text{ GeV}$).

4 Collider Constraints on the Higgs sector

In this section, we study the collider constraints on the Higgs sector in the hMSSM formulation. In section 4.1 we analyze the productions and decays of both the lightest Higgs boson h and the heavier Higgs states (H^0, A^0, H^\pm) of the hMSSM, including the SUSY corrections. In section 4.2, we analyze the current constraints on the parameter space of the hMSSM Higgs sector as imposed by the ATLAS and CMS searches performed during the Run-II phase of the LHC. In section 4.3, we study the decays of the heavier MSSM Higgs bosons into charginos and neutralinos in the context of a light gaugino-higgsino sector, which can be significant in some of the hMSSM parameter space and thus can have important impact on the Higgs phenomenology of the hMSSM.

4.1 Higgs Production and Decay

4.1.1 Higgs Cross Sections and Decay Branching Fractions

We first give a brief summary of the main Higgs production and decay modes in the MSSM [55] and start with the case of the lighter h boson which is SM-like as soon as the mass of the pseudoscalar Higgs state is $M_A \gtrsim 300 \text{ GeV}$, which is indeed the case from the present LHC searches as will be described in the next subsection.

The h mainly decays into $b\bar{b}$ pairs but the channels with WW^* and ZZ^* final states (before allowing the gauge bosons to decay leptonically, $W \rightarrow \ell\nu$ and $Z \rightarrow \ell\ell$ with $\ell = e, \mu$), as well as the $h \rightarrow \tau^+\tau^-$ channel, are also significant. The clean $h \rightarrow \gamma\gamma$ mode, induced by loops of top quarks and W bosons in the SM, can be easily detected albeit its small rates. The decays $h \rightarrow Z\gamma$ and $h \rightarrow \mu^+\mu^-$ will be accessible only at the high-luminosity (HL-LHC) LHC option [20]. The total h decay width is rather small, $\Gamma_h = 4.07 \text{ MeV}$, and any channel beyond the ones above will alter it significantly. This is particularly the case of invisible h decays, which can be probed directly in a more efficient way. We will use the program HDECAY [56] to evaluate the corresponding branching fractions.

As for the Higgs production processes, they will be evaluated using the programs of Refs. [57] which include all relevant higher order QCD corrections. The dominant process is gluon-fusion $gg \rightarrow H$ (ggF) and has rates that are at least an order of magnitude larger than the two subleading channels, vector boson fusion $qq \rightarrow Hqq$ and Higgs-strahlung $q\bar{q} \rightarrow HV$ with $V = W, Z$. Associated $pp \rightarrow t\bar{t}H$ production has an even smaller rate.

Turning to the heavier H, A and H^\pm bosons, they are almost degenerate in mass in the decoupling regime, when $M_A \gtrsim 300\text{--}500 \text{ GeV}$, decouple from the W/Z bosons and interact only with fermions with couplings that are enhanced by powers of $\tan\beta$ for b -quarks and τ -leptons and suppressed as $1/\tan\beta$ for t -quarks. The production and decay

rates strongly depend on $\tan\beta$ [55]. At high values, $\tan\beta \gtrsim 10$, the neutral H, A states are mainly produced in $b\bar{b}$ and gg (through the b -loop contributions) fusion with large rates and decay almost exclusively into $b\bar{b}$ and $\tau^+\tau^-$, with branching ratios of respectively, 90% and 10%. The H^\pm bosons can be produced in the $gb \rightarrow tH^-$ mode and would decay into $t\bar{b}$ and $\tau\nu$ final states, again with branching fractions of 90% and 10%, respectively.

In the low $\tan\beta$ region of $\tan\beta \lesssim 3$, and for Higgs masses above the $2m_t$ threshold, the heavy neutral states will be produced essentially in the $gg \rightarrow H/A$ processes with the top quark loop providing the main contribution and will almost exclusively decay into $t\bar{t}$ final states². The H^\pm bosons will mainly decay into $t\bar{b}$ states with a branching ratio of almost 100%.

For the intermediate $\tan\beta$ region of $3 \lesssim \tan\beta \lesssim 10$, the main Higgs production mode will be $gg \rightarrow H/A$ with some small additional contributions from $b\bar{b}$ fusion; the rates are nevertheless smaller than usual as the coupling $g_t^{H/A}$ is suppressed while $g_b^{H/A}$ is not yet enhanced. For the decays, there will be a competition between the $H/A \rightarrow t\bar{t}$ and $b\bar{b}$ modes. Any additional mode, such as decays into charginos and neutralinos, will impact the rates.

4.1.2 Diphoton Decay Rates of Higgs Bosons

A first effect of the gaugino-Higgsino spectrum on the Higgs sector could be seen in the couplings of the lightest h boson which are rather precisely measured at the LHC. The measurement of the so-called h signal strengths in a given channel, such as the $h \rightarrow XX$ decay, gives a direct constraint on the coupling g_X^h or its reduced form when it is normalized to the coupling of the SM Higgs boson denoted by H_{SM} , which are defined as

$$\kappa_{XX}^{pp \rightarrow h} = \frac{(g_X^h)^2}{(g_X^{H_{\text{SM}}})^2} = \frac{\sigma(pp \rightarrow h) \times \text{BR}(h \rightarrow XX)}{\sigma(pp \rightarrow H_{\text{SM}}) \times \text{BR}(H_{\text{SM}} \rightarrow XX)}. \quad (4.1)$$

These μ_{XX} values depend not only on the angles α and β outside the decoupling regime, when $\alpha \neq \beta - \frac{\pi}{2}$, but also on the loop contributions of the new particles if they are not too heavy. For most of the couplings, these radiative corrections are small but there might be a notable exception with the $h\gamma\gamma$ coupling as the decay $h \rightarrow \gamma\gamma$ proceeds through loops. Besides the standard ones from the top quark and the W boson, there will be those due to SUSY particles which appear at the same order. In our case, there will be only two new contributions: the one due to the charged Higgs boson which, in any case, is rather small and should already be taken into account in the context of the MSSM, but also the contribution due to charginos that we discuss in the following.³

These loops have been discussed in several instances and we will closely follow the relatively recent analysis given in Ref. [59] that we will update. We use the program

²In the process $gg \rightarrow H/A \rightarrow t\bar{t}$, one has to take into account both H and A contributions and also their interference with the $gg \rightarrow t\bar{t}$ QCD background [58]. Nevertheless, as the experimental collaborations are only starting to consider this interference, we will ignore it in our analysis.

³We will ignore here the corresponding chargino (and eventually neutralino) contributions to the other loop induced decay mode, namely $h \rightarrow Z\gamma$ [60], which can be probed only with extremely high statistics and which will provide essentially the same information in the hMSSM context.

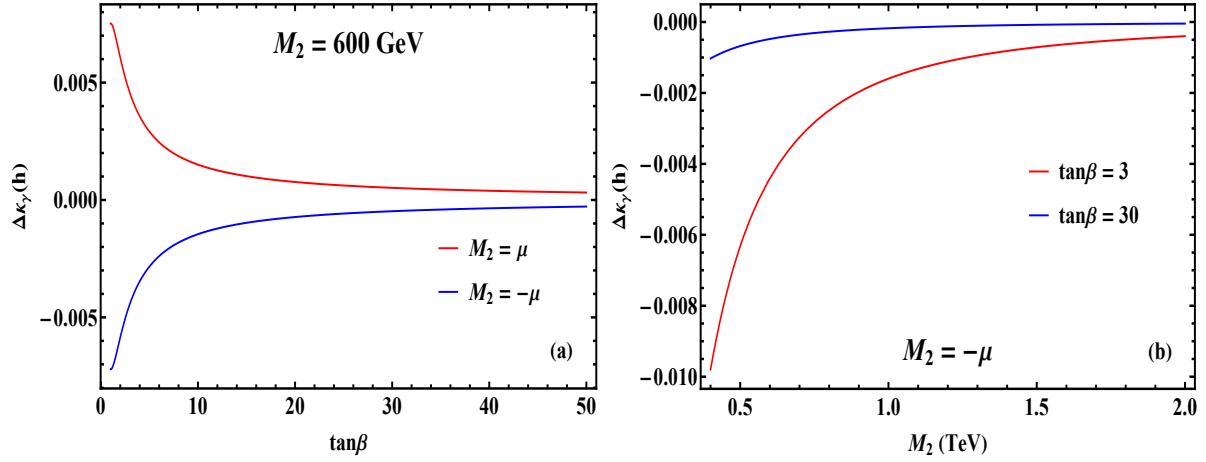


Figure 10: Deviations of the $h\gamma\gamma$ coupling as a function of $\tan\beta$ in the upper panel (a) and of the gaugino mass parameter M_2 in the lower panel (b). For (a), the red (blue) curve corresponds to $M_2 = \mu$ ($M_2 = -\mu$) = 600 GeV. For (b), the red (blue) curve corresponds to $\tan\beta = 3$ ($\tan\beta = 30$) and we set a relation $M_2 = -\mu$.

SUSY-HIT [42] to evaluate the fraction $\text{BR}(h \rightarrow \gamma\gamma)$ including the chargino contributions in the hMSSM context, that is, we use the program HDECAY [56] where all these loop contributions are included at one-loop order (which should be largely sufficient for our purpose here) with the SUSY particle spectrum generated by the package Suspect [25].

The deviation of the $h\gamma\gamma$ coupling when including the SUSY-loop contributions relative to the case without them, $\Delta\kappa_\gamma^h$ will depend on the values of (M_2, μ) that enter the chargino sector in addition to $\tan\beta$. In Fig. 10, we present the deviation $\Delta\kappa_\gamma^h$ for the chargino loop corrections to the h -diphoton coupling as a function of $\tan\beta$ in the upper plot and as a function of the gaugino mass M_2 in the lower plot. In both cases, we fix the pseudoscalar mass to $M_A = 1$ TeV, which makes that we are in the decoupling limit and the Higgs couplings are not affected by the angles α and β . We assume the equality $M_2 = |\mu|$ which maximizes the h couplings to the charginos as described in section 2.2. In the upper panel but we take both signs of μ and vary $\tan\beta$, while in the lower panel, we take $M_2 = -\mu$ only and study the chargino impact as a function of M_2 for the two values $\tan\beta = 3$ and $\tan\beta = 30$. From this figure, we see that the possible deviation $\Delta\kappa_\gamma^h$ has the same sign as the μ parameter. Moreover, $|\Delta\kappa_\gamma^h|$ is smaller than 1% and decreases with the increase of $\tan\beta$ [as in Fig. 10(a)] and the increase of M_2 [as in Fig. 10(b)].

For comparison, we also present the chargino loop corrections to the $H\gamma\gamma$ and $A\gamma\gamma$ couplings in Fig. 11 for $M_A = 1$ TeV. Because the masses of charginos can be smaller than H and A , $\Delta^H\kappa_\gamma$ and $\Delta^A\kappa_\gamma$ can be larger than 1. There are significant differences near $M_A = 2M_2 \approx 2m_{\chi_i^\pm}$ thresholds and the sign of μ has an opposite impact on $\Delta\kappa_\gamma^H$ and $\Delta\kappa_\gamma^A$.

4.1.3 SUSY Corrections to Higgs Production and Decays

As discussed in section 2.4, SUSY particles contribute directly to the Higgs couplings to fermions g_f^Φ and, hence, impact the MSSM Higgs production and decays rates in a way that cannot be absorbed into corrections to the angle α . In particular, at high

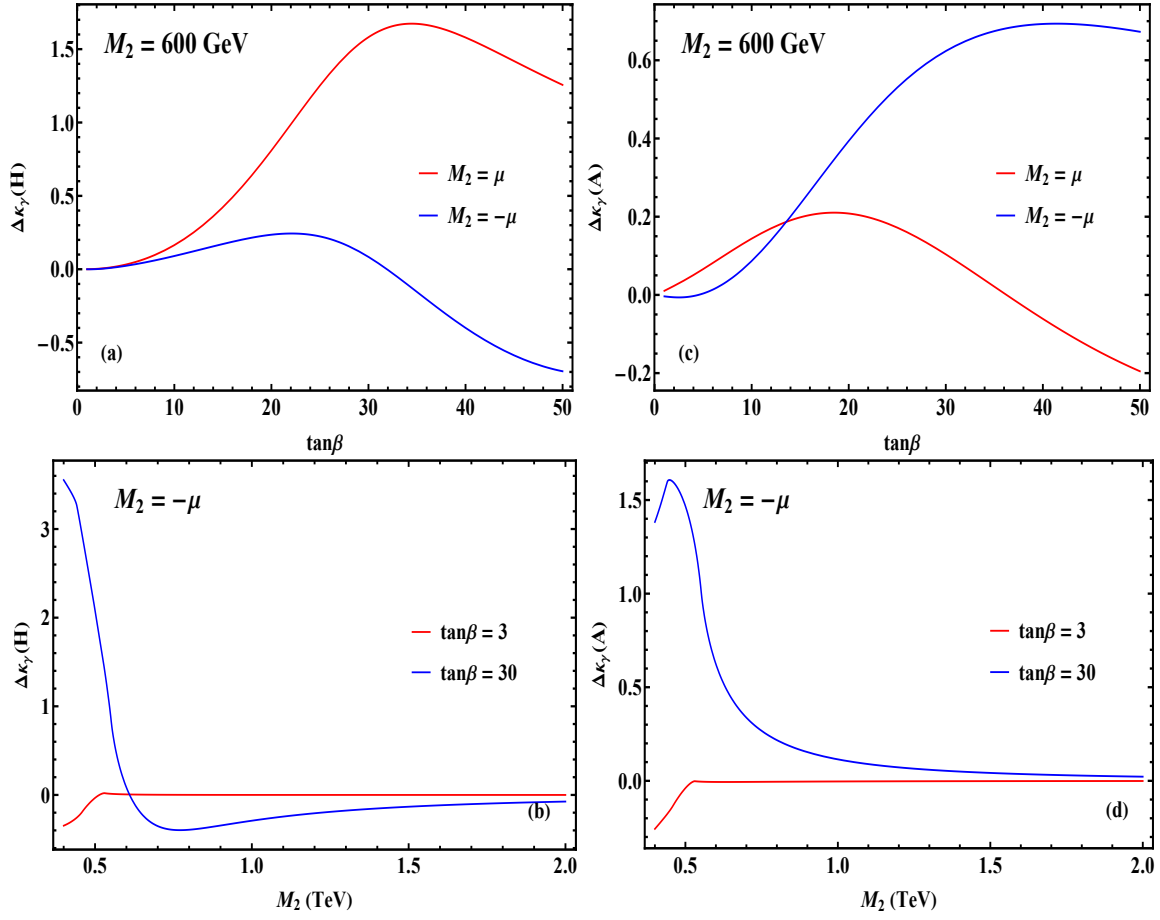


Figure 11: Deviations of the $H\gamma\gamma$ and $A\gamma\gamma$ couplings as a function of $\tan\beta$ in the upper panel (a-c) and of the gaugino mass parameter M_2 in the lower panel (b-d). For (a-c), the red (blue) curve corresponds to $M_2 = \mu$ ($M_2 = -\mu$) = 600 GeV while for (b-d), the red (blue) curve corresponds to $\tan\beta = 3$ ($\tan\beta = 30$) and we set $M_2 = -\mu$.

$\tan\beta$, the direct correction Δ_b to the Higgs- $b\bar{b}$ vertices, the leading part of which is given in eq. (2.26), can be significant when μ is also large. The SUSY-QCD part of the correction, Δ_b^{QCD} , being proportional to $\tan\beta\mu m_{\tilde{g}}/\max(m_{\tilde{g}}^2, M_S^2)$ and the electroweak one $\Delta_b^{\text{EW}} \propto \tan\beta\mu/M_S^2 \times (\mu, M_1, M_2)$, can be made small by setting the SUSY scale M_S , and hence the squark masses since $M_S^2 = m_{\tilde{t}_1}m_{\tilde{t}_2} \approx m_{\tilde{q}}^2$, to very large values as we are assuming in the hMSSM considered here. This would also be the case of the stop-chargino and sbottom-neutralino contributions to the electroweak correction Δ_b^{EW} .

Nevertheless, even if squarks and gluinos are light enough to have sizeable contributions to Δ_b , the latter will have only a limited impact in the main detection channels of the heavy MSSM Higgs states when the full production times decay rates in the dominant processes are taken into account. Indeed, for H/A , the main processes considered at the LHC are $gg, b\bar{b} \rightarrow H/A \rightarrow \tau^+\tau^-$ and while the production cross sections are modified as

$$\sigma(gg, b\bar{b} \rightarrow H/A) \propto (1 + \Delta_b)^{-2}, \quad (4.2)$$

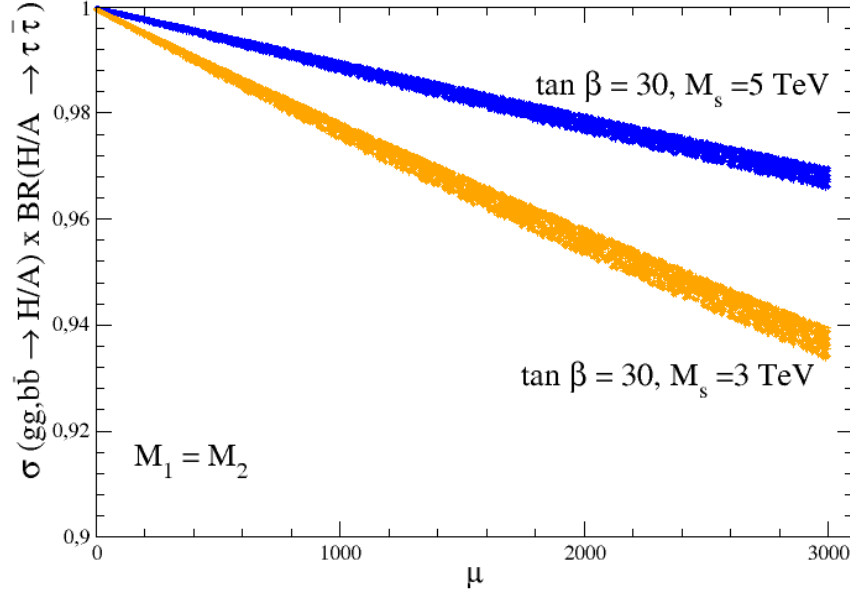


Figure 12: Impact of the Δ_b correction on the production times decay rates $pp \rightarrow H/A \rightarrow \tau^+ \tau^-$ and $pp \rightarrow tbH^\pm \rightarrow tb\tau\nu$ for the large $\tan\beta$ from a scan on the (M_2, μ) parameter space.

one would have the following modification f on the decay branching fractions:

$$\text{BR}(H/A \rightarrow \tau\tau) = \Gamma(H/A \rightarrow \tau\tau) / [(1 + \Delta_b)^{-2} \Gamma(H/A \rightarrow b\bar{b}) + \Gamma(H/A \rightarrow \tau\tau)], \quad (4.3)$$

assuming, as it is generally the case, that the corresponding Δ_τ correction is small enough to be negligible. The Δ_b correction will then largely cancel out in the product of the cross section and branching fraction:

$$\sigma(gg, b\bar{b} \rightarrow H/A) \times \text{BR}(H/A \rightarrow \tau\tau) \simeq 1 - \Delta_b/5. \quad (4.4)$$

Hence, only when the Δ_b correction is very large (say, of order unity), its impact on the $pp \rightarrow H/A \rightarrow \tau\tau$ rate would become of the order of the theoretical uncertainty of the process (stemming from the scale and the PDF uncertainties), which is estimated to be about 20% [55]. Thus the Δ_b effect is insignificant. Such a large Δ_b correction does not occur in our hMSSM scenario as we assume the squarks to be heavy enough. This is illustrated in Fig. 12, from a scan over the parameters M_2 and μ and for a representative large $\tan\beta = 30$ value and not too heavy squark masses, $M_S = (3-5)$ TeV. Note that it would reach about 10% only for values $\tan\beta = 50$, $M_S = 3$ TeV, and large $|\mu| \simeq 3$ TeV. Hence, the limits set by ATLAS and CMS on the heavier MSSM Higgs bosons, which are dominantly derived from the channels above, should not be affected by these SUSY direct corrections.

The discussion above holds partly in the case of the charged Higgs for which the main production process is $bg \rightarrow H^\pm t$. At high $\tan\beta$, its cross section is also modified as in

eq. (4.2) and in one the main detection channels, $H^\pm \rightarrow \tau\nu$, it has the same branching ratio as in eq. (4.3) since $\text{BR}(H/A \rightarrow \tau\tau, b\bar{b})$ should be replaced by $\text{BR}(H^\pm \rightarrow \tau\nu, tb)$. The product of the two, $\sigma(bg \rightarrow H^\pm) \times \text{BR}(H^\pm \rightarrow \tau\nu)$, will then also behave as in eq. (4.4) and, hence, the correction will largely cancel out in the cross section times branching ratio. However, another important channel for the charged Higgs boson at high $\tan\beta$ (as well as low) values, is the $H^\pm \rightarrow tb$ channel which could also be strongly affected by the Δ_b correction. The cross section times decay branching ratio will behave in this case as

$$\sigma(gb \rightarrow H^\pm) \times \text{BR}(H^\pm \rightarrow tb) \simeq 1 - 11\Delta_b/5, \quad (4.5)$$

and will be thus more significantly affected if the Δ_b correction is large. In this case, one will need to take into account the value of the relevant SUSY parameters (in particular the gluino and squarks masses which enter the dominant SUSY-QCD corrections) in order to fix this corrections. But again, one can choose a benchmark scenario in which all these masses are large enough not to affect the Higgs vertices.

In any case, for the charged Higgs boson, the $H^\pm \rightarrow tb$ channel is up to now not as sensitive as the $pp \rightarrow H/A \rightarrow \tau^+\tau^-$ process and will not change the LHC present sensitivity limits of the ATLAS and CMS experiments. Note that we have ignored possible effects in the $H^\pm tb$ vertex stemming from corrections due to the top/stop sector at low $\tan\beta$. The Δ_t corrections, as in the case of the Δ_τ corrections are rather small.

Let us finally make an important remark on the case of the lightest h boson couplings that are now measured rather precisely at the LHC. In principle, the hbb coupling also receives Δ_b corrections, but as discussed recently in Ref. [35] for instance, close to the decoupling limit $M_A \gg M_Z$ the deviation from its SM-like value will be given by

$$\Delta g_d^h \simeq \Delta_b \frac{1 + \tan^2\beta}{\tan\beta} \times \frac{M_Z^2}{2M_A^2} \sin 4\beta \xrightarrow{\tan\beta \gg 1} -\Delta_b \times \frac{M_Z^2}{8M_A^2}, \quad (4.6)$$

which is very strongly suppressed for $M_A \gtrsim 2M_Z$. Hence, these direct corrections should be very small and will not affect the signal strengths of the h boson measured at the LHC to which we turn our attention now.

4.2 Constraints on the Parameter Space of the Higgs Sector

In this subsection, we study the present constraints on the parameter space of the hMSSM Higgs sector as imposed by the ATLAS and CMS searches performed at the Run-II of the LHC. These constraints arise from two sources. The first one is due to the measurements of various couplings of the observed Higgs boson of mass 125 GeV [43][44] which, in our context, corresponds to the lightest h state. Another source of constraints arise from the direct searches of the heavier neutral and charged Higgs bosons in various channels [45][46][47][48]. Both constraints already exclude a significant portion of the $[M_A, \tan\beta]$ parameter space. We recast the two sets of constraints above in our hMSSM context and we start by summarizing our results in Fig. 13 that we will describe below.

For the direct or indirect searches, the main precision measurements of the SM-like Higgs couplings come from the bosonic decays $h \rightarrow ZZ, WW$ and $\gamma\gamma$ with the h boson

dominantly produced from gluon fusion, $gg \rightarrow h$. The measurements of the fermionic couplings in the decays $h \rightarrow \tau^+ \tau^-$ and $b\bar{b}$ are less precise and the contribution of the other production channels such as vector boson fusion $pp \rightarrow hqq$ and associated production $pp \rightarrow hV$ add only little. The measured signal strengths in these main production and decay channels, $\mu_{\gamma\gamma, ZZ, WW}^{\text{ggF}}$ are as defined in eq. (4.1). The combination of measurements of the SM-like Higgs production and decay channels using the full set of 139 or 137 fb $^{-1}$ data collected at the LHC with $\sqrt{s} = 13$ TeV by ATLAS [43] and CMS [44] gives:

$$\text{ATLAS : } \quad \mu_{\gamma\gamma}^{\text{ggF}} = 1.03_{-0.11}^{+0.11}, \quad \mu_{ZZ}^{\text{ggF}} = 0.94_{-0.10}^{+0.11}, \quad \mu_{WW}^{\text{ggF}} = 1.08_{-0.18}^{+0.19}, \quad (4.7a)$$

$$\text{CMS : } \quad \mu_{\gamma\gamma}^{\text{ggF}} = 1.09_{-0.14}^{+0.15}, \quad \mu_{ZZ}^{\text{ggF}} = 0.98_{-0.11}^{+0.12}, \quad \mu_{WW}^{\text{ggF}} = 1.28_{-0.19}^{+0.20}, \quad (4.7b)$$

where the errors correspond to the total theoretical plus experimental uncertainties which have been added in quadrature. As can be seen, up to the level of about 10%, all signal strengths are around unity, meaning that the Higgs particle has SM-like couplings. In the MSSM, as the h couplings should be modified by the angles α and β outside the decoupling regime, one concludes that the value of the pseudoscalar A boson should be large, $M_A \gg M_Z$, in order to be close to this regime. To quantify the implications on these measurements on the $[M_A, \tan \beta]$ parameter space, we perform the following χ^2 fit⁴

$$\chi^2 = \sum (\mu_{\text{hMSSM}} - \mu_{\text{EXP}})^2 / \sigma_{\text{EXP}}^2, \quad (4.8)$$

where the quantities $\mu_{\text{EXP}}, \sigma_{\text{EXP}}$ are the signal strength and uncertainty from the observations given above, and the quantity μ_{hMSSM} is the corresponding signal strength in the hMSSM which is a function of M_A and $\tan \beta$. As shown by the red area in Fig. 13, the hMSSM fit has ruled out the mass range $M_A \lesssim 600$ GeV at the 2σ level. The excluded area does almost not depend on the value of $\tan \beta$. The reason is that $\cos(\beta - \alpha)$ which measures the departure from the decoupling limit reads at high M_A values [35]

$$\cos(\beta - \alpha) \xrightarrow{M_A \gg M_Z} \frac{1}{2} \frac{M_Z^2}{M_A^2} \sin 4\beta \longrightarrow \frac{1}{2} \frac{M_Z^2}{M_A^2} \times \begin{cases} -4/\tan \beta & \text{for } \tan \beta \gg 1 \\ 1 - \tan^2 \beta & \text{for } \tan \beta \sim 1 \end{cases} \rightarrow 0, \quad (4.9)$$

is suppressed not only by M_Z^2/M_A^2 but also by $\tan \beta$, both at high and low $\tan \beta$ values.

Moving to the constraints from direct LHC searches, we will take into account those of heavy Higgs bosons performed by ATLAS [45, 46] and CMS [47, 48] again using the full integrated luminosity of 139 fb $^{-1}$ at $\sqrt{s} = 13$ TeV. The search that provides by far the strongest constraint is the one performed in the channel $pp \rightarrow gg, b\bar{b} \rightarrow H/A \rightarrow \tau^+ \tau^-$ [45, 47] and it excludes at the 95% CL the large part of the $[M_A, \tan \beta]$ plane depicted by the blue area in Fig. 13. Values of M_A below the TeV range are excluded for $\tan \beta \gtrsim 10$.

The search of the charged Higgs boson in the channel $pp \rightarrow tbH^\pm$ with $H^\pm \rightarrow tb$ [46] is much less constraining than the previous one at high $\tan \beta$, since it is sensitive only for $\tan \beta$ close to our upper limit $\tan \beta \approx 50$ and Higgs mass values $M_{H^\pm} \approx M_A$ which are already excluded by the h signal strength measurements. However, the search is also sensitive to very small $\tan \beta$ values, $\tan \beta = 1-2$ for $M_{H^\pm} \lesssim 800$ GeV.

⁴The fit has also been performed by ATLAS (see e.g. [50]) and CMS and in a more accurate way. We nevertheless need to do our own fit as we will extend it later to include some additional SUSY effects.

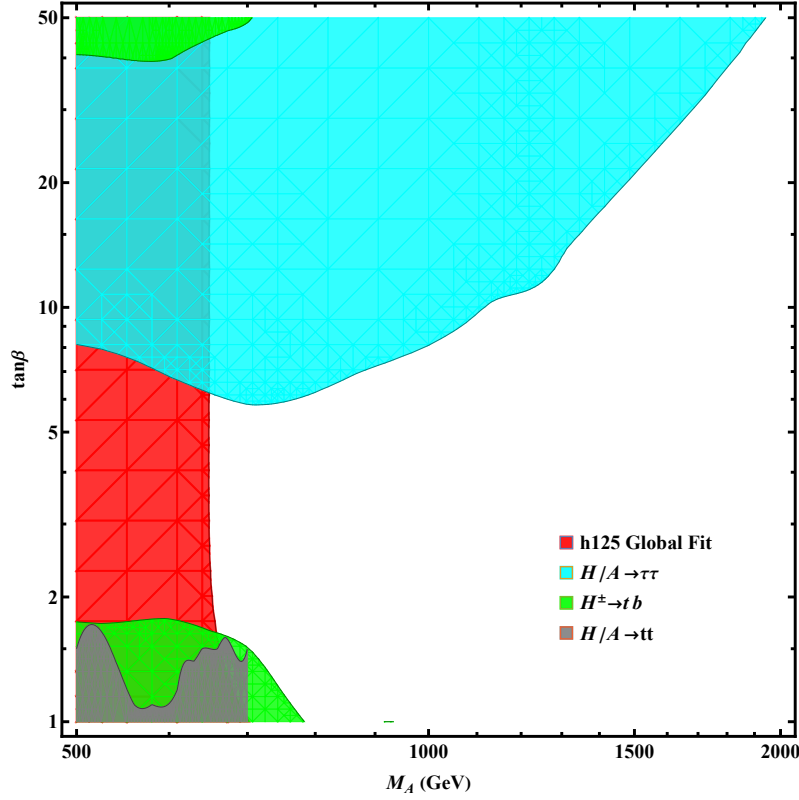


Figure 13: Constraints on the hMSSM viable parameter space in the $[M_A, \tan\beta]$ plane at 95% C.L., using the LHC measurements of the signal strengths of the SM-like Higgs boson h (the red area) as well as the direct searches of the heavier neutral Higgs bosons in the reaction $pp \rightarrow H/A \rightarrow \tau^+\tau^-$ (the blue area), the charged Higgs boson in the reaction $pp \rightarrow H^\pm \rightarrow t\bar{b}$ (the green area) and the neutral Higgs bosons in the channel $pp \rightarrow H/A \rightarrow t\bar{t}$ (the grey area).

Note that in this low $\tan\beta$ area, the search channel $pp \rightarrow gg \rightarrow H/A \rightarrow t\bar{t}$ should be in principle very efficient, in particular when interference effects with the QCD background are taken into account. However, the one performed by the CMS collaboration with only a luminosity of about 36 fb^{-1} [48] is, for the time being, weaker than the one from the $H^\pm \rightarrow t\bar{b}$ mode discussed above. The corresponding ATLAS search, performed with the same integrated luminosity [49], did not include the interference effects and hence, has not been interpreted in the Higgs resonance context. We also find that the bounds imposed by other heavy Higgs search channels [50], including $H \rightarrow WW, ZZ, hh$ and $A \rightarrow hZ$ for instance, are weaker and are already covered by the exclusion regions shown in Fig. 13.

In a next step, we perform the previous χ^2 fit of the h coupling measurements in the $[M_A, \tan\beta]$ parameter space, but this time, taking account the possible effect of the parameters μ and M_2 for which we perform the scan in eq. (3.11) with $M_1 \ll M_2$ and $M_2 = 2M_1$ in, respectively, the left and the right panels. Again, the red dots represent the hMSSM parameter space which obeys all the experimental constraints that we considered here. The blue curves in each panel represent the constraints from the χ^2 fit of the SM-like h coupling measurements with the two parameters $M_A, \tan\beta$ only. Comparing the

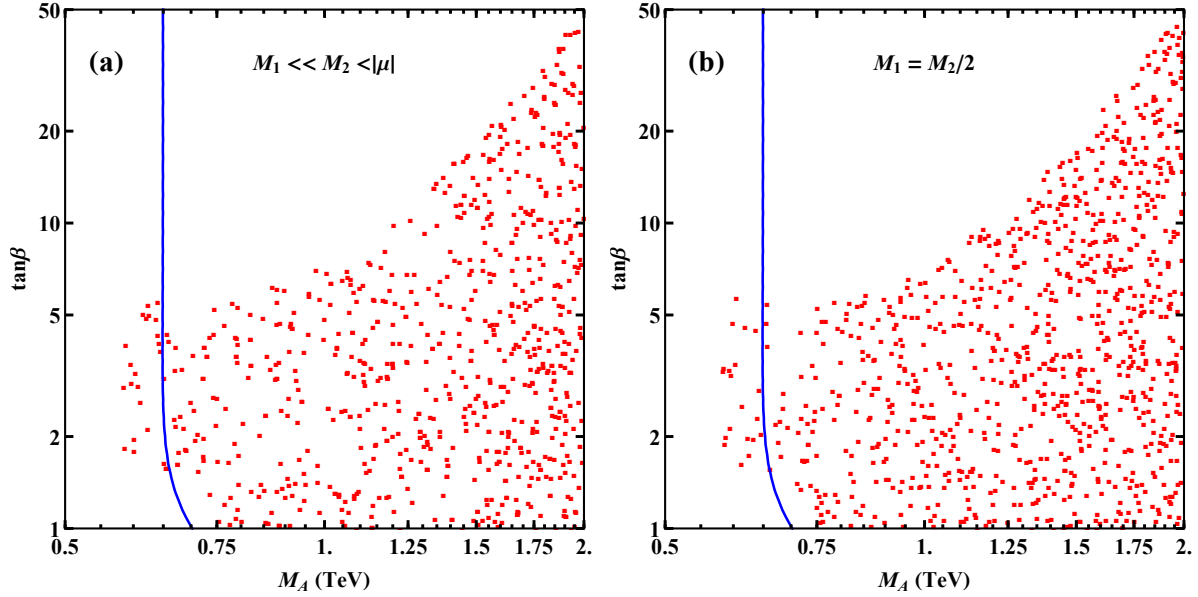


Figure 14: Allowed parameter space in the $(M_A, \tan\beta)$ plane at the 95% C.L., obtained by fitting the h coupling measurements and direct search of H/A at the LHC and including the effects of the parameters M_2 and μ when setting $M_1 \ll M_2$ (left panel) and $M_2 = 2M_1$ (right panel). The regions on the left of the blue curves in each plot are excluded by the LHC h coupling measurements with the parameters $(M_A, \tan\beta)$ only.

allowed region (marked by red dots) by the four-parameter fit of $(M_A, \tan\beta, M_2, \mu)$ with the bound (blue curve) by the two-parameter fit of $(M_A, \tan\beta)$, we see that the lower bound on M_A in four-parameter fit is relaxed modestly.

The reason follows from the fact that the decay channel $h \rightarrow \gamma\gamma$ is very important to the χ^2 fit of the h measurements. Since low M_2 and μ values can affect the $h\gamma\gamma$ coupling, with two more degrees of freedom (M_2, μ) , there is more available parameter space for $(M_A, \tan\beta)$. The red dots satisfy the constraint of heavy Higgs search without considering the impact of charginos and neutralinos. We will discuss the bounds including the decays of heavy Higgs bosons to charginos and neutralinos in the next subsection.

4.3 Higgs Decays into Charginos and Neutralinos

A very important feature in the context of a light gaugino-higgsino spectrum is that it allows for the decays of at least the heavier MSSM Higgs bosons into charginos and neutralinos. These decays can be significant in some of the hMSSM parameter space and thus can make a large impact on the phenomenology of the Higgs sector, as these will affect the LHC Higgs searches, but also the chargino and neutralino sector, as they provide a new window for the detection of these particles. We analyze this aspect in the current subsection.

Denoting as in section 2.2 the MSSM Higgs bosons as H_k [with $k = 1, 2, 3, 4$ for the Higgs states (H, h, A, H^\pm)] and the neutralinos and charginos collectively by χ_i , the partial widths of the Higgs decays $H_k \rightarrow \chi_i \chi_j$ into light gauginos and higgsinos can be written

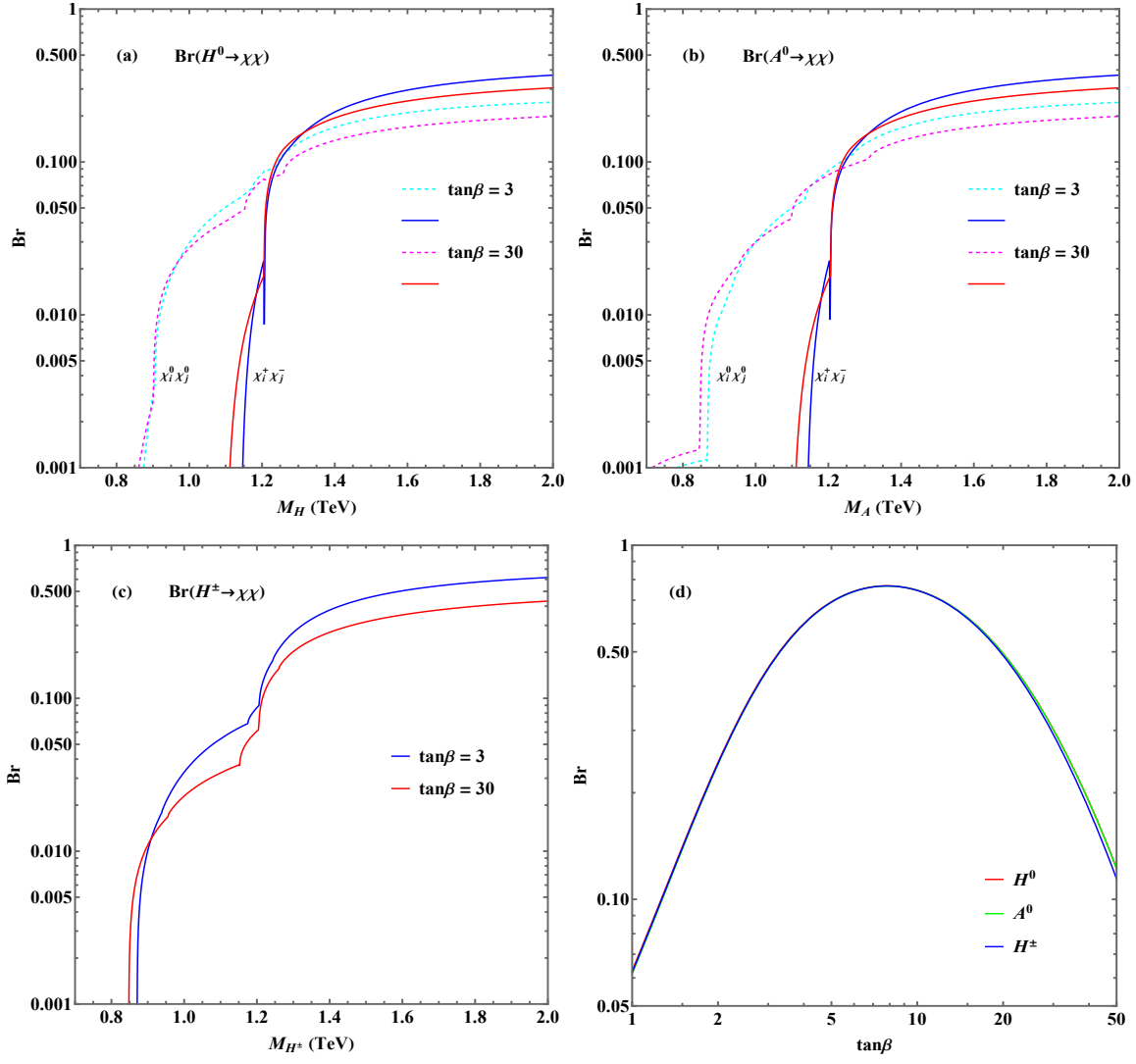


Figure 15: Branching fractions of the heavy Higgs decays into charginos and neutralinos as functions of their masses for the inputs $\tan\beta=3, 30$ and $M_2=2M_1=-\mu=600$ GeV. In the panel (d), we further set the input $M_A=1.5$ TeV, such that all the SUSY-decay channels of the heavy Higgs bosons are open and sum up all the decay modes.

as [61][62][63][64]:

$$\Gamma(H_k \rightarrow \chi_i \chi_j) = \frac{G_\mu M_W^2 s_W^2}{2\sqrt{2}\pi} \frac{M_{H_k} \lambda_{ij}^{\frac{1}{2}}}{1 + \delta_{ij}} \left([(g_{ijk}^L)^2 + (g_{jik}^R)^2] (1 - \kappa_i^2 - \kappa_j^2) - 4\epsilon_i \epsilon_j g_{ijk}^L g_{jik}^R \kappa_i \kappa_j \right), \quad (4.10)$$

where use the abbreviation $\kappa_i = m_{\chi_i}/M_{H_k}$ and where $\delta_{ij} = 0$ unless the final state consists of two identical (Majorana) neutralinos in which case $\delta_{ii} = 1$. $\epsilon_i = \pm 1$ stands for the sign of the i -th eigenvalue of the neutralino mass matrix, but for charginos, one has $\epsilon_i = 1$; $\lambda_{ij} = 1 + \kappa_i^4 + \kappa_j^4 - 2(\kappa_i^2 \kappa_j^2 + \kappa_i^2 + \kappa_j^2)$ is the usual phase space factor. The Higgs couplings to charginos and neutralinos have been already given in eqs. (2.13)-(2.13b).

In the gaugino (higgsino) limit for the lightest χ states $|\mu| \gg M_{1,2}$ (or $|\mu| \ll M_{1,2}$), the neutral Higgs decays into identical neutralinos and charginos $A/H \rightarrow \chi_i \chi_i$, together

with the charged Higgs decays $H^\pm \rightarrow \chi_{1,2}^0 \chi_1^\pm, \chi_{3,4}^0 \chi_2^\pm$, will be strongly suppressed by the couplings even if phase-space favored. The Higgs decays to the mixed heavy and light χ states will in turn be favored by the larger couplings. For example, in the gaugino limit and if one ignores the phase-space suppression by taking $M_{H_k} \gg |\mu| \gg M_2$, the partial widths of the heavy Higgs decays into mixed χ states, in units of the factor $G_F M_W^2 M_{H_k} / (4\sqrt{2}\pi)$, will be simply given by the simple expressions

$$\Gamma(H/A \rightarrow \chi_i^0 \chi_j^0) \propto \frac{1}{2} \xi_i (1 \pm \sin 2\beta), \quad \Gamma(H/A \rightarrow \chi_1^\pm \chi_2^\mp) \propto 1, \quad (4.11)$$

with $\xi_1 = \tan^2 \theta_W$ and $\xi_2 = 1$, so that the decays of one of the neutral Higgs bosons are not suppressed when $\tan\beta$ is either large or close to one. The charged Higgs boson decays $H^\pm \rightarrow \chi_i^\pm \chi_j^0$ do not depend on $\tan\beta$ in this limit and the decay width is simply either 1 or $\tan^2 \theta_W$ in the unit above. We present in Fig. 15 the branching fractions of the three heavy Higgs bosons decaying into the neutral and charged χ states. We note that the turning points around $2M_2 = 1.2 \text{ TeV}$ are due to the mass relation $m_{\chi_2^0}, m_{\chi_1^\pm} \approx M_2$.

For large Higgs masses $M_A \approx M_H \approx M_{H^\pm} \gg M_Z$, when all decay channels are kinematically accessible, the branching fractions can be significant and sometimes can even become dominant, also for the low and large values of $\tan\beta$ which, respectively, enhance the top and bottom decay modes. However, the maximal Higgs decay rates into these states are obtained at moderate $\tan\beta$ when all channels are kinematically accessible. In this case, as a consequence of the unitarity of diagonalizing the χ mixing matrices, the sum of the partial widths does not depend on any supersymmetric parameter when phase space is neglected. For instance, one gets the following expressions for the total branching fraction by summing up all the possible decay modes

$$\text{BR}(\Phi \rightarrow \sum_{i,j} \chi_i \chi_j) = \frac{(1 + \frac{1}{3} \tan^2 \theta_W) M_W^2}{(1 + \frac{1}{3} \tan^2 \theta_W) M_W^2 + \bar{m}_t^2 \cot^2 \beta + (\bar{m}_b^2 + \frac{1}{3} m_\tau^2) \tan^2 \beta}, \quad (4.12)$$

where, besides the decays into the superparticles, only the leading channels $t\bar{t}$, $b\bar{b}$ and $\tau\tau$ for the neutral H/A and the dominant modes tb and $\tau\nu$ for the charged H^\pm bosons are included in the total decay widths, which is indeed the case in the decoupling limit where other decays become negligible, and the mass effects have been neglected.

In Fig. 15, we illustrate the branching fractions for the heavy Higgs decays into charginos and neutralinos. In the panels (a)-(c), these branching fractions are plotted for neutral and charged heavy Higgs bosons as functions of their masses. In all these cases, we choose the sample inputs of $\tan\beta = 3, 30$ and the SUSY parameters $M_2 = 2M_1 = -\mu = 600 \text{ GeV}$. One sees that the pattern for the decay branching fractions of the heavy H , A , H^\pm bosons is quite similar. For the mass values $M_{H_k} \lesssim 2M_2 = 1.2 \text{ TeV}$, the branching ratios are generally below the 10% level, and as the Higgs masses become larger, they can increase up to the level of (40–50)%.

In the last pane (d), we also present the Higgs decay branching fractions into all χ states as function of $\tan\beta$, where a sample input $M_A = 1.5 \text{ TeV}$ is taken, such that all the chargino and neutralino decay modes of the heavy Higgses are open. It shows that the decay branching fractions of the three heavy Higgs bosons nearly coincide and can reach

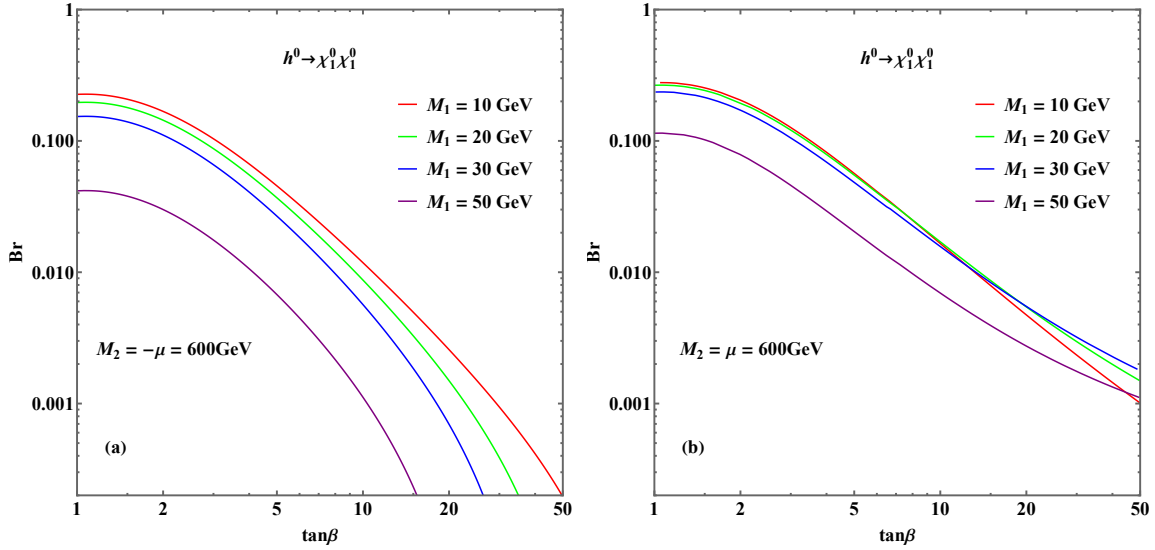


Figure 16: The invisible decay branching fraction $\text{BR}(h \rightarrow \chi_1^0 \chi_1^0)$ as a function of $\tan\beta$, where the (red, green, blue, purple) curves correspond to a gaugino mass parameter $M_1 = (10, 20, 30, 50)$ GeV, respectively. We choose the sample inputs $\mu = -M_2 = 600$ GeV for the plot (a) and $\mu = M_2 = 600$ GeV for the plot (b).

values around 40 – 80% for $\tan\beta$ values in the range $\tan\beta \in [2.5, 25]$.

As mentioned earlier, for very large $\tan\beta$ values, the partial decay widths of the $H/A \rightarrow b\bar{b}, \tau^+\tau^-$ and $H^+ \rightarrow t\bar{b}, \tau^+\nu$ decays are so strongly enhanced, that they leave little room for the SUSY-decay channels. At low $\tan\beta$ values, the decay rates of $H/A \rightarrow t\bar{t}$ when kinematically accessible and $H^+ \rightarrow t\bar{b}$ are large and can be dominating. Thus, the heavy Higgs decays into the neutralinos and charginos could play a significant role mainly for the intermediate values of $\tan\beta$ and possibly for $M_H = M_A \lesssim 350$ GeV. However, two requirements should be fulfilled also in this case. First of all, to make some SUSY decay modes $H_k \rightarrow \chi\chi$ kinematically possible, certain χ states should be light, $M_{H_k} \gtrsim 2m_\chi$ (with $H_k = H, A$). Secondly, the $H_k\chi\chi$ couplings should be large enough, meaning that the χ states should be gaugino-higgsino mixtures as previously discussed.

Finally, let us make a few comments on the SUSY-decay channels of the light CP-even and SM-like h boson. The experimental bound $m_{\chi_1^\pm} \gtrsim 104$ GeV from LEP2 searches does not allow the h boson to decay into any chargino pair or neutralino pair except for the invisible decays into a pair of the LSP neutralinos, $h \rightarrow \chi_1^0 \chi_1^0$. This is especially valid in the case where one equates the gaugino masses at the GUT scale, leading to the relation $M_1 \sim \frac{1}{2}M_2$ at the electroweak scale, is relaxed. This would lead to the possibility of very light LSP neutralinos while the LEP2 bound on $m_{\chi_1^\pm}$ still holds. However, as χ_1^0 should be primarily bino-like in this case, $M_1 \ll M_2, |\mu|$, the $h\chi_1^0\chi_1^0$ coupling is suppressed and leads to small invisible branching fractions. Nevertheless, as it competes with modes that have small partial widths, the rate can still reach a few percent level. Hence, it can be probed by future measurements of the h signal strengths or in the direct searches for invisible decays at HL-LHC or at future e^+e^- and pp colliders.

Nevertheless, even with such a small h branching fraction, one can arrange that the LSP has the required cosmological density, since it will annihilate efficiently through the

exchange of the h Higgs boson, as will be discussed in the following astrophysics section.

In Fig. 16, we present the branching fractions of the lightest h boson when decaying into the LSP neutralinos, $h \rightarrow \chi_1^0 \chi_1^0$, as a function of $\tan\beta$. Here, the (red, green, blue, purple) curves are when the bino mass parameter is fixed to the values $M_1 = (10, 20, 30, 50)$ GeV, respectively. We chosen the other input parameters to be $\mu = -M_2 = 600$ GeV for the panel (a) and $\mu = M_2 = 600$ GeV for the panel (b).

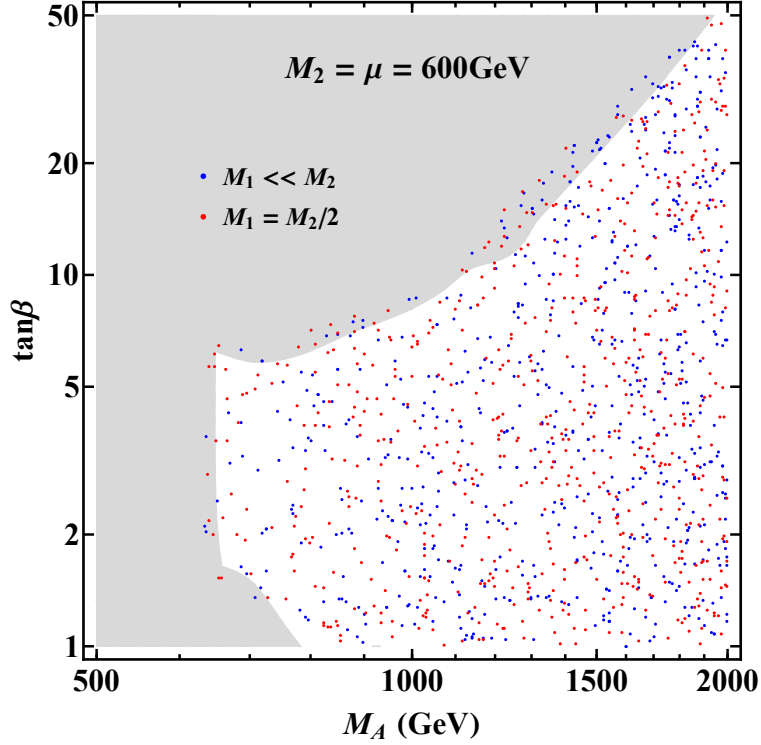


Figure 17: Allowed parameter space in the $[M_A, \tan\beta]$ plane at the 95% CL, obtained by fitting the h coupling measurements and direct search of heavy Higgs bosons at the LHC when setting $M_2 = \mu = 600$ GeV, $M_1 \ll M_2$ (blue dots) and $M_2 = 2M_1$ (red dots). The grey region is the exclusion region under the condition that SUSY particles have no contribution to Higgs production and decays.

One notices that for the small bino mass value $M_1 = (10 - 20)$ GeV, the branching fractions can be around the percent level for $\tan\beta \lesssim 5 - 15$ and can even reach the 20% level for $\tan\beta \lesssim 2$. On the other hand, for larger mass values $M_1 = 50$ GeV, the branching fractions are only around the percent level for $\tan\beta \lesssim 5$. We find that the branching fractions with $\mu = M_2 = 600$ GeV are generally larger than that with $\mu = -M_2 = 600$ GeV.

Fig. 17 presents the parameter space allowed by the combined h coupling measurements and the direct Higgs searches, including contributions of SUSY particles to the decays as discussed in this section. Here, we set the parameters to $M_2 = \mu = 600$ GeV for illustration. For comparison, we also present the exclusion region without the contribution of SUSY particles as in Fig. 13. The presence of SUSY particles reduces the branching fractions of heavy Higgs decays to the SM particles and thus allows for a larger parameter space.

5 Astrophysical Constraints of the hMSSM

The previous discussion about the relation between the invisible decay branching ratio of the SM-like Higgs boson and the relic density of the DM particle allows us to make a smooth transition towards the astrophysical and astroparticle aspects of a neutralino LSP in the context of the hMSSM. As is well known, in an MSSM in which R -parity [21] is conserved, this particle was for a long time considered to be the best candidate for a thermal DM particle [65, 66]. Under this assumption, the requirement of a cosmological relic density compatible with the latest measurement of the PLANCK satellite [67]

$$\Omega_{\chi_1^0} h^2 \simeq 0.12 \pm 0.01, \quad (5.1)$$

as well as compatibility with direct and indirect detection experiments, provide very strong constraints on the MSSM Higgs sector that are complementary to the collider constraints discussed before. We will briefly review below the various DM constraints, focusing on relic density and direct detection, being, in general, the most stringent. Whenever appropriate, will account for indirect detection while illustrating our numerical results.

First, concerning the cosmological relic density of the LSP neutralino that should be compatible with the measured value given in eq. (5.1), it is determined, up to non standard assumptions about the cosmological history of the early universe, by the freeze-out paradigm. According to the latter, the DM abundance is directly related to the thermally averaged cross section $\langle\sigma v\rangle$ of the annihilation of DM pairs into lighter particles, $\Omega_{\chi_1^0} \propto 1/\langle\sigma v\rangle$. In the MSSM, this cross section crucially depends on the composition of the lightest neutralino and on the supersymmetric particle spectrum since co-annihilation processes, occurring when the next-to-lightest supersymmetric particle (NLSP) is almost degenerate in mass with the DM one, play an important role.

In a general MSSM with possibly light sfermions, two main configurations in the model parameter space that lead to an appropriate relic density, have been discussed. A first one, called the “bulk region” [66], is when the main DM annihilation process is into leptonic final states. This is mediated by t -channel slepton exchange and, in particular, the exchange of the $\tilde{\tau}$ state which is expected to be the lightest slepton. The other configuration is when the neutralino χ_1^0 has a mass very close to that of a sfermion \tilde{f} , leading to efficient LSP- \tilde{f} and $\tilde{f}\tilde{f}$ co-annihilations. The possibilities which were advocated most are co-annihilations with again τ -sleptons [68] but also top-squarks [69]. Both sfermions can be made the lightest sfermions by enforcing a strong mixing between the left- and right-handed states.

However, in our hMSSM context in which the sfermions are assumed to be very heavy, these two possibilities become absent. DM annihilations will thus occur only through the s -channel exchange of the Z and neutral bosons, à-la Higgs/ Z -boson portal scenarios [70], or via gauge interactions. The size of such LSP annihilation cross sections and thus, the DM relic abundance, will then primarily depend on the gaugino-higgsino composition of the neutralino DM. This composition also controls the mass difference between the LSP and the other lighter neutralinos and charginos, which is important for co-annihilation.

The correct χ_1^0 relic density can be therefore obtained only in the following situations.

i) A mostly bino-like LSP neutralino. This scenario resembles the Higgs portal simplified models, with the DM mostly annihilating into SM fermions and gauge bosons via the

s -channel exchange of neutral bosons [70]. As the bino annihilation cross sections via the exchange of the CP-even Higgs bosons, as well as the exchange of the Z boson, are p -wave suppressed, only annihilation processes into SM fermions via the exchange of the pseudoscalar A state, are in general relevant as they lead to an s -wave dominated cross section. These processes feature a potentially nice correlation with the LHC Higgs searches illustrated in the previous sections. Nevertheless, for a light DM with a mass $m_{\chi_1^0} \lesssim 100$ GeV, Z and h mediated annihilation channels become relevant but the corresponding cross sections typically lie below the thermally favored value, of order $\langle\sigma v\rangle \approx 10^{-26} \text{cm}^3 \text{s}^{-1}$, unless “pole” enhancements that occur for $m_{\chi_1^0} \simeq \frac{1}{2}M_Z$ or $m_{\chi_1^0} \simeq \frac{1}{2}M_h$ are present [71].

ii) A higgsino or wino-like LSP neutralino. In this case, the pairs of χ_1^0 DM states will annihilate via gauge interactions into pairs of W and Z bosons, with a relic density mainly set by the value of the LSP mass. The cosmologically favored value is achieved for $m_{\chi_1^0} \approx 1$ TeV and $m_{\chi_1^0} \simeq 3$ TeV for, respectively, purely higgsino-like and purely wino-like LSPs [72] and the DM would be under-abundant for lighter masses. In these cases, the correlations with searches of heavy Higgs bosons at the LHC would be very weak or even absent. Hence, dedicated DM searches will be the primary probes for this type of scenario.

iii) The “well tempered” bino-higgsino and bino-wino regimes [73]. Here, the correct relic density is achieved, away from resonances and for DM masses of the order of few hundred GeV, by having a suitable admixture between a bino-like LSP, with very suppressed interactions, and a higgsino and/or wino component, which is more efficiently interacting. As it will be clarified in the discussion below, bino-higgsino DM has enhanced interactions with CP-even Higgs bosons in contrast to the mixed bino-wino lightest neutralinos. The former is thus disfavored by DM direct detection, while the later regime can instead evade these constraints provided that some fine tuning of parameters occurs.

This brings us to the issue of direct detection. In general, the neutralino DM features both spin-independent (SI), mediated by the exchange of the neutral CP-even Higgs bosons and generating a DM–nucleon scattering cross section on the proton of the form

$$\sigma_{\chi_1^0 p}^{\text{SI}} = \frac{\mu_{\chi_1^0 p}^2}{\pi} \frac{m_p^2}{v^2} \left| \sum_q f_q^p \left(\frac{g_{\chi_1^0 \chi_1^0 h} g_q^h}{M_h^2} + \frac{g_{\chi_1^0 \chi_1^0 H} g_q^H}{M_H^2} \right) \right|^2, \quad (5.2)$$

and spin-dependent (SD) interactions, mediated by the Z bosons and leading to a scattering cross-section on protons which reads

$$\sigma_{\chi_1^0 p}^{\text{SD}} = 3 \frac{\mu_{\chi_1^0 p}^2}{\pi M_Z^4} \left[g_{\chi_1^0 \chi_1^0 Z} (g_u^A \Delta_u^p + g_d^A (\Delta_d^p + \Delta_s^p)) \right]^2. \quad (5.3)$$

In these equations, m_p is the proton mass while $\mu_{\chi_1^0 p} = m_{\chi_1^0} m_p / (m_{\chi_1^0} + m_p)$ is the DM–proton reduced mass. For the coefficient f_q^p and Δ_q^p giving the contributions of the various light and heavy quarks, we adopt the numerical values given in Refs. [74].

For both types of interactions, we will impose the most recent constraints provided by the XENON1T collaboration [75, 76]. Analogous constraints have been also obtained by the LUX and PANDA-X experiments and add little so that we do not include them.

In the next subsections, we show how these DM constraints complement the collider ones in the different configurations for the various regimes of the bino and wino mass

parameters that we have identified in the previous sections. In all cases, our numerical results will be based on the implementation of the modified version of the program SuSpec for the hMSSM discussed in section 2 in the program Micromegas [77] for DM.

5.1 $M_1 \simeq \frac{1}{2}M_2$

Let us first consider the case in which the soft SUSY-breaking wino and bino mass parameters are linked by the GUT relation $M_2 \simeq 2M_1$. In such a case, the neutralino DM can be either bino-like or higgsino-like, or a mixture of these two components. Representative examples of the combined DM/LHC constraints in such a scenario are provided in Fig. 18.

The four panels of the figure show the constraints on the bidimensional $[M_2, |\mu|]$ parameter space for two benchmark scenarios with $(M_A, \tan \beta)$ Higgs sector parameters of (1 TeV, 5) for the upper panels and (1.5 TeV, 10) for the lower ones. For each of these two scenarios, we considered the two possibilities $\mu > 0$ and $\mu < 0$. We have then applied on this plane the constraints on the relic density from the PLANCK satellite, the present and future sensitivities of the direct detection experiments and finally, the constraints on this parameter space from LHC searches of charginos and neutralinos discussed previously.

Given the precision in the experimental determination of $\Omega_{\chi_1^0} h^2$, the correct DM relic density, assuming the WIMP paradigm and a standard cosmological evolution for the early universe, is achieved only in the narrow contours of the $[M_2, |\mu|]$ plane marked in black. For the shown benchmarks to be viable, at least one portion of the relic density isocontours should lie outside both the blue regions, corresponding to the exclusion from XENON1T, the yellow regions, corresponding to the exclusion from searches of continuous spectra of γ -rays from DM annihilations as performed by the FERMI collaboration [88], and the gray regions, excluded by neutralino/chargino searches at the LHC. The areas of the $[M_2, |\mu|]$ plane will be, in turn, ruled out if the next future results from XENONnT [78] and LZ [79] (which have comparable sensitivities and, hence, we will represent them in all the plots as a unique region in magenta) as well as DARWIN (purple) [80] experiments will confirm the absence of DM signals.

The outcome shown in Fig. 18 can be understood as follows. In the regions corresponding to $m_{\chi_1^0} < \frac{1}{2}M_{H,A}$, the correct DM relic density can be achieved only for an LSP with a substantial bino-higgsino mixture, a possibility that is ruled out by direct detection limits. For $m_{\chi_1^0} \simeq \frac{1}{2}M_{H,A}$, the vicinity of the Higgs poles enhances the DM annihilation rate, in particular in the pseudoscalar Higgs case. The correct relic density could be then obtained for a bino-like DM that evades, at least partially, the direct detection constraints. The increased sensitivity of upcoming detectors will, however, strongly erode this region in the absence of a signal. Finally, the relic density curve reaches a plateau at around $\mu \simeq 1.1$ TeV. In this region the relic density is saturated by the annihilation processes into gauge boson pairs of a higgsino-like DM state. For $|\mu|$ and $M_{1,2}$ values of the same order, this region appears to be excluded by DM direct detection. Direct detection bounds can be relaxed by considering the possibility $M_{1,2} \gg |\mu|$. This scenario would be not very interesting for what concerns LHC SUSY particle searches.

Comparing the left (for positive μ) and right (for negative μ) panels, one notices that in the latter case, there are regions in which direct detection constraints become sensitively weaker. Indeed, in such regions, the DM scattering cross section is suppressed as a

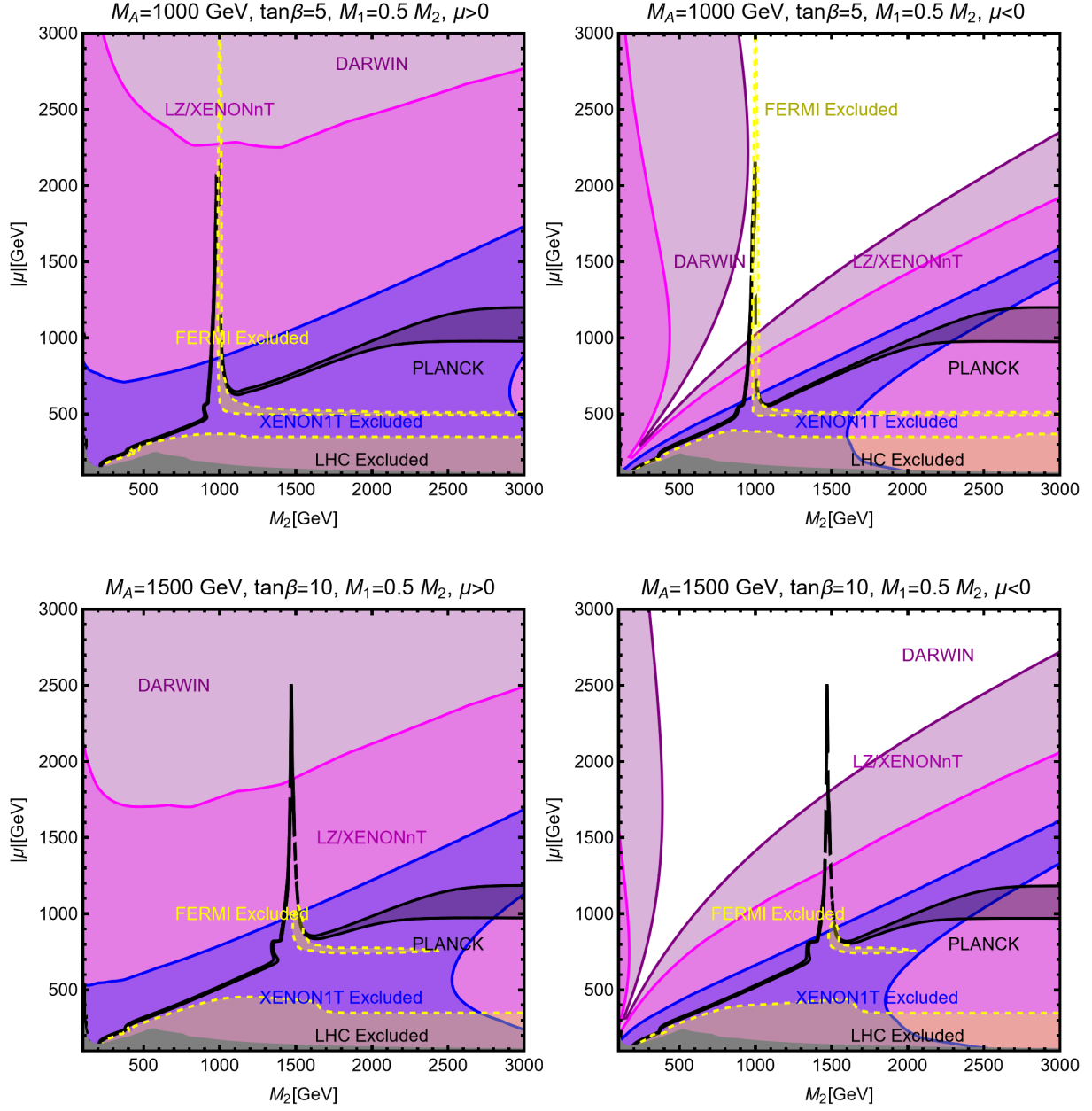


Figure 18: Summary of DM constraints in the $[M_2, |\mu|]$ plane for the $M_2 = 2M_1$ scenario. The upper panels are for the $(M_A, \tan\beta)$ assignments (1 TeV, 5), while the lower panels ones consider (1.5 TeV, 10). For each benchmark we have considered both signs for the μ parameter. In all panels, the black isocontours correspond to regions in which the correct DM relic density is reproduced, the colored contours the present and future sensitivities regions of the XENON1T (XENONnT/DARWIN) direct detection experiments and the regions marked in gray are those ruled out by LHC searches of charginos/neutralinos.

consequence of “blind spots”, i.e. assignments of the model parameters corresponding to a cancellation of the coupling of the DM with the light h boson or destructive interference between the contributions associated with the exchange of the two h and H states [81]. An approximate analytic expression to have these “blind spot” regions reads

$$2 \left(m_{\chi_1^0} + \mu \sin 2\beta \right) / M_h^2 \simeq -\mu \tan \beta / M_H^2. \quad (5.4)$$

In the limit in which the H state is very heavy, $M_H \approx M_A \gg M_Z$, the condition above reduces to $m_{\chi_1^0} + \mu \sin 2\beta \simeq 0$, which requires a negative μ value to be satisfied. Concerning DM indirect detection, limits affect the regions of parameter space with mostly higgsino like DM. This is due to the fact that in the latter case the DM annihilation cross-section is s-wave dominated.

5.2 $M_1 \simeq M_2$

The assignment $M_1 = M_2$ for the gaugino mass parameters leads to bino and wino states with comparable masses and corresponds to one possible option of the so-called “well tempered” LSP neutralino scenario. In this special case, the resulting combined DM and LHC constraints on the $[M_2, |\mu|]$ parameter space are illustrated by Fig. 19. The benchmark scenarios for the Higgs sector and the sign of the μ parameter, as well as the color coding for the various constraints, is exactly the same as in Fig. 18.

Looking first at the relic density contours, one can see that they feature two plateaux: a first one for $|\mu| > M_2 \gtrsim 1 \text{ TeV}$ and another one for $M_2 > |\mu| \gtrsim 1 \text{ TeV}$. It can be noticed, furthermore, that these relic density curves are not sensitive to variations of the $(M_A, \tan \beta)$ parameter sets. The reason is that in the second case, i.e. for $|\mu| < M_{1,2}$, the limit of a pure higgsino DM, already discussed in the previous subsection, is recovered. In the opposite regime, i.e. for $|\mu| > M_{1,2}$, the $M_1 = M_2$ relation imposes a substantial mixing, of the order of the Weinberg angle θ_W , between the bino and wino components of the mixed bino-wino DM neutralino. Consequently, in both limits, the DM relic density is mostly accounted for by DM annihilation into gauge boson pairs, whose cross sections are not sensitive to the Higgs sector parameters. In addition, as one has $m_{\chi_1^0} \approx m_{\chi_2^0} \approx m_{\chi_1^\pm}$, co-annihilation processes (in particular those involving charginos which have stronger couplings) play an important role. In both cases, a multi-TeV DM neutralino is favored.

For what concerns the limits from direct detection experiments, they are again very similar to the ones obtained in the previous $M_1 \simeq \frac{1}{2} M_2$ case. These very strong constraints can be thus evaded only if blind spots, i.e. very specific correlations among the model parameters, are realized as also discussed before. Indirect detection constraints (yellow regions) play a complementary role at low DM masses. This is mostly due to the fact that substantial wino and/or higgsino component for the DM induce high annihilation cross-sections into pairs of gauge bosons, in tension with experimental sensitivity. Notice that, due to Sommerfeld enhancement, also multi-TeV values of the DM mass are potentially subject to constraints from DM indirect detection. As shown e.g. by [89], the latter sensitively affect the parameter space corresponding to wino-like DM and $\mu > 0$. The systematic implementation of Sommerfeld enhancement is beyond the scopes of this work and we hence refer to the dedicated literature.

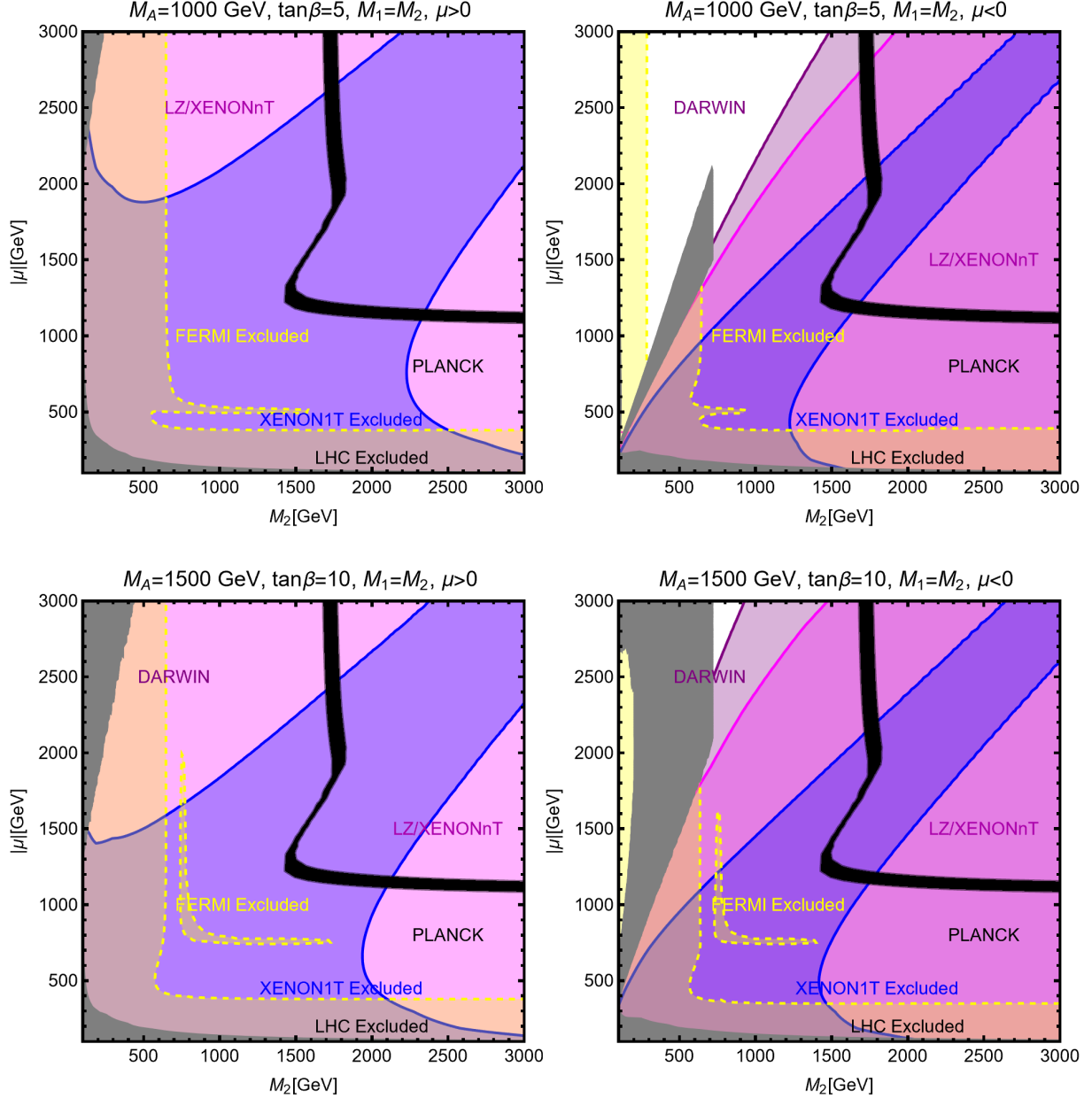


Figure 19: Summary of DM constraints in the $[M_2, |\mu|]$ plane for the $M_2 = M_1$ scenario. The upper panels are for the $(M_A, \tan \beta)$ assignments $(1, \text{TeV}, 5)$, while the lower panels ones consider $(1.5 \text{ TeV}, 10)$. For each benchmark we have considered both signs for the μ parameter. In all panels, the black isocontours correspond to regions in which the correct DM relic density is reproduced, the colored contours the present and future sensitivities regions of the XENON1T (XENONnT/DARWIN) direct detection experiments and the regions marked in gray are those ruled out by LHC searches of charginos/neutralinos.

The picture just depicted can be altered if a slight deviation from the $M_1 = M_2$ relation is considered. This is illustrated in Fig. 20 in which a difference in the two gaugino mass values $M_2 - M_1 \simeq 5 - 10 \text{ GeV}$ is assumed. For $|\mu| \gg M_{1,2}$ as chosen in all panels of the

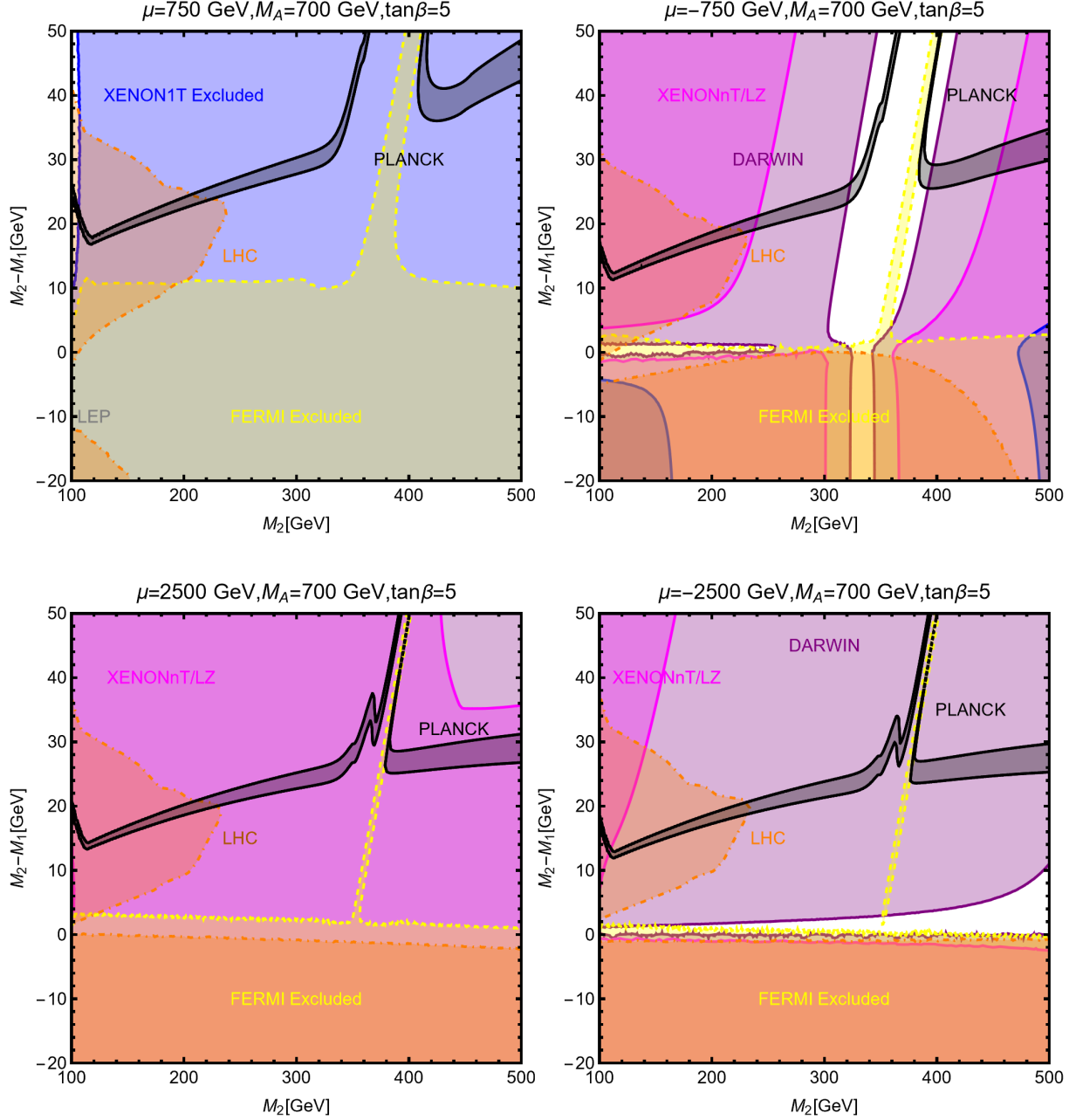


Figure 20: Summary of constraints, in the $[M_1, (M_2 - M_1)]$ parameter space, for some “well-tempered” wino-like neutralino configurations, identified by the Higgs-higgsino parameter assignments on top of each panel. Following the usual color code, the correct DM thermal relic density is identified by the black isocontours, the present (future) excluded regions by the XENON1T (XENONnT/LZ/DARWIN) experiments are marked in blue (magenta/purple) and the regions in orange correspond to those excluded from neutralino/chargino searches at the LHC (see main text for details) while, finally, the yellow regions are excluded by Indirect DM searches by the FERMI experiment.

figure, this leads to small splittings between the masses of the gaugino-like next-to-lightest neutralino and lightest chargino states χ_2^0 and χ_1^\pm and the mass of the LSP neutralino χ_1^0 . This would strongly suppress the co-annihilation processes and allows that the correct DM relic density is achieved for lower DM masses.

As can be seen from the lower panels of Fig. 20 with $\mu = \pm 2.5$ TeV (and also the upper panel with $\mu = -750$ GeV), the direct detection constraints from the XENON1T experiments can be evaded for relatively low values of the gaugino mass parameters M_1 and M_2 , and hence LSP masses, without relying on blind spot configurations. Nevertheless, some of these values are already constrained by LHC searches of charginos and neutralinos given by the orange regions. The portion of parameter space with $M_2 < M_1$, hence wino-like DM, is also ruled out both by DM indirect detection (again because of the very efficient s-wave annihilation cross-section) and both by LHC. For this kind of setup the most effective limits come from searches of disappearing tracks [54, 53]. The upgraded sensitivity expected for the future XENONnT/LZ and DARWIN experiments would allow to probe a very large part of the remaining viable DM parameter space.

5.3 $M_1 \ll M_2$ and $M_2 \ll M_1$

The scenario $M_1 \ll M_2$ is the one in which the bino-like neutralino is lighter than the wino-like neutralino and chargino and, for this reason at least for what concerns DM phenomenology, it has strong similarities with the case $M_1 = \frac{1}{2}M_2$ discussed before. Hence, most of the results presented in subsection 5.1 apply also in this case. Nevertheless, in the case $M_1 \ll M_2$ and for large values of the higgsino mass parameter, $|\mu| \gg M_1$, the LSP can be almost bino-like with no or very small couplings to the Z boson. It is thus no longer constrained by the LEP bounds and, hence, can be very light. We will hence focus the analysis below on the specific $M_1 \lesssim \frac{1}{2}M_h$ sub-case.

Fig. 21 shows the combined constraints in the $[M_1, |\mu|]$ plane for the $(M_A, \tan \beta) = (1 \text{ TeV}, 8)$ and $(M_A, \tan \beta) = (1.5 \text{ TeV}, 15)$ Higgs parameter sets and both signs of μ .

As already mentioned, the DM is mostly bino in the $M_1 \ll M_2$ scenario and the DM cosmological relic density is achieved essentially through DM annihilation processes into SM particle final states, via the SM-like Higgs and the Z boson exchanges in the s -channel. Bino-like neutralinos have, however, strongly suppressed couplings to these particles so that the correct relic density is achieved only around the $m_{\chi_1^0} \simeq \frac{1}{2}M_Z$ or $\frac{1}{2}M_h$ poles.

For $\mu > 0$, the two considered benchmark scenarios are, nevertheless, already ruled out by present constraints from DM direct detection ad exception of very narrow regions around the SM Higgs pole⁵. For $\mu < 0$, direct detection can be evaded in large regions of the parameters space thanks to the occurrence of “blind spots”. However, having “blind spots” means suppressed DM couplings to the SM-like Higgs boson which will then make it difficult to achieve the correct relic abundance. Indeed, as it can be seen from the plots, the PLANCK value of the DM relic density is reproduced only in the h pole region, provided that $|\mu| \lesssim 500$ GeV. The portion of the (M_1, μ) bidimensional space highlighted in orange is excluded by LHC searches. For the considered setup, we adopted the limits determined in [83] for bino DM with higgsino NLSP.

⁵Notice that in such regions the conventional numerical computations of the relic density are not completely reliable [82].

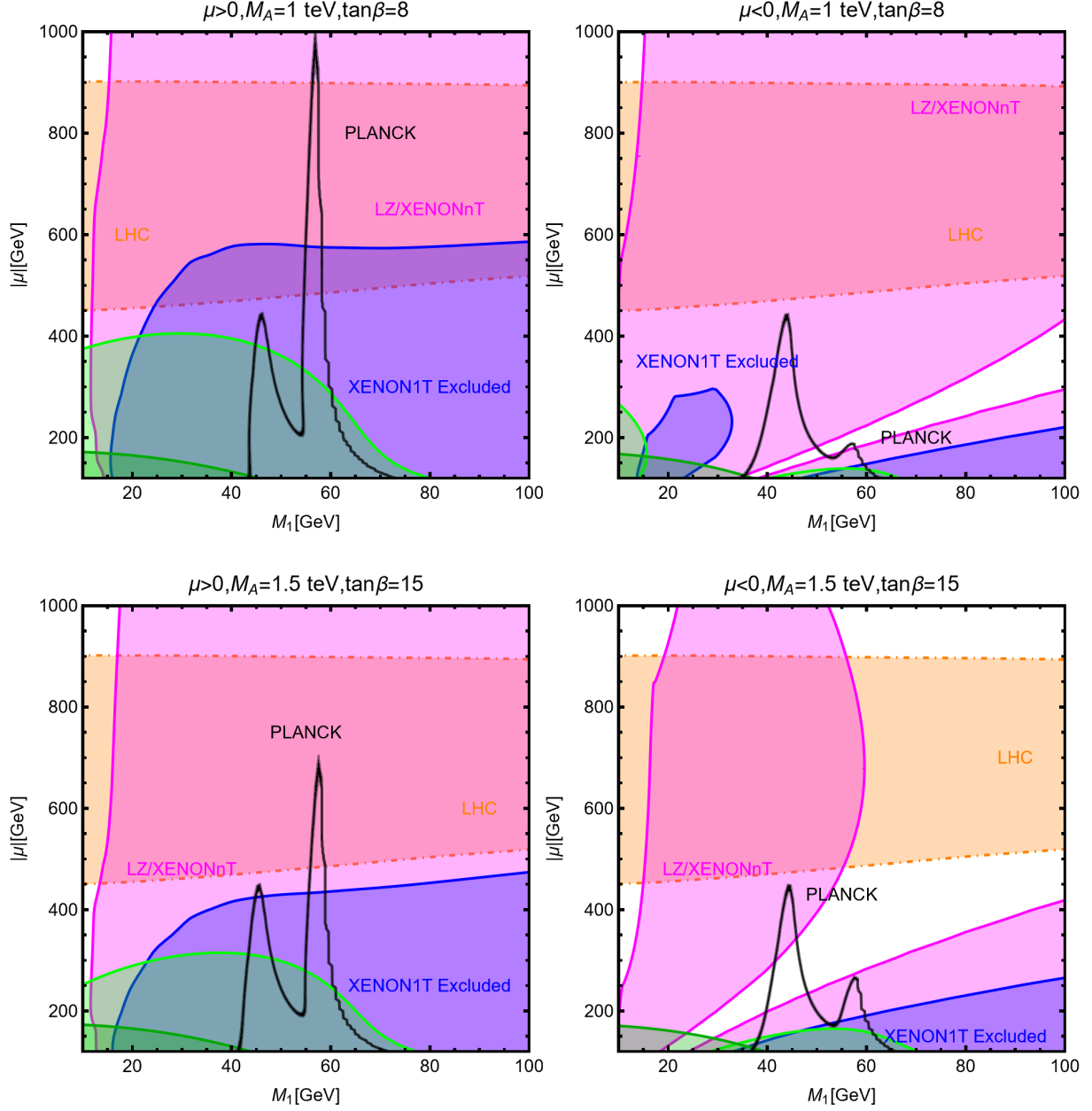


Figure 21: Summary of constraints for the scenario with a light DM neutralino and the choice $M_1 \ll M_2$, in the $[M_1, |\mu|]$ bidimensional space for the benchmark assignments of the parameters M_A , $\tan\beta$ and $\text{sign}(\mu)$ reported on top of the four panels. Following the usual color code, the black isocontours have the correct DM relic density, while the blue (magenta) regions are currently (will be) excluded by the XENON1T (XENONnT) experiments. In addition, shown in orange are the regions excluded by LHC searches of neutralinos and charginos and, in green (dark green), the regions excluded by invisible Higgs (Z) boson.

For completeness, we also display in Fig.21, the excluded region from the invisible decays of the h boson, measured at the LHC (when combining the ATLAS and CMS values) to be [84]

$$\text{BR}(h \rightarrow \text{invisible}) \leq 11\%, \quad (5.5)$$

and the invisible width of the Z bosons, which is constrained from the very precise LEP measurements to be [85]

$$\Gamma(Z \rightarrow \text{invisible}) \leq 2.49 \text{ MeV}. \quad (5.6)$$

One notices that the corresponding constraints are not as competitive as the ones from the XENON1T experiment just discussed before. Contrary to the previous scenario, no limits from DM indirect detection are displayed. This because of the p-wave suppression of the annihilation cross-section of bino-like DM.

Finally, in the $M_2 \ll M_1$ scenario, the DM neutralino is a wino-higgsino admixture for $|\mu|$ values comparable to M_2 and a pure wino (higgsino) for large (small) values of $|\mu|$. The DM relic density is then determined essentially by the gauge interactions. Due to their effectiveness, and further enhanced by Sommerfeld effects [86] and bound state formation [87], the experimental value of Ωh^2 is matched only for multi-TeV lightest neutralino states. Hence, there is almost no complementarity between the phenomenology of the DM state including the constraints from the relic density and direct detection and the LHC searches for neutralinos and charginos. For this reason, we will not discuss this scenario in detail.

5.4 Summary of the DM constraints

We summarize the outcome of the present DM analysis, in the two plots given in Fig. 22 which show the outcome of different scans over the hMSSM parameters, namely M_1, M_2, μ and $M_A, \tan \beta$. Concerning the Higgs-higgsino parameters $M_A, \tan \beta$ and μ , we have assumed in all cases the following ranges of variation:

$$M_A \in [600, 2000] \text{ GeV}, \quad \mu \in [-3, 3] \text{ TeV}, \quad \tan \beta \in [1, 60]. \quad (5.7)$$

For what concerns the gaugino masses $M_{1,2}$ we have considered the following cases:

$$\begin{aligned} M_2 &= 10M_1, \quad M_1 \in [10, 1000] \text{ GeV}, \\ M_1 &= 0.5M_2, \quad M_2 \in [100, 3000] \text{ GeV}, \\ M_1 &= M_2 \pm 50 \text{ GeV}, \quad M_2 \in [100, 3000] \text{ GeV}, \\ M_1 &= 10M_2, \quad M_1 \in [100, 3000] \text{ GeV}, \\ M_1 &= [10, 100] \text{ GeV} \quad M_2 = 2.5 \text{ TeV}. \end{aligned} \quad (5.8)$$

The results are presented in the $[M_1, \mu]$ and $[M_2, \mu]$ planes. The lower range for the value M_2 and μ is chosen to automatically account for the LEP limit on the lightest chargino mass, implying $\min[M_2, \mu] \gtrsim 100 \text{ GeV}$. The panels in the left column of Fig. 22 show the model points evading the constraints from DM direct detection, as given by XENON1T, indirect detection, as given by FERMI, collider constraints from searches of additional

Higgs bosons, invisible decays of the Z/h bosons and searches for neutralinos/charginos. The right column shows the model points which, in addition, feature the correct DM relic density according to the WIMP paradigm. The different colors correspond to, respectively, the $M_2 = 3 \text{ TeV}$ (cyan), $M_1 = 0.1M_2$ (green), $M_1 = \frac{1}{2}M_2$ (blue), $M_1 \simeq M_2$ (red) and $M_1 = 10M_2$ (orange) configurations.

Focusing on the upper left panel, we see that the $M_1 = 0.5M_2$ configuration occupies the smallest region of parameter space. This is due to the limits on LHC searches of chargino/neutralino production which are particularly strong in the case of bino-LSP/wino-NLSP [90]. In agreement with the results shown in the previous subsection, Indirect Detection constraints configurations corresponding to light higgsino-like DM while, bino-higgsino mixtures, namely $M_1 \simeq \mu$, are ruled out by XENON1T⁶. In order that light DM evades observational constraints we need to increase the hierarchy between the M_1 , M_2 . Assuming the latter parameter to be decoupled at a mass scale of 3 TeV, it is possible to access values of the DM mass below 100 GeV. Looking finally at the $M_1 \sim M_2$ case, the model points occupy a relatively large region of parameter space for $M_1 > 100 \text{ GeV}$. While the impact of DM, namely direct and indirect detection, constraints is similar as the previous cases, LHC bounds are weaker due to the compressed neutralino/chargino spectrum. The latter have substantial impact in the case of almost pure wino DM where limits from disappearing tracks apply.

Moving to the bottom left panel, showing the $[M_2, |\mu|]$ bidimensional space, we can assess the viable parameter region for $M_2 = 0.1M_1$. A generic admixture of wino and higgsino components always features s-wave annihilation cross-section which is, hence, constrained by indirect detection. This implies the lower bounds $|\mu| \gtrsim 300 \text{ GeV}$ and $M_2 \gtrsim 700 \text{ GeV}$. Again, the case $M_2 \sim |\mu|$ is ruled by Direct Detection for the whole range of the latter parameters considered in this work. As it can be seen from the right-hand side column of Fig. 22, the strict requirement of the conventional thermal paradigm as mechanism to achieve the correct DM relic density has a dramatic impact on the viable parameter space. This is due to the fact that one has to assume very specific and possibly fine-tuned relations between the model parameters. In the case $M_1 = 0.5M_2$, the correct DM relic density is achieved only for higgsino-like DM with $\mu \simeq 1 \text{ TeV} < M_{1,2}$ or for bino-like DM, provided that $m_{\chi_1^0} \simeq \frac{1}{2}M_A$. In light of this tight relation, the lower bound on M_A from LHC searches of resonances in the $pp \rightarrow A/H \rightarrow \tau\tau$ channel, serves as a lower bound on the DM mass, translating into the constraint $m_{\chi_1^0} \simeq M_1 \gtrsim 350 \text{ GeV}$. In the case $M_1 \simeq M_2$, the occurrence of the well tempered bino-wino regime allows to have M_1 as low as 100 GeV, provided that $|\mu|$ is above the TeV range. Furthermore, the correct DM relic density can be achieved in the case of a wino-like DM, with M_1 at around 2 TeV. No new viable parameter regions open up for $M_1 \gg M_2$. In this last case, all the experimental constraint are passed for pure higgsino or pure wino DM while the mixed composition for the DM is ruled out by direct detection. Finally, for $M_1 \ll M_2$, an additional small region of viable parameter space is present which corresponds to the lightest Higgs pole region $m_{\chi_1^0} \simeq M_1 \simeq \frac{1}{2}M_h$.

⁶Notice that, to apply direct and indirect detection limits in the way described above, one has to implicitly assume that each model points complies with the correct DM relic density, possibly via unknown non-thermal mechanism. Alternatively, one could assume that the neutralino DM represents only a fraction of the DM of the universe and rescale accordingly the experimental exclusion bounds.

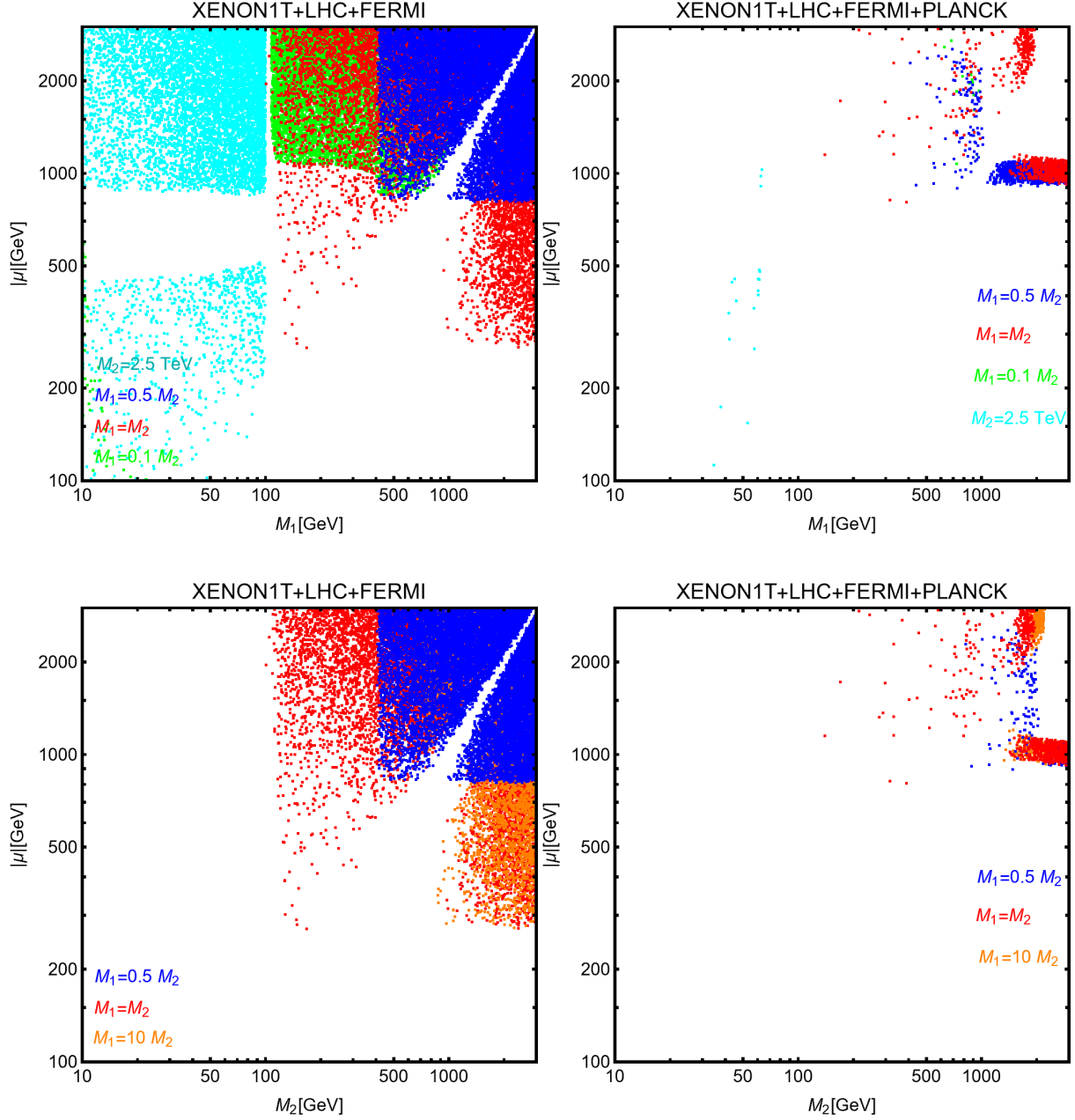


Figure 22: Summary plots of the combined LHC, direct detection and relic density constraints on the hMSSM. The colored points represent the outcome of different parameter scans (see main text for details) conducted assuming $M_1 = 0.1M_2$ (green points), $M_1 = 0.5M_2$ (blue points), $M_1 \simeq M_2$ (red points), $M_1 = 10M_2$ (orange points) and $M_2 = 3 \text{ TeV}$. The left panel shows the points evading constraints from DM direct detection and from LHC while the right panels shows, in addition, the model points complying with the correct relic density.

6 Conclusions

The hMSSM, in which the MSSM Higgs sector is parameterized in such a way that the mass of the lightest Higgs boson is automatically set to the value $M_h = 125$ GeV measured at the LHC, has become one of the two main benchmark scenarios used by the ATLAS and CMS collaborations in constraining the parameter space of the model either by interpreting their measurements of the SM-like lightest h couplings to fermions and gauge bosons [2] or in their searches of the heavier H , A and H^\pm states in various discovery channels. A nice feature of this approach, which tremendously simplifies the experimental and theoretical analyses, is that only two basic input parameters, generally taken to be $\tan\beta$ and M_A exactly like at the tree-level, are then needed in order to describe the Higgs sector. This is particularly true in the case where the masses of scalar quarks or, alternatively, the SUSY-breaking scale M_S , are large as suggested by the LHC data. It is nevertheless useful and in fact mandatory in view of future LHC upgrades, to allow for the possibility of light weakly interacting particles which are much less constrained by current data and which will be subjects to intensive searches at these upgrades.

This is the main scope of the present paper: to extend the by now traditional hMSSM [13, 14] in order to incorporate the effects of possibly light charginos χ_i^\pm and neutralinos χ_i^0 and study the implications at both colliders such as the LHC and in astroparticle physics experiments searching for the dark matter particle which, in our context, is represented by the lightest neutralino χ_1^0 . Still assuming large values of the SUSY scale M_S and the gluino mass parameter M_3 , which implies that squarks and gluinos are too heavy to have any direct impact on Higgs phenomenology, we define an hMSSM with three extra inputs parameters in addition to $\tan\beta$ and M_A , namely the bino, wino and higgsino mass parameters M_1 , M_2 and μ . In this extended hMSSM benchmark, we then explore in the most comprehensive way all possible effects of charginos and neutralinos and their interplay with the Higgs sector.

We first start by summarizing the way we implement such an hMSSM scenario in one of the numerical codes that generate the superparticle and Higgs spectra in the MSSM, the program SuSpect [25], which we then use in the subsequent numerical analyses (eventually after linking it with codes that calculate production cross sections and decay branching ratios such as HDECAY [56] and SDECAY [41]). We then evaluate the one-loop radiative corrections of charginos and neutralinos to the Higgs boson masses and couplings and show that their impact, compared to the hMSSM as traditionally defined, is rather modest for reasonable values of the additional SUSY parameters. In particular, the one-loop corrections to the Higgs boson self-energies modify the mass of the h boson by less than 1%, which is well below the admitted theoretical uncertainty in determining this mass in a general MSSM. These corrections have an even smaller impact on the determination of the masses of the heavier CP-even H and charged H^\pm states as well as on the angle α . There are also direct corrections that affect the Higgs- $b\bar{b}$ vertices at large $\tan\beta$ and μ values, but it turns out that they are also modest if squarks and gluinos are assumed to be sufficiently heavy and, hence, they do not alter the global picture.

We then study the collider implications of the charginos and neutralinos in this hMSSM. We first summarize their production and detection channels at the LHC and adapt the present experimental constraints on these particles derived by ATLAS and

CMS to our hMSSM with 5 parameters, $M_A, \tan \beta, M_1, M_2$ and μ and delineate the still allowed parameter space. We then discuss all possible sources of impact of these charginos and neutralinos on the MSSM Higgs sector: the χ_i^\pm contributions to the decays of the neutral h, H, A states into two photons, the direct corrections to heavier H, A, H^\pm production and decays in the main channels, and their impact on the lighter h boson signal strengths as measured at the LHC. We close this collider part by discussing the possible impact of Higgs decays into charginos and neutralinos on present LHC constraints.

We finally, perform a complete analysis in the hMSSM of the astroparticle implications of the lightest neutralino, considered as the dark matter particle. In particular, we update the constraints from the relic abundance of this neutralino as well as the constraints and prospects in direct and indirect detection experiments, paying a special attention to the complementarity between these searches and those performed at colliders.

All in all, we show that extending the original hMSSM scenario to incorporate the possibility of light chargino and neutralino states can be done at a minimal cost. Such an hMSSM can still parameterize in an accurate manner the MSSM Higgs sector and, at the same time, be a very good benchmark in describing the interplay between this sector and the one involving the electroweak gauginos and higgsinos. This will ease future simultaneous analyses of the two sectors at the next LHC runs, future colliders and astrophysical experiments.

Acknowledgements

We thank Luciano Maiani for discussions and collaboration at an early stage of this work. A.D. is supported by the Estonian Research Council grants MOBTT86 and by the Junta de Andalucia through the Talentia Senior program as well as by the grants A-FQM-211-UGR18 and P18-FR-4314 with ERDF. HJH and RQX are supported in part by the National NSF of China (under grants Nos. 11835005 and 11675086) and by the National Key R & D Program of China (No. 2017YFA0402204).

References

- [1] The ATLAS Collaboration, Phys. Lett. **B716** (2012) 1; The CMS Collaboration, Phys. Lett. **B716** (2012) 30.
- [2] The ATLAS and CMS Collaborations, JHEP **1608** (2016) 045; The ATLAS Collaboration, ATLAS-CONF-2019-005; The CMS Collaboration, JHEP **01** (2021) 148.
- [3] For reviews on supersymmetric theories, see M. Drees, R. Godbole and P. Roy, *Theory and phenomenology of sparticles*, World Scientific, 2005; H. Baer and X. Tata, *Weak scale Supersymmetry: from superfields to scattering events*, Cambridge U. Press, 2006; S. Martin, hep-ph/9709356; P. Binétruy, *Supersymmetry: Theory, Experiment, and Cosmology*, Oxford University Press, 2006.
- [4] H.E. Haber and G.L. Kane, Phys. Rept. **117** (1985) 75.
- [5] A. Djouadi *et al.*, The MSSM working Group, hep-ph/9901246.

- [6] J. Gunion, H. Haber, G. Kane and S. Dawson, “The Higgs Hunter’s Guide”, Reading 1990; A. Djouadi, Phys. Rept. **457** (2008) 1; M. Spira, Prog. Part. Nucl. Phys. **95** (2017) 98.
- [7] A. Djouadi, Phys. Rept. **459** (2008) 1.
- [8] Heavy Higgs searches at the LHC have been discussed recently in e.g.: M. Kakizaki et al., Int. J. Mod. Phys. **A30** (2015) no.33, 1550192; J. Baglio, A. Djouadi and J. Quevillon, Rept. Prog. Phys. **79** (2016) no.11, 116201; P. Athron et al. [GAMBIT], Eur. Phys. J. **C77** (2017) no.12, 824; P. Athron et al. [GAMBIT], Eur. Phys. J. **C77** (2017) no.12, 879; L.-C. Lü, C. Du, Y. Fang, H.-J. He, and H. Zhang, Phys. Letts. B **755** (2016) 509; J. Ren, R.-Q. Xiao, M. Zhou, Y. Fang, H.-J. He, and W. Yao, JHEP **06** (2018) 090; E. Bagnaschi et al., Eur. Phys. J. **C78** (2018) no.3, 256; E. Bagnaschi et al., Eur. Phys. J. **C79** (2019) no.2, 149.
- [9] G.C. Branco, P.M. Ferreira, L. Lavoura, M.N. Rebelo, M. Sher and J.P. Silva, Phys. Rept. **516** (2012) 1.
- [10] For reviews, see: M. Carena and H. Haber, Prog. Part. Nucl. Phys. **50** (2003) 63; S. Heinemeyer, W. Hollik and G. Weiglein, Phys. Rept. **425** (2006) 265; S. Heinemeyer, Int. Jour. Mod. Phys. **A21** (2006) 2659; B. Allanach et al., JHEP 0409 (2004) 044; P. Slavich et al., Eur. Phys. J. C **81**, no.5, 450 (2021).
- [11] M. Carena et al., Eur. Phys. J.C **26** (2003) 601; Eur. Phys. J. **C73** (2013) 2552; E. Bagnaschi et al, Eur. Phys. J.C **79** (2019) 7, 617.
- [12] E. Bagnaschi et al., Report LHCHXSWG-2015-002.
- [13] A. Djouadi, L. Maiani, G. Moreau, A. Polosa, J. Quevillon and V. Riquer, Eur. Phys. J. **C73** (2013) 2650.
- [14] A. Djouadi, L. Maiani, A. Polosa, J. Quevillon and V. Riquer, JHEP **06** (2015) 168.
- [15] G. Lee and C. E. M. Wagner, Phys. Rev. D **92** (2015) no.7, 075032.
- [16] J. Ellis, G. Ridolfi and F. Zwirner, Phys. Lett. **B257** (1991) 83; Y. Okada, M. Yamaguchi and T. Yanagida, Prog. Theor. Phys. **85** (1991) 1; H. Haber and R. Hempfling, Phys. Rev. Lett. **66** (1991) 1815.
- [17] M. Carena, J.R. Espinosa, M. Quiros and C.E. Wagner, Phys. Lett. **B355** (1995) 209; H. Haber, R. Hempfling and A. Hoang, Z. Phys. **C75** (1997)539; S. Heinemeyer, W. Hollik and G. Weiglein, Phys. Rev. **D58** (1998) 091701; Eur. Phys. J. **C9** (1999) 343; G. Degrassi, P. Slavich and F. Zwirner, Nucl. Phys. **B611** (2001) 403; A. Brignole, G. Degrassi, P. Slavich and F. Zwirner, Nucl. Phys. **B631** (2002) 195; Nucl. Phys. **B643** (2002) 79; S. Martin, Phys. Rev. **D75** (2007) 055005; P. Kant, R. Harlander, L. Mihaila and M. Steinhauser, JHEP **1008** (2010) 104.
- [18] R. El-Kosseifi, J. L. Kneur, G. Moulataka and D. Zerwas, [arXiv:2202.06919 [hep-ph]].

- [19] W. Adam and I. Vivarelli, *Int. J. Mod. Phys.* **A37** (2022) 02, 2130022.
- [20] The ATLAS collaboration, ATL-PHYS-PUB-2018-054; the CMS collaboration, contribution to CSS2013, 1307.7135 [hep-ex]; M. Cepeda, CERN Yellow Report, Monogr. **7** (2019) 221-584; arXiv:1902.00134; J. de Blas et al., *JHEP* **01** (2020), 139.
- [21] G. Farrar and P. Fayet, *Phys. Lett.*, **76B** (1978) 575.
- [22] M. Drees and G. Gerbier, Mini-Review of Dark Matter for the Review of Particle Physics, arXiv:1204.2373 [hep-ph].
- [23] G. Arcadi, A. Djouadi and M. Raidal, *Phys. Rept.* **842** (2020) 1.
- [24] J.F. Gunion and H.E. Haber, *Nucl. Phys.*, **B272** (1986) 1; *Nucl. Phys.* **B278** (1986) 449.
- [25] A. Djouadi, J.L. Kneur and G. Moultaka, *Comput. Phys. Commun.* **176** (2007) 426.
- [26] A. Arbey et al., *Phys. Lett.* **B708** (2012) 162; *Phys. Lett.* **B720** (2013) 153; *JHEP* **1209** (2012) 107.
- [27] L. Maiani, A.D. Polosa and V. Riquier, *New J. Phys.* **14** (2012) 073029; *Phys. Lett.* **B718** (2012) 465; and *Phys. Lett.* **B724** (2013) 274; A. Djouadi and J. Quevillon, *JHEP* **1310** (2013) 028; G. Chalons, A. Djouadi and J. Quevillon, *Phys. Lett.* **B780** (2018) 74; S. Liebler, M. Mühlleitner, M. Spira and M. Stadelmaier, *Eur. Phys. J.* **C79** (2019) no.1, 65.
- [28] A. Brignole, *Phys. Lett.* **B277** (1992) 313; M. Frank et al., *Phys. Rev.* **D88** (2013) 055013.
- [29] D.M. Pierce, J.A. Bagger, K.T. Matchev and R.-J. Zhang, *Nucl. Phys.* **B491**, 3 (1997).
- [30] G. Passarino and M. J. G. Veltman, *Nucl. Phys. B* **160**, 151-207 (1979).
- [31] P.H. Chankowski, S. Pokorski and J. Rosiek, *Nucl. Phys.* **B423** (1994) 437.
- [32] A. Dabelstein, *Nucl. Phys.* **B456** (1995) 25.
- [33] See e.g., A. Djouadi, M. Spira and P. M. Zerwas, *Z. Phys.* **C70**, 427 (1996).
- [34] M. Carena, D. Garcia, U. Nierste and C. M. Wagner, *Nucl. Phys.* **B577**, 88 (2000); J. Guasch, P. Häfliger and M. Spira, *Phys. Rev.* **D68**, 115001 (2003); D. Noth and M. Spira, *Phys. Rev. Lett.* **101**, 181801 (2008); and *JHEP* **1106**, 084 (2011); L. Mihaila and C. Reisser, *JHEP* **1008**, 021 (2010); A. Crivellin and C. Greub, *Phys. Rev.* **D87** (2013) 015013 Erratum: [*Phys. Rev.* **D87** (2013) 079901]; L. Mihaila and N. Zerf, *JHEP* **1705** (2017) 019; M. Ghezzi, S. Glaus, D. Mueller, T. Schmidt and M. Spira, *Eur. Phys. J.* **C81** (2021) no.3, 259.
- [35] A. Arbey et al., arXiv:2201.00070 [hep-ph].

- [36] W. Beenakker et al., Phys. Rev. Lett. **83** (1999) 3780-3783; J. Fiaschi and M. Klasen, Phys. Rev. **D98** (2018) 5, 055014.
- [37] W. Beenakker, R. Hopker and M. Spira, e-Print: hep-ph/9611232; T. Plehn, hep-ph/9809319; M. Spira, hep-ph/0211145.
- [38] J.F. Gunion and H.E. Haber, Nucl. Phys. **B307** (1988) 445; (E) hep-ph/9301205.
- [39] J.F. Gunion et al., Int. J. Mod. Phys. **A2** (1987) 1145; A. Bartl, W. Majerotto and N. Oshimo, Phys. Lett. B **216** (1989) 233; H. Baer, M. Bisset, X. Tata and J. Woodside, Phys. Rev. **D46** (1992) 303; D. Denegri, W. Majerotto and L. Rurua, CMS-NOTE-1997-094, hep-ph/9711357; S. Abdullin et al. (CMS collaboration), J. Phys. **G28** (2002) 469; I. Hinchliffe et al. (ATLAS collaboration), Phys. Rev. **D55** (1997) 5520.
- [40] A.K. Datta et al., Phys. Rev. **D65** (2002) 015007; A.K. Datta et al., Nucl. Phys. **B681** (2004) 31; A. Djouadi, Y. Mambrini and M. Muhlleitner, Eur. Phys. J. **C20** (2001) 563; M. Bisset, M. Guchait and S. Moretti, Eur. Phys. J. **C 19** (2001), 143-154; H. Baer, A. Mustafayev, S. Profumo, A. Belyaev and X. Tata, JHEP **07** (2005), 065; K. Huitu, R. Kinnunen, J. Laamanen, S. Lehti, S. Roy and T. Salminen, Eur. Phys. J. **C 58** (2008), 591-608; A. Djouadi et al., JHEP **07** (2008) 002; P. Bandyopadhyay et al., JHEP **03** (2010) 04; G. D. Kribs, A. Martin, T. S. Roy and M. Spannowsky, Phys. Rev. D **82** (2010), 095012; A. C. Fowler and G. Weiglein, JHEP **01** (2010), 108; S. Gori, P. Schwaller and C. E. M. Wagner, Phys. Rev. D **83** (2011), 115022; F. Yu, Phys. Rev. D **90** (2014) no.1, 015009; T. Han, S. Padhi and S. Su, Phys. Rev. D **88** (2013) no.11, 115010; A. Arbey, M. Battaglia and F. Mahmoudi, Eur. Phys. J. **C 75** (2015) no.3, 108.
- [41] M. Muhlleitner, A. Djouadi and Y. Mambrini, Comput. Phys. Commun. **168** (2005) 46-70.
- [42] A. Djouadi, M.M. Muhlleitner and M. Spira, Acta Phys. Polon. **B38** (2007) 635-644.
- [43] The ATLAS collaboration, ATLAS-CONF-2020-027.
- [44] The CMS collaboration, CMS-PAS-HIG-19-005.
- [45] The ATLAS collaboration, Phys. Rev. Lett. **125**, no.5, 051801 (2020).
- [46] The ATLAS collaboration, ATLAS-CONF-2020-039.
- [47] The CMS collaboration, CMS-PAS-HIG-21-001.
- [48] The CMS collaboration, JHEP **04**, 171 (2020).
- [49] The ATLAS collaboration, Eur. Phys. J. **C 78** (2018) no.7, 565.
- [50] The ATLAS collaboration, ATL-PHYS-PUB-2021-030.

- [51] The ATLAS collaboration, Phys. Rev. D **98**, no.9, 092012 (2018); Phys. Rev. D **101**, no.5, 052005 (2020); Eur. Phys. J. C **81**, no.12, 1118 (2021); ATLAS-CONF-2021-022; Eur. Phys. J. C **80**, no.8, 691 (2020); JHEP **05**, 071 (2014); Eur. Phys. J. C **80**, no.2, 123 (2020); Phys. Rev. D **93**, no.5, 052002 (2016); Eur. Phys. J. C **78**, no.12, 995 (2018); JHEP **10**, 096 (2014); Eur. Phys. J. C **78**, no.2, 154 (2018).
- [52] The CMS collaboration, Phys. Rev. D **90**, no.9, 092007 (2014); JHEP **10**, 045 (2021); arXiv:2106.14246 [hep-ex]; JHEP **04**, 123 (2021); JHEP **06**, 077 (2011).
- [53] The CMS collaboration, Phys. Lett. **B806**, 135502 (2020); arXiv:2111.06296 [hep-ex].
- [54] ATLAS collaboration, Phys. Rev. D **101**, 052005 (2020); ATLAS-CONF-2021-015 (2021); arXiv:2201.02472 [hep-ex].
- [55] LHC Higgs Cross Section Working Group]: S. Dittmaier *et al.*, arXiv:1101.0593 [hep-ph]; arXiv:1201.3084 [hep-ph]; S. Heinemeyer *et al.*, arXiv:1307.1347; J. Baglio and A. Djouadi, JHEP **03** (2011) 055; JHEP **10** (2010) 064.
- [56] A. Djouadi, J. Kalinowski and M. Spira. Comput. Phys. Commun. **108** (1998) 56–74; A. Djouadi, J. Kalinowski, M. Muehlleitner and M. Spira, Comput. Phys. Commun. **238** (2019) 214-231.
- [57] Michael Spira, Fortsch. Phys. **46** (1998) 203-284; hep-ph/9510347. See the website: <http://tiger.web.psi.ch/proglist.html>.
- [58] See e.g. A. Djouadi, J. Ellis, A. Popov and J. Quevillon, JHEP **03** (2019) 119.
- [59] A. Djouadi, V. Driesen, W. Hollik and J. I. Illana, Eur. Phys. J. C **1** (1998), 149-162; A. Djouadi, Eur. Phys. J. **C73** (2013) 2498; A. Djouadi, J. Quevillon and R. Vega-Morales, Phys. Lett. **B757** (2016) 412.
- [60] A. Djouadi, V. Driesen, W. Hollik and A. Kraft, Eur. Phys. J. C **1** (1998), 163.
- [61] K. Griest and H. E. Haber, Phys. Rev. D **37**, 719 (1988).
- [62] J. F. Gunion and H. E. Haber, Nucl. Phys. B **307**, 445 (1988) [erratum: Nucl. Phys. B **402**, 569 (1993)].
- [63] A. Djouadi, J. Kalinowski, and P. M. Zerwas, Z. Phys. C **57**, 569-584 (1993).
- [64] A. Djouadi, J. Kalinowski, P. Ohmann, and P. Zerwas, Z. Phys. C **74**, 93-111 (1997).
- [65] J. R. Ellis, J. S. Hagelin, D. V. Nanopoulos, K. A. Olive and M. Srednicki, Nucl. Phys. B **238** (1984), 453-476; H. Goldberg, Phys. Rev. Lett. **50** (1983), 1419; K. Griest, Phys. Rev. D **38** (1988), 2357.
- [66] M. Drees and M. M. Nojiri, Phys. Rev. D **47** (1993), 376-408.
- [67] N. Aghanim *et al.* [Planck], Astron. Astrophys. **641** (2020), A6 [erratum: Astron. Astrophys. **652** (2021), C4].

- [68] J. R. Ellis, T. Falk and K. A. Olive, Phys. Lett. B **444** (1998), 367-372; J. R. Ellis, T. Falk, K. A. Olive and M. Srednicki, Astropart. Phys. **13** (2000), 181-213; M. E. Gomez, G. Lazarides and C. Pallis, Phys. Lett. B **487** (2000), 313-320; H. Baer, C. Balazs and A. Belyaev, JHEP **03** (2002), 042.
- [69] C. Boehm, A. Djouadi and M. Drees, Phys. Rev. D **62** (2000), 035012; A. Djouadi, M. Drees and J.L. Kneur, JHEP **08** (2001) 055; J. R. Ellis, K. A. Olive and Y. Santoso, Astropart. Phys. **18** (2003), 395-432; R. L. Arnowitt, B. Dutta and Y. Santoso, Nucl. Phys. B **606** (2001), 59-83; J. Ellis, K. A. Olive and J. Zheng, Eur. Phys. J. C **74** (2014), 2947.
- [70] G. Arcadi, Eur. Phys. J. C **78** (2018) no.10, 864; G. Arcadi, M. Dutra, P. Ghosh, M. Lindner, Y. Mambrini, M. Pierre, S. Profumo and F. S. Queiroz, Eur. Phys. J. C **78** (2018) no.3, 203; M. Escudero, A. Berlin, D. Hooper and M. X. Lin, JCAP **12** (2016), 029, L. Calibbi, A. Mariotti and P. Tziveloglou, JHEP **10** (2015), 116; G. Arcadi, Y. Mambrini and F. Richard, JCAP **03** (2015), 018.
- [71] K. Griest and D. Seckel, Phys. Rev. D **43** (1991), 3191-3203, H. Baer, A. Belyaev, T. Krupovnickas and A. Mustafayev, JHEP **0406** (2004) 044; A. Djouadi, M. Drees and J.L. Kneur, Phys. Lett. **B624** (2005) 60.
- [72] A. Hryczuk, R. Iengo and P. Ullio, JHEP **03** (2011), 069; L. Roszkowski, E. M. Sessolo and A. J. Williams, JHEP **02** (2015), 014; M. Beneke et al., JHEP **03** (2016), 119; M. Beneke et al., JHEP **01** (2017), 002; L. Roszkowski, E. M. Sessolo and S. Trojanowski, Rept. Prog. Phys. **81** (2018) no.6, 066201.
- [73] N. Arkani-Hamed, A. Delgado and G. F. Giudice, Nucl. Phys. B **741** (2006), 108-130; H. Baer, A. Mustafayev, E. K. Park and X. Tata, JCAP **01** (2007), 017; N. Bernal, A. Djouadi and P. Slavich, JHEP **07** (2007), 016; M. Badziak, M. Olechowski and P. Szczerbiak, Phys. Lett. B **770** (2017), 226-235; S. Profumo, T. Stefaniak and L. Stephenson Haskins, Phys. Rev. D **96** (2017) no.5, 055018.
- [74] J. M. Alarcon, J. Martin Camalich and J. A. Oller, Annals Phys. **336** (2013), 413-461; A. Crivellin, M. Hoferichter and M. Procura, Phys. Rev. D **89** (2014), 054021; B. Kubis, J. Ruiz de Elvira, M. Hoferichter and U. G. Meißner, PoS **CD15** (2015), 021; M. Hoferichter, P. Klos, J. Menéndez and A. Schwenk, Phys. Rev. Lett. **119** (2017) no.18, 181803.
- [75] E. Aprile *et al.* [XENON], Phys. Rev. Lett. **121** (2018) no.11, 111302.
- [76] E. Aprile *et al.* [XENON], Phys. Rev. Lett. **122** (2019) no.14, 141301.
- [77] G. Belanger, F. Boudjema, A. Pukhov and A. Semenov, Comput. Phys. Commun. **185** (2014), 960-985; Comput. Phys. Commun. **149** (2002) 103-120; G. Belanger, F. Boudjema, P. Brun, A. Pukhov, S. Rosier-Lees, P. Salati and A. Semenov, Comput. Phys. Commun. **182** (2011), 842-856.
- [78] E. Aprile *et al.* [XENON], JCAP **11** (2020), 031.

- [79] K. Pushkin [LZ], Nucl. Instrum. Meth. A **936** (2019), 162-165.
- [80] J. Aalbers *et al.* [DARWIN], JCAP **11** (2016), 017.
- [81] P. Huang and C. E. M. Wagner, Phys. Rev. D **90** (2014) no.1, 015018; J. R. Ellis, A. Ferstl and K. A. Olive, Phys. Rev. D **63** (2001), 065016; H. Baer, A. Mustafayev, E. K. Park and X. Tata, JCAP **01** (2007), 017.
- [82] M. Duch and B. Grzadkowski, JHEP **09** (2017), 159; T. Binder, T. Bringmann, M. Gustafsson and A. Hryczuk, Phys. Rev. D **96** (2017) no.11, 115010.
- [83] The ATLAS collaboration, Phys. Rev. D **104** (2021) no.11, 112010.
- [84] The ATLAS collaboration, Phys. Rev. Lett. **122** (2019) no.23, 231801; Phys. Lett. B **829** (2022), 137066.
- [85] P.A. Zyla *et al.* [Particle Data Group], PTEP **2020** (2020) no.8, 083C01.
- [86] M. Beneke, R. Szafron and K. Urban, JHEP **02** (2021), 020, A. Hryczuk and R. Iengo, JHEP **01** (2012), 163.
- [87] A. Mitridate, M. Redi, J. Smirnov and A. Strumia, JCAP **05** (2017), 006, T. Binder, L. Covi and K. Mukaida, Phys. Rev. D **98** (2018) no.11, 115023; T. Binder, B. Blobel, J. Harz and K. Mukaida, JHEP **09** (2020), 086.
- [88] M. L. Ahnen *et al.* [MAGIC and Fermi-LAT], JCAP **02** (2016), 039; S. Hoof, A. Geringer-Sameth and R. Trotta, JCAP **02** (2020), 012.
- [89] M. Beneke *et al.*, JHEP **01** (2017), 002.
- [90] The ATLAS collaboration, Phys. Rev. D **104** (2021) no.11, 112010; arXiv:2204.13072.